ISSN 0869-5911, Petrology, 2015, Vol. 23, No. 6, pp. 576–622. © Pleiades Publishing, Ltd., 2015.
Original Russian Text © I.S. Peretyazhko, E.A. Savina, N.S. Karmanov, 2015, published in Petrologiya, 2015, Vol. 23, No. 6, pp. 624–672.

Comendites and Pantellerites of Nemrut Volcano, Eastern Turkey: Genesis and Relations between the Trachyte-Comenditic, Comenditic, and Pantelleritic Melts

I. S. Peretyazhko[a], E. A. Savina[a], and N. S. Karmanov[b]

[a] *Vinogradov Institute of Geochemistry, Siberian Branch, Russian Academy of Sciences, ul. Favorskogo 1a, Irkutsk, 664033 Russia*

e-mail: pgmigor@igc.irk.ru

[b] *Sobolev Institute of Geology and Mineralogy, Siberian Branch, Russian Academy of Sciences, pr. Akademika Koptyuga 3, Novosibirsk, 630090 Russia*

Received April 10, 2015; in final form, June 30, 2015

Abstract—The paper reports data on the mineralogy, geochemistry, phase composition of comendites and pantellerites from Nemrut volcano, eastern Turkey; estimates of the crystallization conditions of minerals, composition of matrix glasses and melt inclusions in anorthoclase, fayalite, hedenbergite phenocrysts. LA-ICP-MS was applied to analyze the matrix glasses and phenocryst minerals. The distribution coefficients between phases and glass were calculated for P, B, Li, Rb, Cs, Ba, Sr, Zr, Hf, Ta, Nb, Sc, V, Cr, Ni, Cu, Pb, Th, U, Y, REE. Mass balance simulations of the comenditic and pantelleritic compositions, experimental data, data on melt inclusions are utilized to analyze the processes responsible for the derivation of the magmas, accumulation of components in them and to elucidate genetic links between the trachyte-comenditic, comenditic and pantelleritic melts. The origin of the residual comenditic and pantelleritic melts is explained by variations in the crystallization conditions of anorthoclase (dominant phase), hedenbergite, fayalite, Fe and Ti oxides in the parental trachyte-comenditic magma depending on the pressure and concentration of water dissolved in the melts. The accessory phases (REE- and Sr-bearing fluorapatite and zircon) were likely involved in the fractionation of the melts. The following crystallization parameters were obtained by QUILF calculations for the hedenbergite, fayalite, and ilmenite phenocrysts (minimum values for quartz-free melts): 3 kbar, 763°C, ΔFMQ = –1.27 for the Fe-comendites; 3.3–3.8 kbar, 715°C, ΔFMQ = –1.8 for the pantellerites; 2.3 kbar, 748°C, ΔFMQ = –1.16 for the low-Fe comendites. The equilibrium crystallization of anorthoclase phenocrysts in the comenditic melts proceeded at temperature ~750°C. Data on glasses of melt inclusions indicate that the comenditic and pantelleritic melts contained 1–3 wt % H_2O. Analysis of literature data and estimates of the conditions under which the Nemrut magmas were derived suggest that the local chambers with H_2O-undersaturated comenditic and pantelleritic melts could occur at centers of alkaline volcanism at depths within the range of 5 to 10–15 km (lithostatic pressure of 1–4 kbar), at temperatures <750°C and oxygen fugacity below the FMQ buffer.

DOI: 10.1134/S0869591115060041

INTRODUCTION

Conditions under which comendites and pantellerites can be formed were evaluated in numerous publications. These rocks show broad compositional variations, are often anomalously enriched in trace elements (Zr, Nb, Ta, Th, U, REE), and can be generated in various geodynamic environments. Areas of alkaline volcanism with comendites and pantellerites among differentiated rocks are most commonly found in continental rifts (Yarmolyuk, 1983), for example, in the Late Paleozoic rift association in the Noen and Tost ranges in southern Mongolia (Kozlovskii et al., 2007), in Cenozoic rift systems in East Africa, and in the Basin and Range province in North America. The rocks were lately studied in Paleogene–Quaternary volcanic complexes in the Olkaria and Eburru in the Kenya Rift (Heumann and Davies, 2002; Ren et al., 2006; Macdonald et al., 2008; Marshall et al., 2009), Dabbahu volcano in the Afar Rift (Field et al., 2012, 2013), Gedemsa and Boseti volcanoes in the Central Ethiopian Rift (Peccerilo et al., 2003; Ronga et al., 2010), Pektusan volcano (also known as Baitoshan, or Changbaishan Tianshi) in the Tanlu Rift System at the boundary between China and North Korea (Horn and Schmincke, 2000; Popov et al., 2005, 2008; Sakhno, 2007a, 2007b; Andreeva et al., 2014). In the West Antarctic Rift (Marie Byrd Land), Antarctica studied volcanoes with pantelleritic trachytes, pantellerites and phonolites (LeMasurier et al., 2011). Comendites and pantellerites were also found in geodynamic environments of oceanic islands and were studied, for example, in the Azores (Mungall and Martin, 1995), Pan-

telleria Island (Civetta et al., 1998; White et al., 2009) and Socorro Island (Bohrson and Reid, 1997).

No consensus has been reached so far concerning the origin of comenditic and pantelleritic melts, which are usually thought to be the most alkaline and silicic residual products of the evolution of trachytic magmas, which were, in turn, formed by the fractional crystallization of trachybasaltic or alkali basaltic magmas in isolated crustal magma chambers (Mungall and Martin, 1995; Bohrson and Reid, 1997; Civetta et al., 1998; Gavnegin et al., 2003; Peccerillo et al., 2003; White et al., 2009; Ronga et al., 2010; LeMasurier et al., 2011; Field et al., 2013; Andreeva et al., 2014; and others). In an alternative model suggested for the origin of residual high-Fe alkali comenditic and pantelleritic melts, these rocks are reportedly generated via the fractional crystallization of low-Fe comenditic melts (Macdonald et al., 1987; Scaillet and Macdonald, 2001, 2003, 2006; Marshall et al., 2009).

Centers of trachybasalt–trachyte–comendite ± pantelleritic volcanism are very rare in environments of convergent lithospheric plates. One of these areas is Nemrut volcano in eastern Turkey, which was formed in a collision zone between the Anatolian and Arabian plates (Çubukçu et al., 2012; Ulusoy et al., 2012). Our earlier paper reported data obtained on samples of trachybasalt, mugearite, benmoreite, trachydacite, comendite and hybrid volcanic rocks from Nemrut (Peretyazhko et al., 2015). These data and the results of our mass-balance calculations were later employed in discussing the most probable processes that could produce mugearitic and benmoreitic magmas. This paper reports the results of comprehensive study of the mineralogy and geochemistry of Nemrut comendites and pantellerites. These studies were undertaken to elucidate the conditions under which the rocks were formed and possible genetic links between the trachyte-comenditic, comenditic and pantelleritic melts during the pre-caldera and post-caldera stages of the volcano. Below we discuss data on melt inclusions in phenocrysts, the composition of the matrix glasses, conditions of melts crystallization, mass-balance models for the magmatic evolution and the accumulation processes of the comenditic and pantelleritic residual melts.

METHODS

The rocks were analyzed by XRF on a CPM-25 X-ray spectrometer at the Vinogradov Institute of Geochemistry. Trace elements were determined by ICP-MS on a NexION300D (Agilent Technologies Inc.) quadrupole mass spectrometer at the Baikal Analytical Center of Collective Use at the Irkutsk Research Center of the Siberian Branch, Russian Academy of Sciences. Samples were prepared for ICP-MS analysis with the use of open acid decomposition.

Minerals and glasses were analyzed by a MIRA-3 LMU (Tescan Ltd.) scanning electron microscope equipped with an Inca Energy 450 XMax 80 (Oxford Instruments Ltd.) energy-dispersive spectrometer (SEM-EDS analysis) at the Sobolev Institute of Geology and Mineralogy in Novosibirsk. The reference samples were quartz, feldspars and metals. Matrix effects were taken into account using the XPP algorithm of the proprietary software of the scanning microscope. The analyses were carried out at an accelerating voltage of 20 kV, beam current of 1.5 nA, counting time of 20 s. For these analytical conditions metrological characteristics were determined for analysis of rock-forming minerals (Lavrent'ev et al., 2015). The detection limit for SEM-EDS was 0.2–0.3 wt %, and the average random error was 0.9% for elements whose concentrations were >10 wt %, 3% for concentrations of 1–10 wt %, and 13% for concentrations of 0.3–1 wt %. Glasses and minerals were analyzed by scanning over rectangular areas >10 μm^2 (if the sizes of mineral and glass grains were larger). These analytical conditions allowed us to preclude significant losses of alkalis from glasses. The average compositions of rock matrixes were determined by scanning over areas greater than 300 to 400 μm^2.

Glasses in rock matrixes and melt inclusions (MI) in anorthoclase, hedenbergite, fayalite phenocrysts were analyzed by LA-ICP-MS using a UP213QA/S (Perkin Elmer) laser ablation system and NexION300D mass spectrometer. The quality of the analysis was controlled by analyzing NIST-612, NIST-610, NIST-614 standard samples. The concentrations of elements were normalized to SiO_2 and Al_2O_3 concentrations (analyzed by SEM-EDS) in minerals and glasses.

The thermometric study of MI was carried out on Linkam-TS1500 and Linkam-TS1400XY stages at the Vinogradov Institute. To monitor the process of melting, MI were heated and held for 3–9 h at temperatures of 700 to 1200°C. Long-lasting heating of MI was done using a TS-1500 stage. The heating/freezing stages were calibrated on the melting temperatures of $K_2Cr_2O_7$, NaCl, Au with temperature controlled accurate to ±5°C within the temperature range of 700–1000°C and to ±5–8°C at temperatures >1000°C. Upon exposing MI, their glasses and crystalline phases were analyzed by SEM-EDS and LA-ICP-MS.

Mass balance models and ion proportions in the crystallochemical formulas of minerals were calculated using the CRYSTAL software (Peretyazko, 1996). The crystallization parameters of minerals were evaluated by geothermometers (Ghiorso and Evans, 2008; Putirka, 2008) and the QUILF-95 program (Andersen et al., 1993).

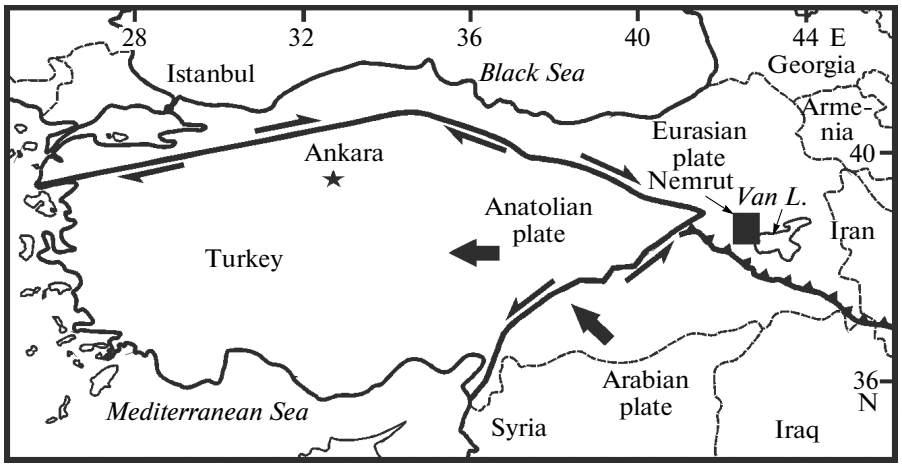

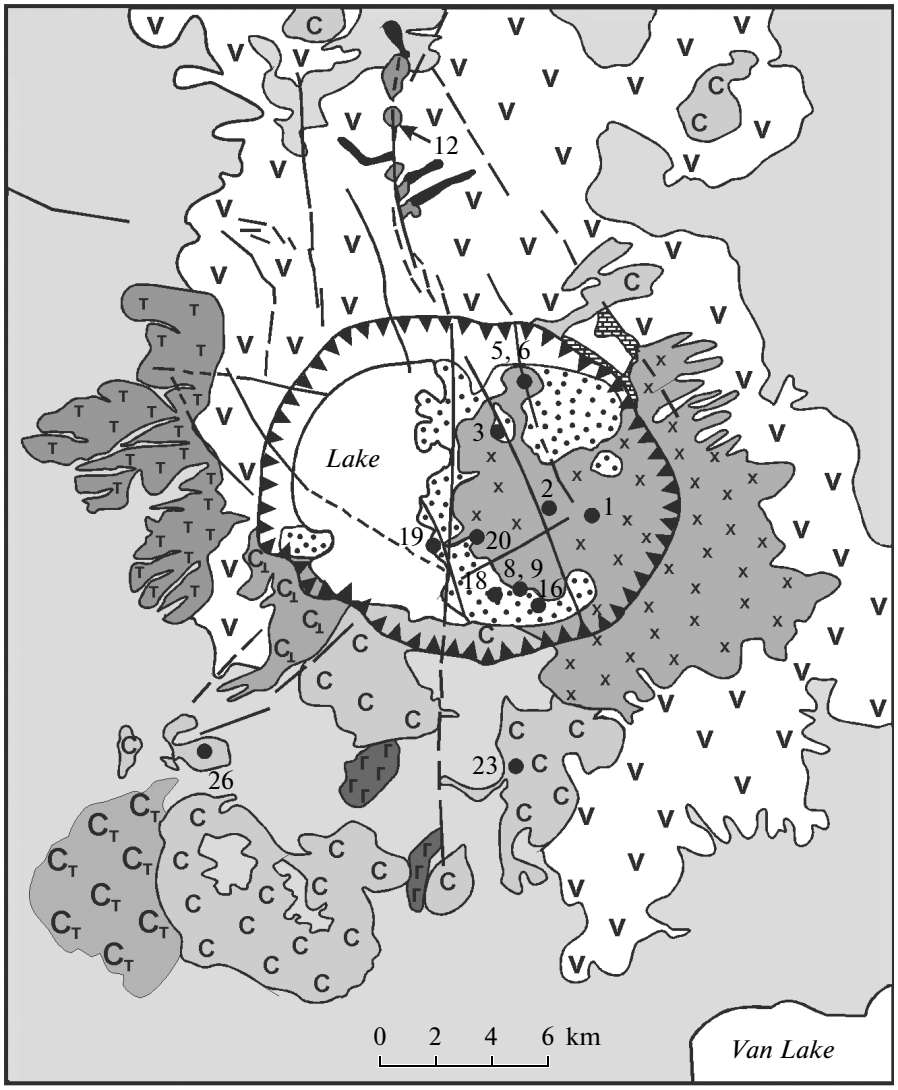

Pre-caldera stage

1 2 3 4 5 6

Post-caldera stage

7 8 9 10 11

COMENDITES AND PANTELLERITES OF NEMRUT VOLCANO

The geological setting of Nemrut volcano, the succession of its eruptions, and its stratigraphy are described in (Yilmaz et al., 1998; Yadar et al., 2003; Karaoğlu et al., 2005; Özdemir et al., 2006; Ulusov et al., 2012: Çubukçu et al., 2012). Figure 1 shows the tectonic setting of volcano and geological map of this Anatolian region.

Nemrut volcano is located on the eastern shore of Lake Van, 12 km east of the collisional boundary between the Anatolian and Arabian plates. During the pre-caldera stage of the volcano at 1 Ma to 89–93 ka (Çubukçu et al., 2012), the edifice of the stratovolcano was formed. This edifice is dominated by eruption products (lava and pyroclastic material) of trachytic, trachyte-comenditic, and high-Fe comenditic magmas containing more than 63 wt % SiO_2. Isotopic ages (K-Ar data; Çubukçu et al., 2012) make it possible to distinguish a number of successive eruption cycles of the stratovolcano: 1010 ± 40 ka, 384 ± 23 ka (trachytes); 333 ± 41, 264 ± 6, 89 ± 2 ka (comenditic trachytes); 567 ± 23, 384 ± 23, 99 ± 3 (pantellerites); 310 ± 100, 242 ± 15, 158 ± 4, <89 ± 2 ka (high-Fe comendites). The trachytes and comenditic trachytes are variably recrystallized aphyric and porphyritic (or much more rarely vitreous) rocks. The high-Fe comendites and pantellerites consist of glass, phenocrysts and microlites (rarely more than 10 vol % crystals), with occasionally occurring partly recrystallized varieties.

According to (Çubukçu et al., 2012), the caldera was formed between 90 and 30 ka as a result of the collapse of the stratovolcano edifice triggered by large eruptions of trachytic ignimbrites. After this, low-Fe comenditic magma was erupted in the caldera and produced comendites varieties dated at 30 ± 2, 24 ± 1, 15 ± 1, 8 ± 3 ka. The rocks compose lava flows and domes. The longest of the flows is made up of glassy comenditic lava extends sublatitudinally for 3 km at a width of 1–1.5 km and a thickness of 20–25 m, and descends to the lake (Fig. 1). The top portion of the flow consists of perlite (swelled comendite), which is readily desintegrated and composes peculiar landforms. The vitreous low-Fe comendites (sometimes obsidian almost devoid of phenocrysts) form lava domes in the caldera, which hosts perlite beds and domains and rocks with spherulitic, lenticular and patchy segregations of partly devitrified glass. Low-Fe comenditic magma was also erupted as pyroclastic material within the caldera itself.

Outside the caldera, in the northern face of the volcano (Fig. 1) a so-called rift zone up to 50 m wide and bounded by two faults up to 5000 m long was formed approximately 500 years ago (Ulusov, 2008; Ulusov et al., 2012). The low-Fe comendites composes there a number of lava flows, which were erupted after the trachybasaltic magma. The trachybasalts and low-Fe comendites in the "rift" zone are the youngest volcanic rocks of Nemrut volcano. The post-caldera low-Fe comendites typically contains benmoreitic enclaves and domains with relics (glass of trachyrhyodacite–trachyrhyolite composition and xenocrysts of magnesian olivine, plagioclase, augite) of the post-caldera benmoreitic magma (Çubukçu et al., 2012; Peretyazhko et al., 2015).

ROCK SAMPLES

We studied samples of the pre-caldera stage high-Fe comendite (sample NR-23), pantellerite (NR-7), a number of samples of the post-caldera low-Fe comendites. Samples of other rocks of the pre-caldera stage and those from the "rift" zone (trachybasalt, mugearite, trachydacite, benmoreite, a hybrid rock of benmoreitic composition and low-Fe comendites) are described in (Peretyazhko et al., 2015). The sampling sites are shown in Fig. 1, and their coordinates are listed in Table 7.

Sample NR-23 of high-Fe *comendite* was taken from a lava flow in the southern slope of the volcano (Fig. 1). The rock consists of 95% glass. The dominant phenocryst mineral is anorthoclase, and hedenbergite, fayalite, ilmenite phenocrysts are more rare. Anorthoclase phenocrysts are large (up to 1–2 mm) euhedral colorless semitransparent crystals and their aggregates, sometimes showing dissolution embayments. The phenocrysts of dark green hedenbergite and semitransparent yellow fayalite are up to 200–300 μm, euhedral and subhedral, occur not far from one another or from aggregates (Fig. 2b). Ilmenite is very rare, occurs as single grains 100–200 μm across and as inclusions, together with REE- and Sr-bearing fluorapatite in hedenbergite (Fig. 2a). The glass shows clear fluidal textures, which are seen in transmitted light around phenocrysts and are accentuated by various tints of the semitransparent pale glass and oriented hedenbergite microlites (3–5 μm long, <1 μm in cross section). The glass abounds in small (<1 μm) grains of Fe and Ti oxides (likely ilmenite and/or titanomagnetite) and contains rare patches (<1 mm) of devitrified glass (Fig. 2a).

Fig. 1. Geological setting of Nemrut volcano shown in schematic geological map (modified after Çubukçuet al., 2012; Ulusoy et al., 2012). Numerals are the numbers of sampling sites (see note to Table 7 for their coordinates). Pantellerite sample NR-7 was taken from comenditic talus in the caldera, and trachyte sample NR-21 is from an enclave in an ignimbritic sheet. *Pre-caldera rocks*: (1) Nemrut ignimbrite; (2) Kantaşi ignimbrite; (3) comenditic trachyte (lava, dome); (4) (a) pantellerite (lava), (b) mugearite (lava); (5) comendite (lava, dome); (6) (a) comenditic trachyte (lava, dome), (b) trachyte (lava). Post-caldera rocks: (7) Base Surge comendite; (8) comendite (lava, dome); (9) trachybasalt from "rift" zone; (10) comendite from "rift" zone; (11) caldera contours and faults.

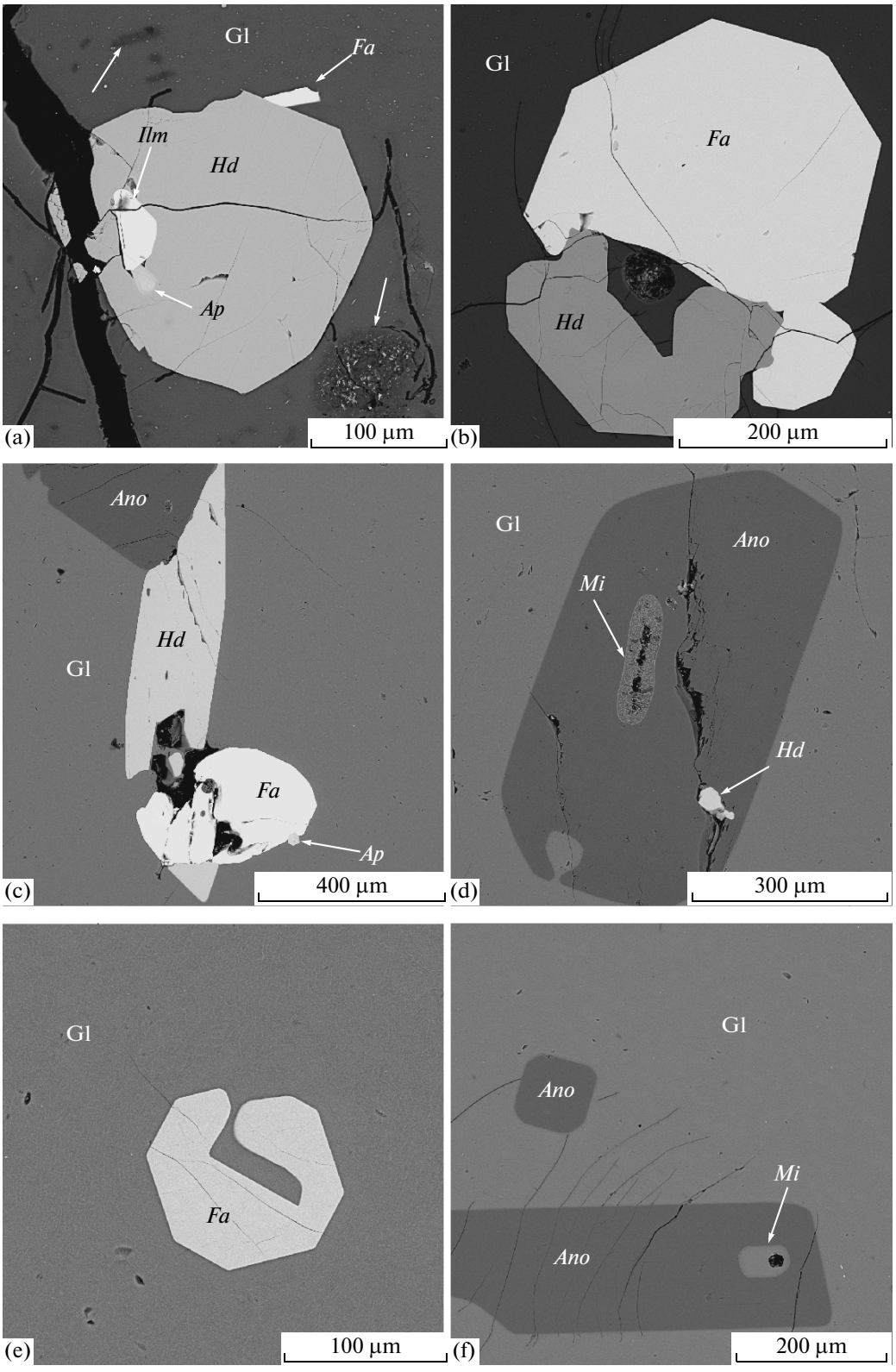

Fig. 2. BSE images of fragments of samples of high-Fe comendite NR-23 and pantellerite NR-7. Sample NR-23: (a) Inclusion Fayalite microlite with hedenbergite phenocryst containing ilmenite and fluorapatite inclusions (arrows point to domains of devitrified glass); (b) aggregate of hedenbergite and fayalite phenocrysts (interstices between the phenocrysts are filled with glass). Sample NR-23: (c) aggregate of anorthoclase, hedenbergite and fayalite phenocrysts (fluorapatite grain near the margin of a phenocryst); (d) anorthoclase phenocryst with a partly overgrown embayment, recrystallized MI and hedenbergite inclusion; (e) fayalite microlite in glass; (f) anorthoclase phenocrysts with MI filled with primary quenched glass. Symbols: Gl—glass, *Hd*—hedenbergite, *Fa*—fayalite, *Ano*—anorthoclase, *Ilm*—ilmenite, *Ap*—apatite, *Mi*—melt inclusion.

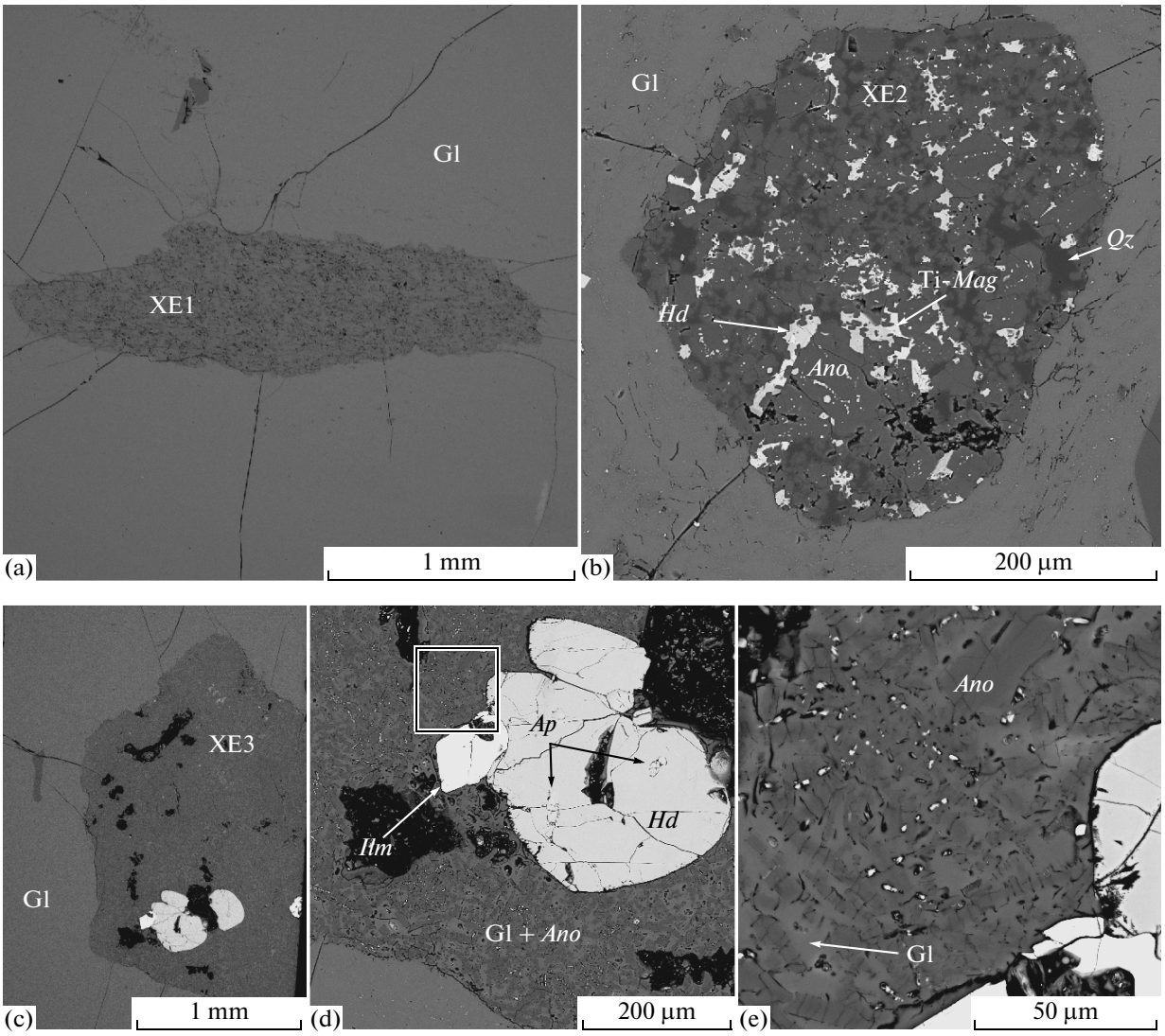

Fig. 3. BSE images of fragments of pantellerite sample NR-7. (a) Enclave XE1, perlite of high-Fe comendite; (b) enclave XE2, recrystallized comenditic trachyte (quartz–anorthoclase symplectite with hedenbergite and titanomagnetite); (c) enclave XE3, comenditic trachyte; (d) detailed image of enclave XE3 with a hedenbergite phenocryst that contains ilmenite and fluorapatite inclusions; (e) portion of the matrix of enclave XE3 with anorthoclase microlites (which differ in Fe concentrations) and pantelleritic interstitial glass. Ti-*Mag* is titanomagnetite, other symbols are as in Fig. 2.

Sample *NR-7 of pantellerite* was taken from loose blocks of comenditic lava in the caldera. The pantellerite fragments perhaps form talus from the pre-caldera pantelleritic lava exposed in a caldera wall. It should be mentioned that the pre- and post-caldera comendites and pantellerites are indistinguishable in hand-specimens. The rocks are dominated by semitransparent glass with intricately bent dark and pale stripes "enveloping" large (up to 2 mm) elongate crystals of semitransparent colorless anorthoclase, which are sometimes corroded by small dissolution embayments (Fig. 2d). Anorthoclase is the dominant phenocryst mineral. The rocks contain fayalite phenocrysts, which display evidence of dissolution and/or growth of crystal faces (Fig. 2e), crystals of dark green hedenbergite, microlites of fluorapatite (up to 30–40 μm), and aggregates of phenocrysts of anorthoclase, hedenbergite, fayalite and fluorapatite (Fig. 2c). The anorthoclase sometimes contains hedenbergite inclusions (Fig. 2d). The fluidal glass hosts rare submicrometer-sized phases, likely Fe and Ti oxides.

The sample contains single enclaves (0.5 mm to 2 cm across) of high-Fe comendite and comenditic trachyte. Judging by their appearance and composition, some of the enclaves (labeled XE1 in Fig. 3a) are perlite of high-Fe comendite. Other enclaves are variably recrystallized comenditic trachyte. Some of these enclaves are dominated by quartz–feldspar symplectite with hedenbergite and titanomagnetite inclusions (XE2 in Fig. 3b). In the context of data interpretation,

Table 1. Composition (wt %) of feldspars

Component	NR-7 (22)	XE2 (2)	XE3 (2)	XE3 (2)	NR-23 (9)	NR-1 (12)	NR-2 (10)	Mc (2)	NR-5 (11)	PL (2)	PLc (1)	NR-16 (12)	NR-18 (18)	NR-19 (5)	NR-20 (10)	Mc (7)
SiO_2	68.01	68.03	68.03	68.62	67.39	66.90	67.54	68.79	68.18	57.10	68.05	67.59	67.38	68.54	67.14	68.36
Al_2O_3	18.43	19.01	19.4	19.27	18.47	18.59	18.92	16.71	18.99	26.27	19.37	18.68	18.62	19.19	18.63	18.32
$Fe_2O_3^*$	0.82	0.33	0.63	1.37	0.60	0.31	0.32	1.06	0.28	0.70	0.44	0.28	0.33		0.37	0.55
CaO			0.32	0.35		0.11	0.13		0.11	8.67	0.60	0.10	0.12	0.19	0.19	0.10
Na_2O	7.80	7.39	7.67	8.66	7.77	7.23	7.37	8.35	7.45	6.34	9.35	7.10	7.24	7.48	7.32	9.27
K_2O	5.64	6.25	6.00	4.15	5.65	6.17	6.13	3.23	6.22	0.42	3.96	6.16	6.18	6.13	5.91	2.97
Total	100.74	100.97	101.99	101.18	99.89	99.31	100.41	98.12	101.23	99.50	100.77	99.92	99.88	101.53	99.57	99.57
Ab, %	67.76	64.25	65.03	74.76	67.66	63.73	64.32	79.74	64.21	55.58	80.40	63.36	63.78	64.59	64.75	82.25
Or, %	32.24	35.75	33.47	23.57	32.34	35.80	35.17	20.26	35.28	2.42	16.75	36.19	35.85	34.88	34.41	17.34
An, %			1.50	1.67		0.47	0.50		0.51	42.00	2.85	0.45	0.37	0.53	0.84	0.41

$Fe_2O_3^*$ is total Fe; *Ab*, *Or*, *An* are the albite, orthoclase, anorthite end members; XE2 and XE3 are anorthoclase with variable Fe concentrations from enclaves (Figs. 3b–3e), sample NR-7; Mc is microlites in glass; PL and PLc, respectively, are the core and rims of andesine xenocryst from benmoreitic magma (Fig. 4e); numerals in parentheses show the numbers of analyses.

the most interesting enclaves are those of comenditic trachyte, which consists of a mixture of anorthoclase with variable Fe concentrations and pantelleritic glass (XE3 in Figs. 3c–3e). The matrix of these enclaves contains hedenbergite phenocrysts with ilmenite and fluorapatite inclusions (Fig. 3d).

Samples of *low-Fe* comendites were collected from lava flows and lava domes in the caldera and a lava flow in the "rift" zone (Fig. 1). These are vitreous rocks that usually contain no more than 10 vol % phenocrysts. The phenocrysts are dominated by large (up to 2–3 mm) euhedral anorthoclase crystals. Phenocrysts of hedenbergite, fayalite, fluorapatite, ilmenite and titanomagnetite are much more rare, as also are anorthoclase microlites (Figs. 4a–4d). The matrix glass contains single andesine xenocrysts with anorthoclase rims (Fig. 4e) and augite aggregates with titanomagnetite (Fig. 4f). According to (Peretyazhko et al., 2015), the andesine, augite and titanomagnetite xenocrysts crystallized from the benmoreitic magma, which was repeatedly injected into the low-Fe comenditic melt. Several samples contain chevkinite, zircon, and pyrrhotite microlites (Figs. 4b, 4f). The matrix glasses are semitransparent, not fluidal, and sometimes contain submicrometer-sized grains of Fe and Ti oxides. Glasses in some samples host numerous gas bubbles (up to 2–5 mm long), which are flattened along layers of melt flow. In sample NR-8, matrix glass alternates with linear elongate stripes of devitrified glass (Fig. 4g). Sample NR-20 contains spherulites up to 1–2 mm across consisting of feldspar–quartz symplectite and blebs (1–3 mm) of devitrified glass (Figs. 4h, 4i).

MINERAL CHEMISTRIES

Feldspars

Data in Table 1 illustrate the composition of the feldspars, which are also shown in the *Ab–An–Or* diagram in Fig. 5. In sample NR-23 of comendite and sample NR-7 of pantellerite, feldspar phenocrysts are unzoned and correspond to anorthoclase ($Ab_{66\text{-}69}Or_{34\text{-}31}$) with insignificant variations in the concentrations of the albite end member (Fig. 5a). Anorthoclase in samples NR-23 and NR-7 contains slightly different Fe concentrations: 0.6 and 0.8 wt % Fe_2O_3 on average, respectively. Anorthoclase microlites in enclave XE3 of comenditic trachyte (Figs. 3c–3e) in pantellerite of sample NR-7 are zoned: their cores have a composition close to that of phenocrysts in matrix glass of the pantellerite, whereas their outermost rims are more sodic ($Ab_{72\text{-}77}Or_{28\text{-}33}$) and richer in Fe (1–1.7 wt %

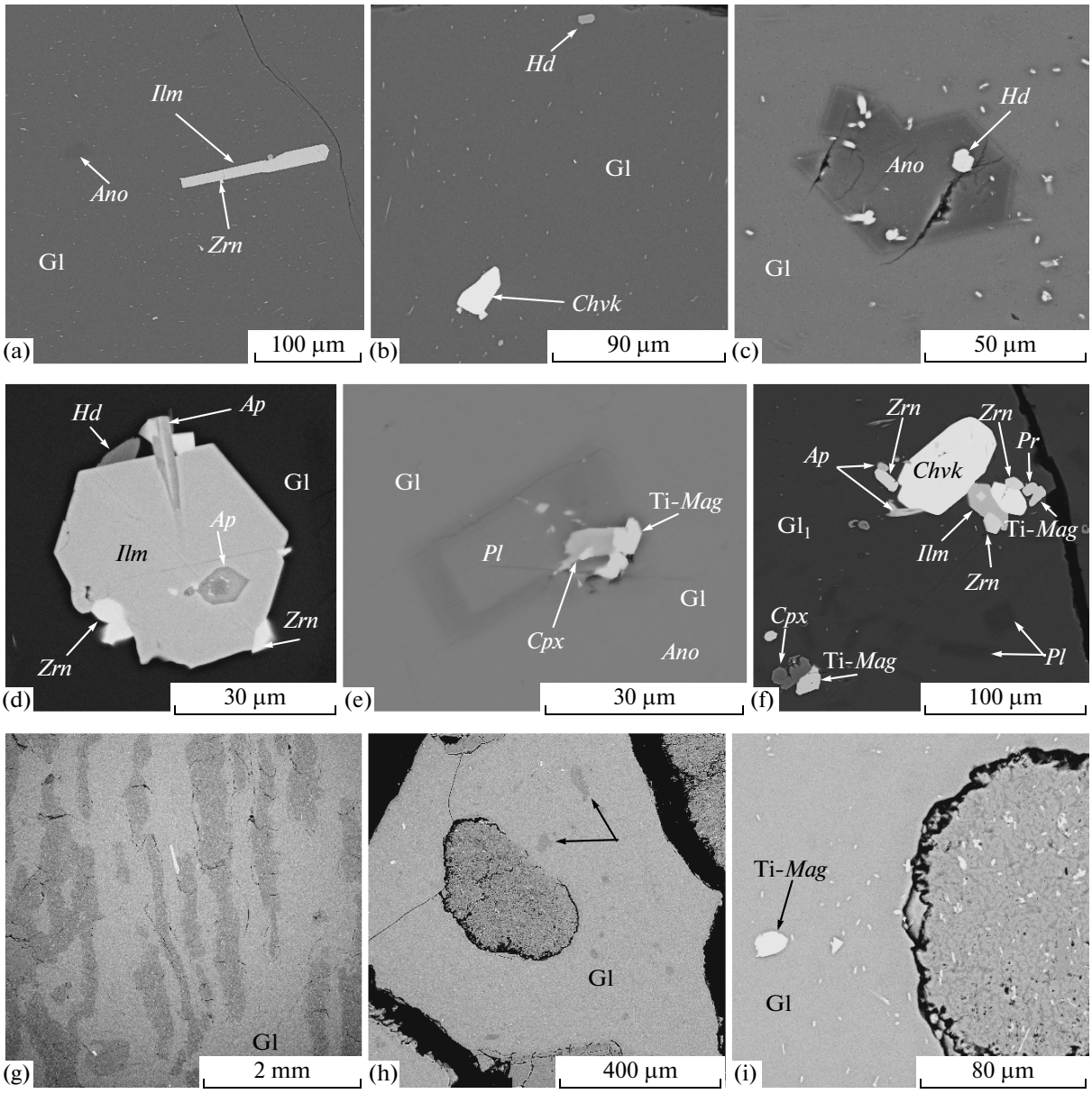

Fig. 4. BSE images of fragments of low-Fe comendite samples. (a) Ilmenite phenocryst with a zircon grain and anorthoclase microlite in matrix glass, sample NR-16; (b) chevkinite and hedenbergite microlites in glass, sample NR-16; (c) anorthoclase microlite with hedenbergite inclusions, the microlite is zoned: its core has the composition $Ab_{67}Or_{33}$, and the outer zones is more sodic, $Ab_{85}Or_{15}$, sample NR-20; (d) ilmenite microlite (crystal) with a fluorapatite ingrowth and inclusion at the contact of a zircon microlite and hedenbergite, sample NR-18; (e) andesine microlite with anorthoclase rim in aggregate with augite and titanomagnetite microlites in glass (the xenocrysts are relics from benmoreitic magma), sample NR-5; (f) fragment of matrix glass with microlites of the comenditic mineral association (chevkinite, zircon, apatite, ilmenite, titanomagnetite, pyrrhotite), with augite and titanomagnetite microlites, and with andesine crystals that have oligoclase rim from benmoreitic magma, sample NR-12; (g) banded fluidal devitrified glass in the matrix, sample NR-8; (h) quartz-feldspathic symplectite spherulite and patches of devitrified glass in the matrix, sample NR-20; (i) fragment of a quartz-feldspathic symplectite spherulite with titanomagnetite inclusions, sample NR-20. *Chvk*—chevkinite, *Pr*—pyrrhotite, *Pl*—plagioclase, *Cpx*—clinopyroxene, other symbols are as in Figs. 2 and 3.

Fe_2O_3). The anorthoclase of enclave XE2 (Fig. 3b) contains 0.3 wt % Fe_2O_3.

Anorthoclase phenocrysts in the low-Fe comendites is unzoned. It is usually more potassic ($Ab_{61\text{-}68}An_{0\text{-}2}Or_{34\text{-}38}$) than in samples NR-23 and NR-7, and its composition points plot around the boundary line between the anorthoclase and Na-sanidine fields (Fig. 5b). The anorthoclase contains admixtures of CaO (0.25 wt %) and Fe_2O_3 (up to 0.4 wt %). Microlites in the glass (Fig. 4c) contain more Na, typically show significant

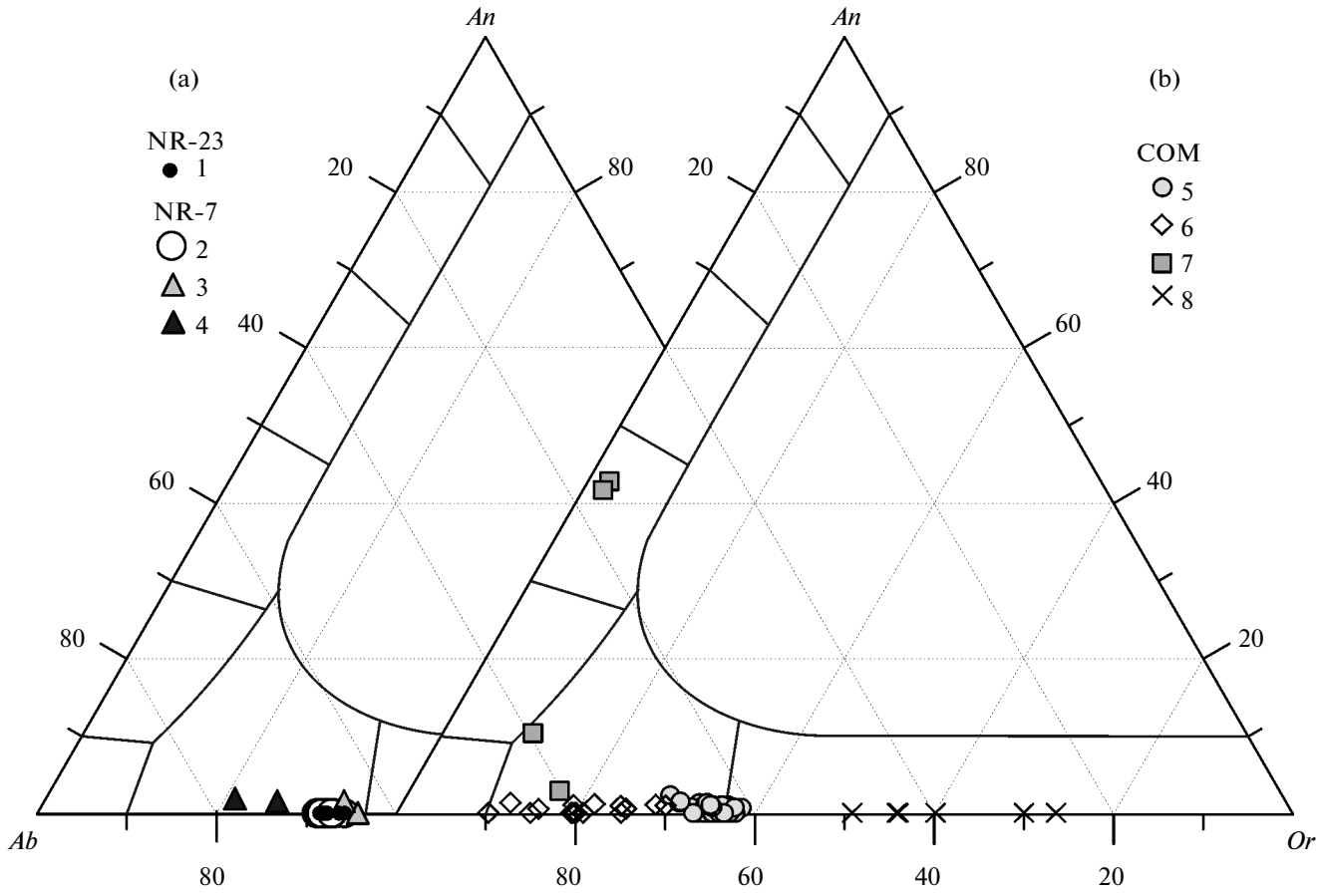

Fig. 5. Compositional evolution of feldspars in (a) pantellerite NR-7, high-Fe comendite NR-23 and (b) low-Fe comendite. (1) Phenocrysts, sample NR-23; (2) phenocrysts, sample NR-7; (3) microlites in matrix glass, sample NR-7; (4) Fe-enriched anorthoclase microlites in enclave XE3, sample NR-7; (5) phenocrysts in low-Fe comendite samples (COM); (6) microlites in matrix glass; (7) andesine xenocrysts with anorthoclase rims, sample NR-5; (8) microlites in glasses of melt inclusions in anorthoclase phenocrysts. *Ab*—albite, *An*—anorthite, *Or*—orthoclase.

variations in the content of the albite end member ($Ab_{71\text{-}90}An_{0\text{-}1}Or_{10\text{-}30}$), and are richer in Fe_2O_3 (0.6–1 wt %) than the anorthoclase phenocrysts. Single crystals from the benmoreite magma (Fig. 4e) are andesine with anorthoclase rims, whose composition is closely similar to that of the matrix microlites of the low-Fe comendite (Fig. 5b). The K- and Fe-richest microlites are those in the glass of MI in anorthoclase phenocrysts. They have intermediate compositions ($Ab_{26\text{-}49}Or_{74\text{-}51}$), plot within the sanidine field (Fig. 5b), and are the richest in Fe_2O_3 (3.3 wt % on average).

Clinopyroxene

Clinopyroxene is the second most abundant phenocryst and microlite mineral after anorthoclase. The composition of the mineral varies insignificantly from sample to sample ($En_{3\text{-}5}$,$Fs_{43\text{-}57}$,$Wo_{42\text{-}45}$), and its composition points plot near the hedenbergite field (Fig. 6). The mineral typically contains elevated Mn concentrations (1–2.4 wt % MnO). The Mg concentration in the hedenbergite is different in various rocks: the mineral contains 0.2–0.3 wt % MgO in comendite of sample NR-23 and pantellerite of sample NR-7 and 0.5–1.3 wt % MgO in the low-Fe comendite (Table 2). MI in anorthoclase phenocrysts sometimes contain aegirine-augite microlites (Table 2, analysis 2), and the matrix of the low-Fe comendite contains augite xenocrysts from benmoreitic magma (Figs. 4e, 4f; Table 2, analysis 11). Figure 6 shows the composition points of clinopyroxene from the trachyte (sample NR-21) and the compositional trend of the mineral in the rocks containing more than 63 wt % SiO_2.

Fayalite

Fayalite phenocrysts and microlites were found in all comendite samples and in the pantellerite of sample NR-7. Analyses of the mineral are listed in Table 3. The fayalite is characterized by a composition extremely rich in Fe and by very insignificant variations in the Mg and Mn concentrations. Fayalite in comendite NR-23 and pantellerite NR-7 is poorer in MgO (0.1–0.2 wt %, LA-ICM-MS data) and richer

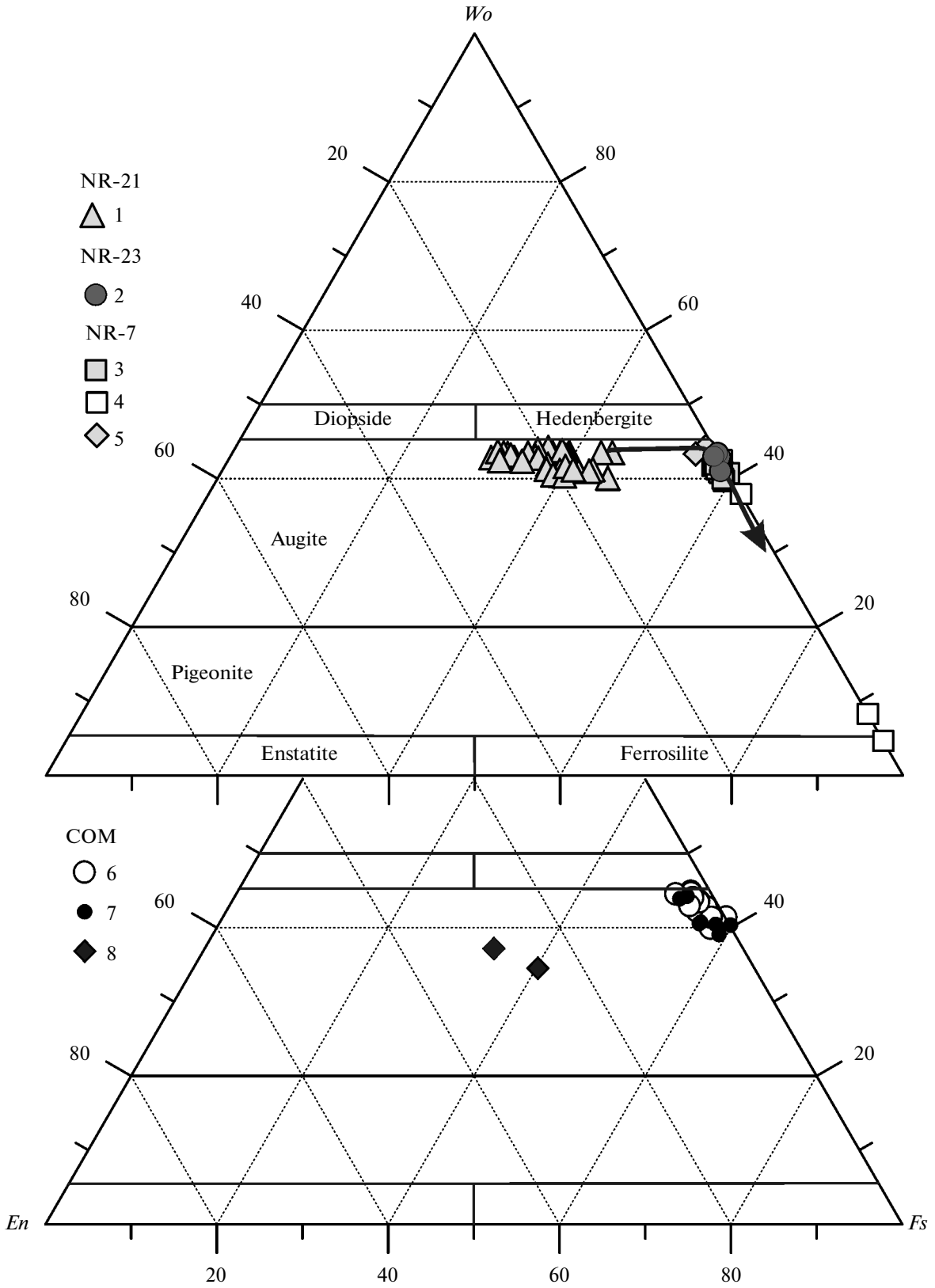

Fig. 6. Compositional evolution of clinopyroxene in the rocks. (1) Phenocrysts in trachyte, sample NR-21; (2) phenocrysts in sample NR-23; (3) phenocrysts, sample NR-7; (4) microlites in glasses of melt inclusions in anorthoclase phenocrysts, sample NR-7; (5) phenocryst in enclave XE3, sample NR-7; (6) phenocrysts in low-Fe comendites (COM); (7) microlites in low-Fe comendites; (8) augite xenocryst from benmoreitic magma. The arrow shows the compositional trend of clinopyroxene in rocks and MI glasses from the trachytes to comendites and pantellerites.

Table 2. Composition (wt %) of hedenbergite

Component	NR-7		XE1	XE3	NR-23	NR-1		NR-5				NR-16	NR-18		NR-19	NR-20
	(13)	(2)	(1)	(1)	(5)	(2)	(2)	(2)	(1)	(1)	(1)	(1)	(1)	(2)	(1)	(1)
	1	2	3	4	5	6	7	8	9	10	11	12	13	14	15	16
SiO_2	48.58	54.69	48.22	48.01	48.64	49.15	47.95	49.12	49.72	51.73	46.89	48.33	48.71	49.01	49.25	49.33
TiO_2	0.46	3.02	1.12	0.58	0.26	0.32	2.05	0.28	0.33		3.12	0.35	0.32	1.13		
Al_2O_3	0.22	1.21	0.87	0.26	0.21	0.35	0.79	0.25	0.60	0.72	1.36	0.43	0.34	0.55	0.28	
Fe_2O_3	4.51	22.42	1.77	2.46	2.65	0.56	9.34	0.94	0	5.97	4.25	1.78	0.63	0	0.28	0.02
FeO	26.54	5.41	27.87	28.10	28.18	28.56	18.43	29.42	29.14	20.54	19.94	28.31	30.83	29.25	28.53	28.23
MnO	1.29	0.66	1.46	1.46	1.26	1.35	2.36	1.32	1.21	1.32	0.89	1.21	1.28	1.11	1.05	1.11
MgO	0.30		0.80	0.30	0.24	0.77	0.43	0.61	0.90	0.85	8.37	0.48		0.63	1.28	1.33
CaO	16.87	1.33	18.30	19.00	17.65	19.02	14.27	18.43	17.46	14.58	15.77	17.85	17.21	18.14	18.81	19.07
Na_2O	1.85	12.75	0.96	0.75	1.32	0.74	4.19	0.77	0.93	2.11	0.47	0.94	0.94	0.83	0.63	0.61
K_2O							0.18		0.23	0.24	0.24	0.16				
Total	100.63	101.48	101.18	100.68	100.40	100.81	99.80	101.12	100.29	99.82	101.06	99.84	100.26	100.64	100.11	99.70
Wo, %	41.04	6.17	43.15	44.11	42.44	44.46	40.18	42.96	42.11	40.52	34.31	42.64	41.25	43.35	43.69	44.38
En, %	0.87		2.63	0.97	0.31	2.49	0.84	1.96	3.02	3.29	25.34	1.60		2.10	4.14	4.30
Fs, %	58.09	93.83	54.22	54.92	57.25	53.05	58.98	55.08	54.86	56.20	40.35	55.77	58.75	54.56	52.18	51.32

Analyses (1, 5, 8, 12, 16) are phenocrysts and microlites; (2) aegirine-augite in MI; (3) in symplectite of enclave XE2 (Table 3b); (4) phenocryst (Fig. 3d) in enclave XE3; (6, 10, 15) microlites in MI; (7, 9, 13) inclusions in anorthoclase phenocrysts; (11) augite xenocryst from benmoreitic magma; (14) inclusion in ilmenite phenocryst. FeO and Fe_2O_3 are calculated from stoichiometric proportions of the mineral; *Wo*, *En*, *Fs* are the wollastonite, enstatite, ferrosilite end members, respectively; numerals in parentheses show the numbers of analyses.

Table 3. Composition (wt %) of fayalite

Component	NR-7	NR-23			NR-1	NR-18	NR-20	
	(3)	(1)	(1)	(3)	(2)	(1)	(2)	(5)
SiO_2	29.50	29.48	29.35	29.50	30.18	29.65	29.55	30.39
Fe_2O_3	0.26	0	0	0	0	0	0.52	0
FeO	66.70	65.84	65.38	67.59	67.82	66.31	65.79	61.79
MnO	3.46	3.46	3.53	3.54	3.08	3.20	3.06	2.81
MgO					0.41	0.46	0.95	0.79
CaO	0.29	0.24	0.39	0.25	0.25	0.20	0.25	0.24
Total	100.21	99.02	101.18	101.47	101.73	99.80	101.12	96.01
Tp, %	4.97	5.05	5.18	5.03	4.35	4.61	4.36	4.31
Fo, %	0	0	0	0	1.01	1.17	2.37	2.12
Fa, %	95.03	94.95	94.82	94.97	94.64	94.23	93.27	93.56

FeO and Fe_2O_3 are calculated from stoichiometric of the mineral; *Tp*, *Fo*, and *Fa* are the tephroite, forsterite, fayalite end members; numerals in parentheses show the numbers of analyses.

Table 4. Composition (wt %) of ilmenite and titanomagnetite

Component	XE3	NR-23	NR-2	NR-5	NR-16	NR-18		NR-20	
	(2)	(1)	(1)	(1)	(3)	(3)	(1)	(1)	(2)
SiO_2	0.30		0.24	0.26			0.40	0.34	1.58
TiO_2	52.66	50.49	50.43	49.79	50.32	50.32	19.69	51.01	2.52
Al_2O_3							0.33		0.49
Fe_2O_3	2.27	3.78	2.17	4.52	3.14	3.71	28.04	2.21	57.69
FeO	45.46	43.61	44.74	43.23	44.14	43.67	48.17	45.44	33.97
MnO	2.05	1.59	1.59	1.52	1.61	1.56	1.03	1.25	0.61
CaO		0.14		0.64					
Nb_2O_5			0.66	0.47	0.48			0.40	
Total	102.42	99.23	99.83	100.43	99.69	99.25	97.65	100.65	96.85
Ti, %	49.92	49.13	49.23	48.45	49.06	48.98	19.45	49.23	2.59
Fe^{2+}, %	47.93	47.20	48.72	46.91	47.87	47.45	52.90	48.72	38.52
Fe^{3+}, %	2.15	3.67	2.05	4.64	3.07	3.57	27.65	2.05	58.89

FeO and Fe_2O_3 are calculated from stoichiometric of the mineral; XE3 is ilmenite inclusion in hedenbergite from enclave XE3 (Fig. 3d) in pantellerite NR-7; Ti, Fe^{2+}, and Fe^{3+} are component in the crystal chemical formula of ilmenite and titanomagnetite; numerals in parentheses show the numbers of analyses.

in MnO (3.3–3.5 wt %) than in the low-Fe comendite (0.4–1 wt % MgO and 2.8–3.2 wt % MnO).

Fe and Ti Oxides

The comendites and pantellerite NR-7 contain ilmenite in the form of both small single phenocrysts (microlites) and inclusions in hedenbergite and anorthoclase. Titanomagnetite is more typical of the low-Fe comendites, which contain this mineral in the form of microlites and submicrometer-sized grains in the glass. The composition of the mineral is illustrated by data of Table 4. All rocks contain ilmenite whose composition is close to the ilmenite end member and which contains 2–5 wt % of the hematite end member and 1.6–2 wt % MnO. Ilmenite in the low-Fe comendite contains 0.4–0.7 wt % Nb_2O_5. We have also analyzed a few titanomagnetite microlites. The mineral is dominated by varieties containing 50–53% of the ulvospinel end member (Table 4). Small (<2–3 μm) microlites in glass have a composition close to the ideal magnetite formula and contain 2.3–2.7 wt % TiO_2.

Accessory Minerals

Fluorapatite microlite in glass and inclusions in hedenbergite phenocrysts are abundant in comendite NR-23 and pantellerite NR-7 (Figs. 2a, 4d, 4f). Microlites of this mineral were found only in two samples of the low-Fe comendites. Analyses of the fluorapatite and the coefficients in its crystallochemical formula are presented in Table 5. The mineral contains up to 10 wt % REE (La, Ce, Pr, Nd) and 0.5–3 wt % FeO. Fluorapatite in samples NR-23 and NR-7 and in enclave XE3 contains up to 1 wt % SrO.

Chevkinite and zircon were identified in the low-Fe comendites. Chevkinite was found among microlites in the matrix glass and, more commonly, as inclusions in anorthoclase, hedenbergite and fayalite phenocrysts. In all of the samples the composition of the mineral varies insignificantly and can be readily recalculated to the ideal crystallochemical formula (Table 6). The chevkinite contains 2.5–3 wt % CaO, 0.6–1 wt % ThO_2 and sometimes also 0.7–1 wt % Y_2O_3, 0.9 wt % ZrO_2, 0.7–1.1 wt % Nb_2O_5. Judging from literature data (Macdonald and Belkin, 2002; Macdonald et al., 2009), chevkinite from Nemrut is merely insignificantly different from this mineral from other volcanic complexes with comendites and pantellerites.

Zircon microlites were found in the matrix and as inclusions in anorthoclase and ilmenite phenocrysts. The mineral contains 1 wt % HfO_2 and up to 1 wt % FeO.

GEOCHEMISTRY OF THE ROCKS AND THEIR MATRIX GLASSES

The compositions of Nemrut rocks are reported in Table 7 and portrayed in classification diagrams. In the TAS diagram (Fig. 7), in which the boundary line between the rhyolite and trachyte fields is shown according (Sharpenok et al., 2009), the composition point of NR-7 lies within the pantelleritic field. The composition points of the high-Fe comendites plot within the trachyrhyolitic field, and two data points fall into the comenditic field. Most of the pre-caldera rocks containing >63 wt % SiO_2 correspond to trachytes. On the Al_2O_3–FeO_{tot} diagram (Macdonald,

Table 5. Composition (wt %) and crystallochemical formulas of fluorapatite

Component	NR-23	NR-7		XE3	NR-2	NR-12	
	4(1)	2a(1)	14(1)	10a(2)	10a(1)	7(1)	15b(1)
	1	2	3	4	5	6	7
SiO_2	3.12	2.14	1.67	1.98	5.95	6.82	8.43
FeO	0.89	0.48	0.72	0.78		3.05	
CaO	46.58	50.26	50.26	50.71	44.47	41.18	39.88
P_2O_5	36.59	39.48	39.96	39.52	32.33	30.61	29.22
SrO	1.01	1.02	1.05	1.03			
La_2O_3	1.27	0.65	0.81	0.64	1.43	1.83	2.01
Ce_2O_3	3.24	1.73	1.78	1.60	3.51	5.53	6.18
Pr_2O_3	0.71						0.90
Nd_2O_3	1.73	0.68	0.87	0.90	2.13	3.01	3.52
F	4.04	3.97	4.08	3.07	4.30	4.18	4.67
Total	99.18	99.88	101.21	100.21	94.12	96.21	99.16
Si	0.28	0.18	0.14	0.17	0.56	0.65	0.81
Fe^{2+}	0.07	0.03	0.05	0.06		0.24	
Ca	4.47	4.65	4.63	4.72	4.47	4.18	4.09
P	2.78	2.88	2.91	2.9	2.57	2.45	2.37
Sr	0.05	0.05	0.05	0.05			
La	0.04	0.02	0.03	0.02	0.05	0.06	0.07
Ce	0.11	0.05	0.06	0.05	0.12	0.19	0.22
Pr	0.02	0	0	0	0	0	0.03
Nd	0.06	0.02	0.03	0.03	0.07	0.1	0.12
F	1.14	1.08	1.11	0.84	1.28	1.25	1.41

(2, 3, 7) are phenocrysts and microlites in matrix glass, inclusions in phenocrysts: (5) anorthoclase, (6) fayalite; (1) hedenbergite, (4) in hedenbergite from enclave XE3 (Fig. 3d); the crystallochemical formulas of fluorapatite based on13 oxygens; numerals in parentheses show the numbers of analyses.

1974) for alkaline rocks enriched in SiO_2, the composition points of rocks plot within the field of comenditic trachytes (Fig. 8). In this diagram, the composition points of the rocks with >70 wt % SiO_2 define a linear trend between the low-Fe comendites and pantellerite NR-7. The agpaitic coefficient (NK/A) of the rocks is greater than one. Their concentrations of alkalis and iron increase from the comendites to pantellerites (Table 7).

The devitrification and recrystallization of the matrix glass of alkaline volcanic rocks can result in significant Na and K losses, even if the rocks are vitreous varieties or obsidian. The composition points of the insignificantly altered rocks lie within the field of a linear trend (Fig. 9) in the NK/A–FK/A [$(K_2O + FeO_{tot})/Al_2O_3$, mole ratio] diagram (White et al., 2003). Judging from this diagram, all comendite samples and pantellerite NR-7 have not lost alkalis.

The rocks were analyzed for trace elements by ICP-MS. The compositions of Nemrut rocks normalized to the primitive mantle are shown in multielemental plots in Fig. 10. The geochemical characteristics of the trachybasalts are intermediate between OIB and E-MORB model types. An unusual feature of the rocks is their low Ba concentrations (70–83 ppm). As was demonstrated in (Peretyazhko et al., 2015), fractional crystallization of trachybasaltic melt and its mixing with trachydacitic or low-Fe comenditic magmas predetermined the geochemical specifics of the mugearites, trachydacites, and pre- and post-caldera benmoreites.

Pantellerite NR-7 and the high-Fe comendites (NR-23 and NR-26) exhibit the deepest negative Ba, Sr, P, and Ti anomalies, the highest concentrations of Cs, Rb, Th, U, Nb, Ta, REE, Y, Pb, Zr, Hf (Fig. 10). The comendites and pantellerites are richer than other Nemrut rocks in Li (70–108 ppm), Be (9–11 ppm), Ga (28–32 ppm), Mo (6–11 ppm), Sn (12–14 ppm), W (5–6 ppm) but are poorer in Sc, V, Cr, Co, Ni, Cu (Table 7). The low-Fe comendites and pre-caldera comenditic trachytes contain lower concentrations of Cs, Rb, Th, U, Nb, Ta, REE, Y, Pb, Zr, Hf, and their negative Ba, Sr, P, Ti anomalies in multielemental diagrams are shallower (Fig. 10). It is worth mentioning that negative Y anomalies, which are merely insignificantly pronounced in the trachybasalts, are enhanced

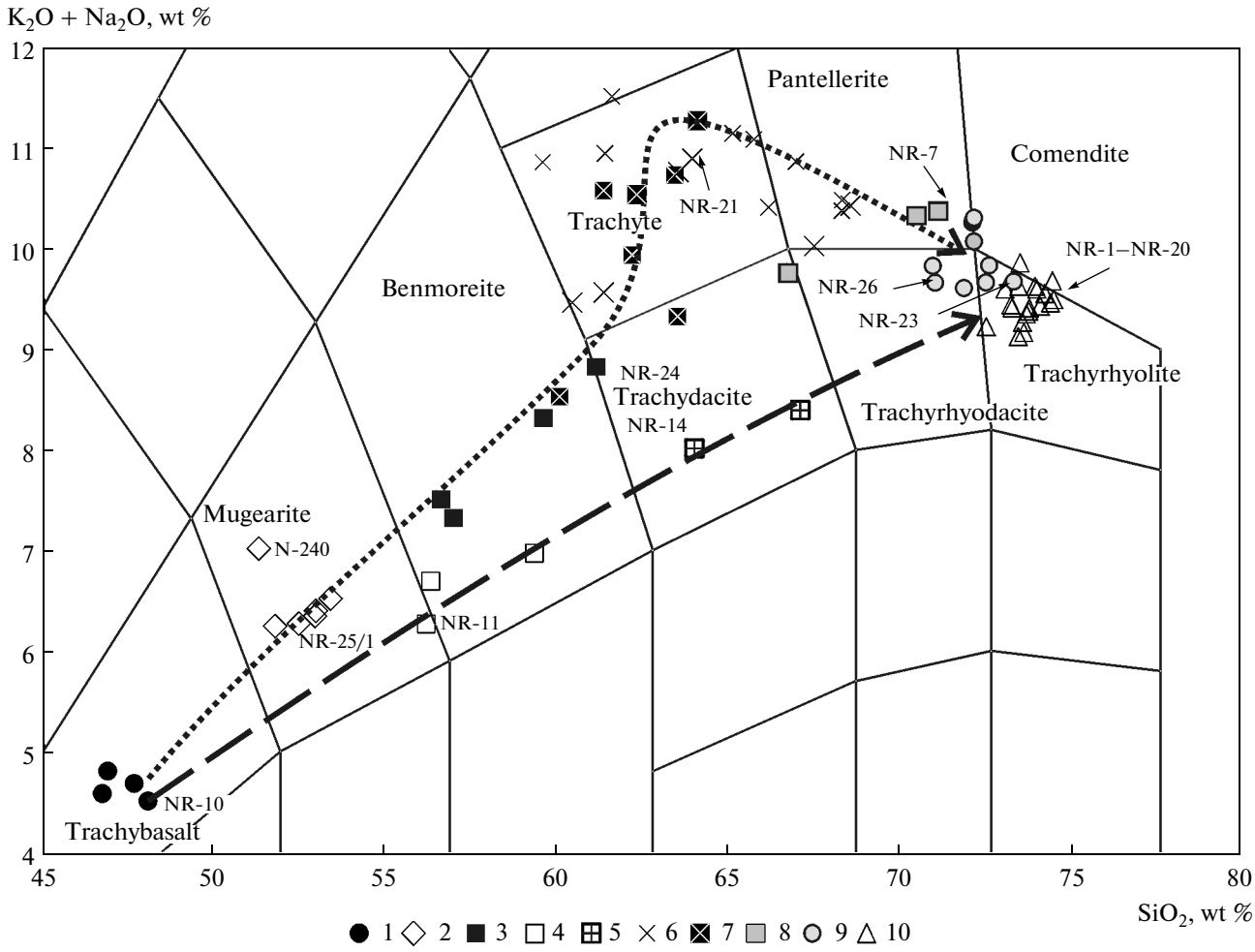

Fig. 7. TAS diagram showing the fields of rhyolite, dacite, trachydacite, and trachyte (Sharpenok et al., 2009) and composition points of rocks from Nemrut volcano. (1) Trachybasalt; (2) mugearite; (3) pre-caldera benmoreite; (4) post-caldera benmoreite; (5) hybrid rocks of composition intermediate between benmoreite and low-Fe comendite; (6) trachyte and comenditic trachyte; (7) pumice and trachyte ignimbrite; (8) pantellerite; (9) pre-caldera high-Fe comendite; (10) pre-caldera and "rift"-zone low-Fe comendite. The dashed line shows the compositional evolution of the pre-caldera rocks, and the heavy dashed line corresponds to the composition of the hybrid rocks produced by mixing trachybasaltic magma with low-Fe comenditic melt (Peretyazhko et al., 2015).

in the mugearites, trachytes, comenditic trachytes, and low-Fe comendites. The highest F concentrations are typical of trachyte NR-21 (800 ppm) and pantellerite NR-7 (750 ppm), and these concentrations in the comendites are lower: 440–670 ppm (Table 7).

Composition of Matrix Glasses

The average composition of the matrix glasses recalculated to anhydrous basis are reported in Table 8 and represented in Fig. 11. The most alkaline and Fe-richest (6.3–7.1 wt % FeO) glass whose NK/A = 1.48–1.60 was found in pantellerite NR-7. In the TAS diagram, the composition points plot near the boundary line between the pantelleritic and comenditic fields (Fig. 11a). High-Fe comendite NR-23 contains less alkaline glass (NK/A = 1.25–1.34), whose FeO concentration is 4–4.5 wt % (Fig. 11c). The composition points of glass in this sample lie in the comenditic field. Glasses from the low-Fe comendites have the lowest NK/A = 1.04–1.11 and the lowest FeO concentration of 1.8–2.1 wt %. Most composition points of the glasses define a linear trend from the low-Fe comendites to pantellerite NR-7 (Figs. 11a, 11c). The interstitial (residual) glass of enclave XE3 (Table 8) in comenditic trachyte of sample NR-7 has a pantelleritic composition but is different from the matrix glass of the rocks in bearing higher Al_2O_3 concentrations and lower concentrations of alkalis (Fig. 11) at an agpaitic coefficient NK/A = 1.14.

Similar to the rocks, their matrix glasses are richer in Na than K (Tables 7, 8). Only the glasses of samples NR-8 and NR-20, in which numerous devitrification domains were found (Figs. 4g–4i), are more potassic than the bulk-rock composition (Table 8). This is

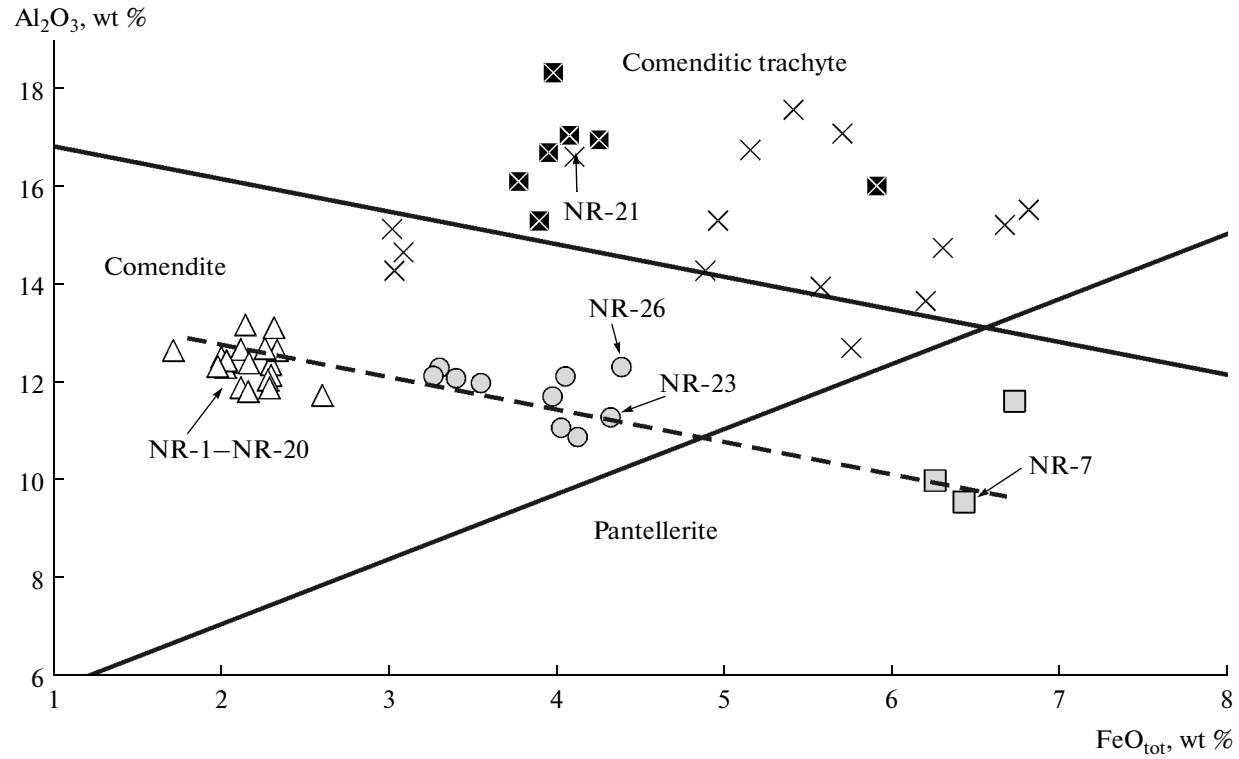

Fig. 8. Classification diagram (Macdonald, 1974) for Nemrut rocks containing more than 63 wt % SiO_2. Data from Table 7 and (Çubukçu et al., 2012; Peretyazhko et al., 2015). The dashed line shows the compositional trend of rocks between the low-Fe comendites and pantellerites. See Fig. 7 for symbol explanations.

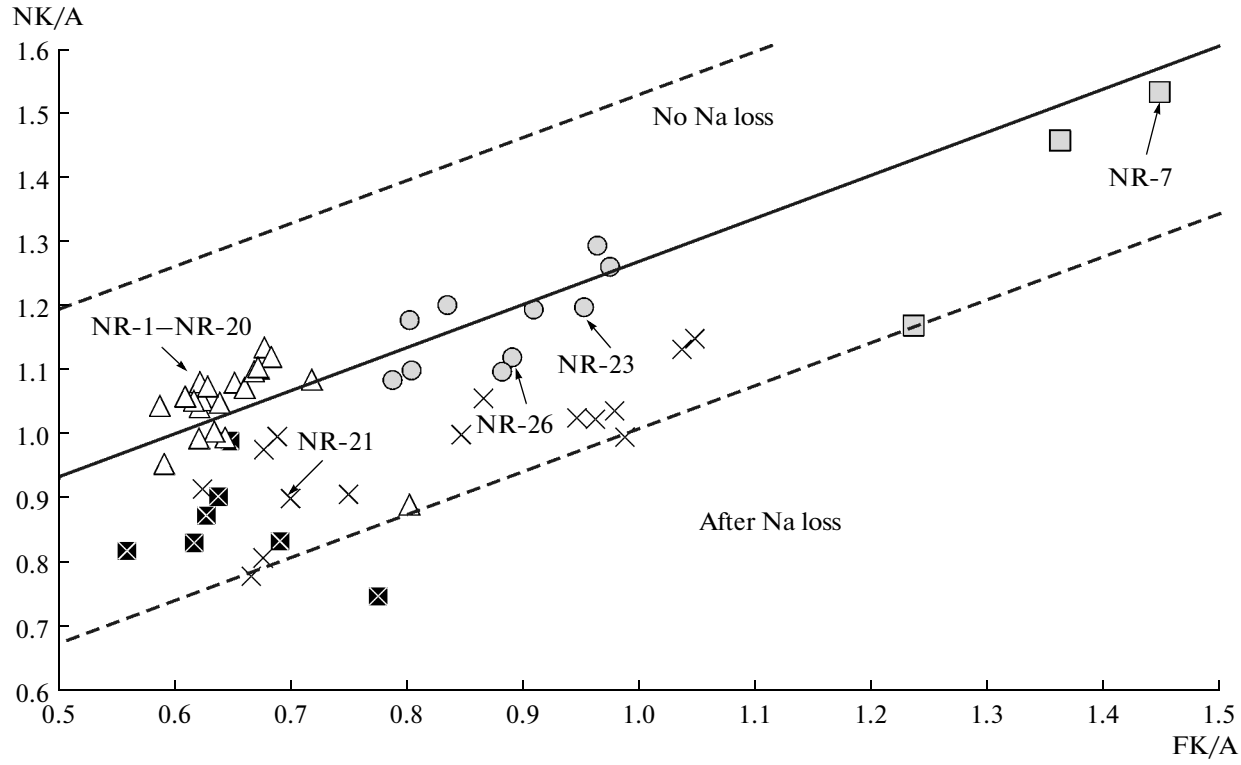

Fig. 9. Relations between the agpaitic coefficient NK/A and FK/A ratio in Nemrut rocks. Rock fields are presented according to (White et al., 2003). FK/A = $(K_2O + FeO_{tot})/Al_2O_3$, mol %. See Fig. 7 for symbol explanations.

Table 6. Composition (wt %) and crystallochemical formulas of chevkinite

Component	NR-2	NR-5	NR-16	NR-18	NR-20	NR-12			NR-14	
	10a(1)	7b(1)	5-6b(3)	3a(1)	7a(1)	5(2)	5(1)	15b(4)	2-2(1)	11(1)
	1	2	3	4	5	6	7	8	9	10
SiO_2	19.10	19.49	19.55	20.24	19.62	19.55	19.34	19.75	18.89	21.14
Al_2O_3						0.15	0.25		0.30	0.81
TiO_2	18.88	18.15	18.56	18.98	18.87	19.08	18.50	18.51	18.37	18.47
Fe_2O_3	3.21	5.68	2.35	1.94	2.75	1.76	2.76	2.47	3.69	5.30
FeO	8.08	7.14	8.64	9.29	8.55	9.16	9.00	8.70	8.62	8.82
CaO	2.97	3.67	2.82	2.50	3.05	2.98	2.60	2.75	2.49	2.90
La_2O_3	11.42	10.05	10.75	11.89	11.08	11.65	11.18	11.64	11.38	10.59
Ce_2O_3	21.90	21.48	21.97	22.69	21.87	22.28	22.11	22.23	22.21	20.95
Pr_2O_3	1.84	2.39	2.07	2.55	1.52	1.86	1.88	1.86	1.51	1.97
Nd_2O_3	6.86	7.17	6.87	6.95	6.30	6.97	6.82	6.67	6.84	7.24
Sm_2O_3				0.88			1.23			
Y_2O_3		1.02				0.71	0.79		0.55	
ThO_2	0.75	0.58	0.68	0.73	1.07	0.83	0.85	0.81	0.73	0.53
ZrO_2		0.88				0.89				
Nb_2O_5		0.82				0.70	1.14		0.90	0.70
Total	95.01	98.52	94.26	98.64	94.69	98.57	98.45	95.40	96.48	99.42
La	0.90	0.76	0.85	0.91	0.86	0.88	0.85	0.91	0.88	0.77
Ce	1.70	1.60	1.72	1.71	1.69	1.68	1.68	1.72	1.71	1.52
Pr	0.14	0.18	0.16	0.19	0.12	0.14	0.14	0.14	0.12	0.14
Nd	0.52	0.52	0.52	0.51	0.48	0.51	0.50	0.50	0.51	0.51
Sm				0.06			0.09			
Y		0.11				0.08	0.09		0.06	
Th	0.04	0.03	0.03	0.03	0.05	0.04	0.04	0.04	0.03	0.02
Ca	0.68	0.80	0.65	0.55	0.69	0.66	0.58	0.62	0.56	0.61
A	3.97	4.00	3.93	3.97	3.89	3.99	3.97	3.94	3.87	3.58
B(Fe^{2+})	1.00	1.00	1.00	1.00	1.00	1.00	1.00	1.00	1.00	1.00
Fe^{2+}	0.44	0.22	0.54	0.60	0.51	0.58	0.56	0.54	0.51	0.46
Fe^{3+}	0.51	0.87	0.38	0.30	0.44	0.27	0.43	0.39	0.58	0.79
Ti	1.02	0.78	0.98	0.95	1.00	0.95	0.88	0.95	0.90	0.75
Al						0.04	0.06		0.07	0.19
Zr		0.09				0.09				
Nb^{5+}		0.08				0.07	0.11		0.09	0.06
C	1.97	2.03	1.90	1.85	1.95	1.99	2.03	1.88	2.16	2.24
D (Ti)	2.00	2.00	2.00	2.00	2.00	2.00	2.00	2.00	2.00	2.00
Si	4.06	3.97	4.17	4.18	4.15	4.02	4.00	4.18	3.97	4.18

Chevkinite in phenocrysts of the following minerals: (1, 4) anorthoclase, (2) hedenbergite, (10) fayalite. All other analyses are microlites in matrix glass. The crystallochemical formulas based to 22 oxygens and 13 cations. FeO and Fe_2O_3 are according to the ideal stoichiometry; A, B, C, D are the totals of crystallochemical coefficients on structural sites; numerals in parentheses show the numbers of analyses.

Table 7. Compositions of rocks Nemrut volcano

Component	NR-21	NR-7	NR-26	NR-23	NR-1	NR-2	NR-3	NR-5	NR-6	NR-8	NR-9	NR-16	NR-18	NR-19	NR-20	NR-12
SiO_2	64.17	71.38	71.37	72.84	73.81	74.12	72.85	74.35	74.29	74.85	74.75	73.96	73.92	73.80	73.58	74.11
TiO_2	0.38	0.40	0.30	0.25	0.14	0.13	0.15	0.15	0.14	0.13	0.13	0.14	0.14	0.14	0.13	0.25
Al_2O_3	16.61	9.56	12.32	11.29	12.37	12.15	11.74	12.05	11.89	11.90	11.82	12.66	12.70	13.18	13.12	11.27
Fe_2O_3	2.74	2.60	2.17	1.38	0.80	0.80	1.14	0.94	0.79	0.96	0.81	0.37	0.84	0.88	0.58	1.57
FeO	1.65	4.09	2.44	3.09	1.58	1.58	1.58	1.44	1.58	1.26	1.44	2.01	1.51	1.36	1.80	1.36
MnO	0.09	0.17	0.11	0.10	0.05	0.05	0.06	0.05	0.05	0.05	0.05	0.05	0.05	0.05	0.05	0.06
MgO	0.37	0.05	0.10	0.06	0.06	0.05	0.09	0.05	0.05	0.05	0.05	0.05	0.05	0.05	0.06	0.28
CaO	1.34	0.46	0.59	0.36	0.47	0.43	1.02	0.41	0.39	0.41	0.42	0.39	0.38	0.52	0.45	0.71
Na_2O	5.55	6.04	5.39	5.41	5.20	5.02	4.86	5.11	5.13	4.93	4.97	4.71	4.80	4.75	4.96	5.12
K_2O	5.35	4.35	4.28	4.26	4.43	4.39	4.37	4.49	4.50	4.56	4.49	4.46	4.47	4.38	4.48	4.35
P_2O_5	0.10	0.04	0.07	0.03	0.05	0.04	0.02	0.02	0.03	0.03	0.02	0.03	0.03	0.04	0.04	0.03
L.O.I.	1.58	0.65	0.91	0.95	1.02	1.21	1.32	0.91	1.06	0.75	0.93	1.08	1.09	0.89	0.79	0.70
Total	99.91	99.80	100.04	100.02	99.98	99.98	99.21	99.97	99.91	99.88	99.87	99.91	99.97	100.03	100.05	99.81
NK/A	0.90	1.53	1.10	1.20	1.08	1.07	1.08	1.10	1.12	1.10	1.10	0.99	1.00	0.95	0.99	1.17
F	800	750	670	660	560	590	660	550	530	580	550	610	600	480	610	440
Li	29.8	108	85.8	93.1	71.4	73.4	71.2	74.1	74.3	70.0	77.8	74.1	82.9	72.7	69.8	74.8
Rb	222	279	268	285	236	243	237	239	241	239	241	247	271	243	237	238
Cs	5.6	10.7	9.5	10.1	8.9	9.3	8.9	9.1	9.2	9.2	9.7	9.3	10.3	9.2	8.8	9.3
Ba	339	9.9	65.3	1.54	18.1	12.5	12.4	17.9	19.7	30.9	31.5	11.7	12.2	31.5	31.6	13.8
Sr	69.40	1.63	13.30	0.50	2.6	1.0	2.2	3.4	3.3	2.0	2.0	1.5	1.1	2.0	2.4	16.9
Zr	948	1782	1694	1836	736	754	721	746	747	669	663	754	832	677	649	827
Hf	16.8	36.5	34.4	37.1	19.1	19.4	18.6	19.0	19.0	17.3	17.4	19.4	21.5	17.8	17.1	21.0
Ta	3.50	5.90	5.79	6.2	4.9	5.0	4.8	4.9	4.9	4.8	4.8	5.1	5.6	4.9	4.7	5.0
Nb	46.3	77.5	73.8	80.2	60.8	63.1	60.6	62.4	63.0	59.7	58.6	63.1	69.6	59.9	57.1	64.0
Be	6.0	10.4	9.8	10.5	9.0	9.4	9.1	9.3	9.2	9.1	9.0	9.6	10.1	9.1	8.9	9. 5
Sc	3.99	1.34	1.47	0.97	1.09	1.03	1.12	1.12	1.10	1.33	1.28	1.07	1.15	1.35	1.30	2.1
V	0.54	0.29	2.13	0.23	0.40	0.21	1.05	0.52	0.49	0.24	0.26	0.38	0.20	0.21	0.33	11.4
Cr	2.65	3.02	4.72	2.95	1.54	1.95	1.58	2.22	2.54	5.99	2.48	1.82	8.06	4.47	5.08	5.4
Co	1.33	0.27	0.59	0.21	0.33	0.29	0.39	0.27	0.27	0.29	0.36	0.35	0.24	0.26	0.46	2.12
Ni	1.64	1.85	2.37	1.30	1.11	10.69	1.20	1.69	1.95	1.33	1.13	1.14	1.85	1.55	3.70	2.77
Cu	5.60	5.89	6.13	5.4	4.20	3.51	5.11	4.71	5.70	3.90	4.18	4.00	6.04	4.01	5.55	5.6

Table 7. (Contd.)

Component	NR-21	NR-7	NR-26	NR-23	NR-1	NR-2	NR-3	NR-5	NR-6	NR-8	NR-9	NR-16	NR-18	NR-19	NR-20	NR-12
Zn	104	230	189	196	117	118	116	119	120	111	110	118	134	111	106	125
Ga	25.0	31.9	32.1	32.4	28.30	28.50	27.47	29.09	28.28	29.16	28.45	28.72	31.75	28.63	28.03	28.8
Ge	1.67	2.92	2.64	2.65	2.07	2.23	2.21	2.33	2.25	2.22	2.27	2.33	2.55	2.27	2.21	2.28
Mo	4.7	10.7	11.0	10.9	5.7	6.2	5.9	6.4	6.8	8.5	7.2	5.8	7.7	7.8	7.6	8.2
Sn	7.4	14.2	13.0	13.9	12.7	13.1	12.9	12.7	13.3	12.7	12.7	13.0	14.6	12.8	12.5	13.1
Sb	0.87	1.44	1.23	1.33	1.54	1.63	1.55	1.60	1.59	1.64	1.62	1.64	1.78	1.68	1.74	1.56
W	1.9	5.7	5.8	6.3	5.2	5.4	5.2	5.5	5.3	5.5	5.4	5.4	6.1	5.4	5.3	5.4
Pb	24.4	34.8	32.3	33.8	25.9	27.4	26.0	26.1	26.6	25.8	25.7	30.3	30.3	26.1	25.7	26.1
Th	20.3	30.3	31.4	33.6	26.3	26.7	26.1	26.2	26.3	25.7	26.0	26.8	29.5	26.5	25.9	26.2
U	6.7	10.1	10.1	10.9	9.0	9.2	9.1	9.1	9.2	8.9	9.0	9.3	10.2	9.1	8.8	8.9
Tl	0.74	1.09	1.07	1.16	0.94	1.01	0.95	0.98	0.99	0.95	0.98	1.54	1.12	0.97	0.96	0.93
Bi	0.06	0.70	0.35	0.48	0.41	0.53	0.42	0.84	0.47	0.39	0.41	0.83	0.51	0.44	0.47	0.33
Y	42.8	163	144	153	91.7	93.8	90.6	91.9	93.0	88.7	89.8	93.6	105	89.2	84.4	91.7
La	62.0	128	126	134	73.2	74.8	70.4	71.4	75.3	71.5	71.2	73.4	82.5	75.0	71.3	71.5
Ce	143	275	266	281	174	177	167	171	179	171	170	175	199	179	169	174
Pr	14.5	29.2	27.2	28.8	18.2	18.2	17.2	17.7	18.3	17.5	17.5	18.1	20.3	18.1	17.2	18.2
Nd	54.8	120	109	114	70.0	71.2	67.1	69.0	70.9	67.9	67.3	70.6	79.0	70.1	66.8	71.3
Sm	10.3	26.0	22.7	23.8	15.1	15.3	14.7	14.9	15.2	14.6	14.5	15.4	17.0	14.8	14.2	15.5
Eu	1.22	1.66	1.09	0.90	0.33	0.32	0.31	0.34	0.35	0.37	0.37	0.32	0.35	0.39	0.36	0.39
Gd	9.9	27.7	24.3	25.6	16.5	16.7	16.2	16.3	17.0	15.9	15.8	16.9	18.6	16.5	15.6	17.0
Tb	1.46	4.35	3.75	3.99	2.73	2.82	2.73	2.73	2.83	2.64	2.63	2.84	3.10	2.71	2.62	2.82
Dy	9.3	28.0	24.6	26.2	18.5	18.9	18.3	18.6	18.8	17.9	18.0	19.2	21.1	18.3	17.5	19.2
Ho	1.90	5.9	5.2	5.5	3.9	4.0	3.9	4.0	4.0	3.8	3.8	4.0	4.5	3.9	3.7	4.1
Er	5.6	17.1	15.2	16.2	11.7	12.1	11.7	11.8	11.9	11.5	11.5	12.3	13.4	11.6	11.2	12.3
Tm	0.85	2.52	2.25	2.38	1.73	1.82	1.76	1.77	1.77	1.73	1.73	1.85	1.99	1.76	1.68	1.84
Yb	5.9	17.1	15.3	16.3	11.9	12.3	11.9	11.9	12.0	11.5	11.6	12.4	13.5	11.9	11.4	12.5
Lu	0.92	2.56	2.30	2.48	1.75	1.81	1.75	1.76	1.76	1.71	1.70	1.82	1.97	1.74	1.67	1.83

Pre-caldera rocks: NR-21—trachyte; NR-7—pantellerite; NR-23, NR-26—high-Fe comendite. Post-caldera rocks: NR-1, NR-2, NR-3, NR-5, NR-6, NR-8, NR-9, NR-16, NR-18, NR-19, and NR-20—low-Fe comendites in caldera; NR-12—low-Fe comendite in "rift" zone.

See Fig. 1 for sampling sites. The coordinates of the sampling sites are as follows: NR-21: 38°33.989′ N, 42°13.08′ E; NR-7: 38°37.679′ N, 42°16.094′ E; NR-26: 38°34.137′ N, 42°10.628′ E; NR-23: 38°34.378′ N, 42°15.996′ E; NR-1: 38°37.810′ N, 42°16.510′ E; NR-2: 38°37.609′ N, 42°15.739′ E; NR-3: 38°38.128′ N, 42°15.054′ E; NR-5, NR-6: 38°38.582′ N, 42°14.932′ E; NR-8, NR-9: 38°37.347′ N, 42°15.713′ E; NR-16: 38°36.213′ N, 42°15.885′ E; NR-18: 38°36.258′ N, 42°15.648′ E; NR-19: 38°36.716′ N, 42°14.170′ E; NR-20: 38°36.730′ N, 42°14.701′ E; NR-12: 38°40.509′ N, 42°13.693′ E.

Analytical methods: major elements (wt %)—XRF, F (ppm)—atomic emission analysis (powder blow-in), and other elements (ppm)—ICP-MS (with preparatory acid decomposition). FeO was analyzed by titration. LOI is the loss on ignition, calculated with regard for Fe distribution between FeO and Fe_2O_3; agpaitic index NK/A = $(Na_2O + K_2O)/Al_2O_3$, mol %.

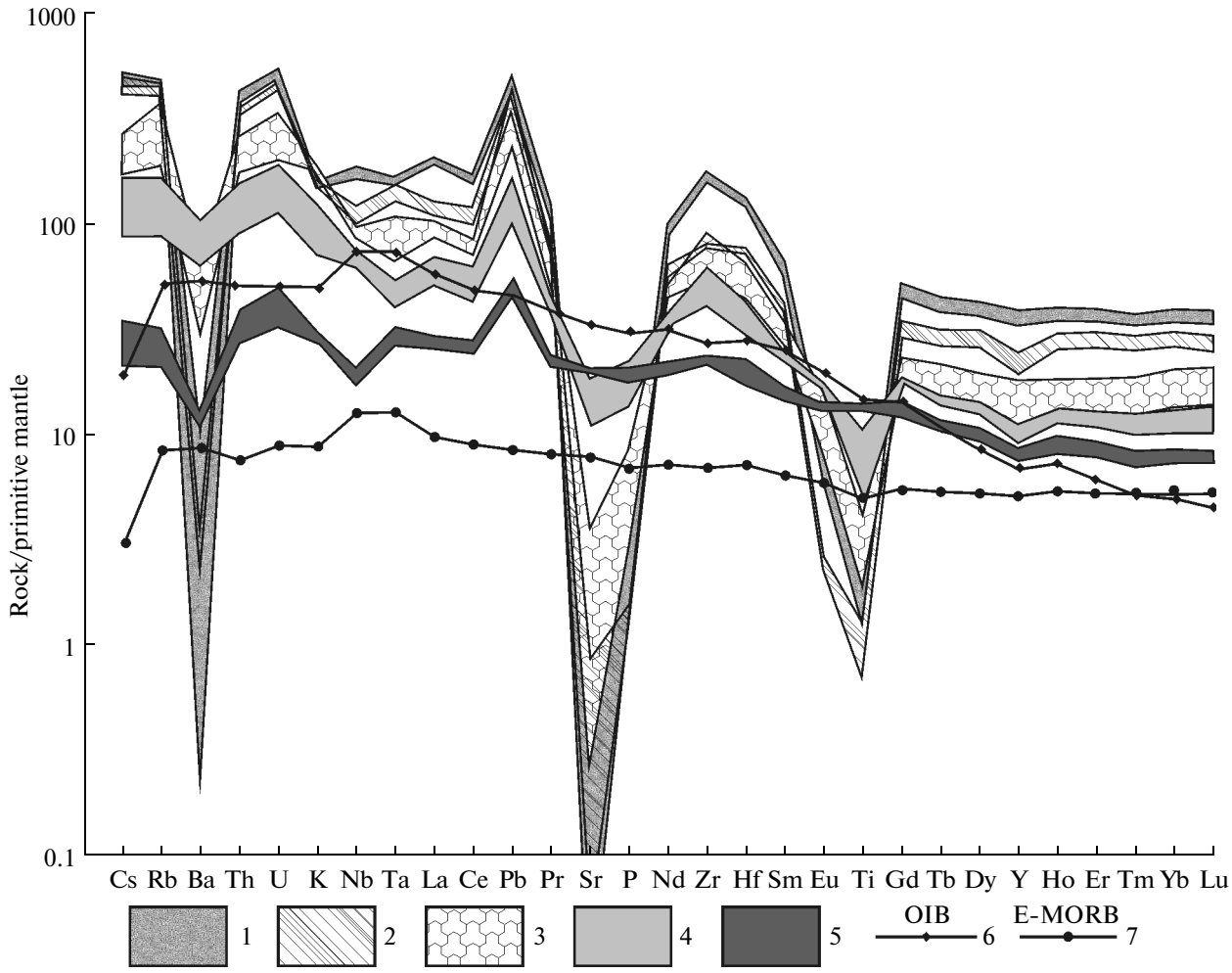

Fig. 10. Primitive mantle-normalized (McDonough and Sun, 1995) multielemental pattern of Nemrut rocks. Based on data on rock composition in Table 7 and in (Peretyazhko et al., 2015; Çubukçu et al., 2012). (1) Pantellerite NR-7, high-Fe comendite NR-23 and NR-26; (2) low-Fe comendites in the caldera and "rift" zone; (3) trachytes and comenditic trachyte NR-21; (4) mugearites; (5) trachybasalts in the "rift" zone; (6, 7) OIB and E-MORB basalts.

likely explained by the diffusion-driven redistribution of alkalis (without their significant losses, judging by the composition of the rocks) between the glass and devitrification domains, in which Na dominates over K. Such phenomena are typical of processes of alteration acid volcanic glasses (Ewart, 1981). The analytical totals of the oxides are no more than 3 wt % lower than 100%, which is likely accounted for by H_2O contents in the glasses (Fig. 12a). These values for the post-caldera low-Fe comendites are usually lower than 2 wt %.

LA-ICP-MS Analyses and Distribution Coefficients of Elements between Phases and Glasses

We made use of LA-ICP-MS analysis to determine concentrations of trace elements in the glasses and anorthoclase, hedenbergite, fayalite phenocrysts in pantellerite NR-7, high-Fe comendite NR-23, low-Fe comendites NR-1 and NR-5. The matrix glasses were analyzed at four to six spots near phenocrysts, and these data were later used to calculate the average concentrations of elements. Anorthoclase was analyzed at two to five spots in a number of phenocrysts in all of the samples. We have also analyzed one fayalite and one hedenbergite phenocrysts in each of the samples. The results of the analyses (Table 9) were used to calculate the distribution coefficients between the phenocrysts and matrix glasses of the rocks (Table 10). The coefficients were then used in mass balance calculations, which are discussed below. The trace-element composition of the glasses and phenocryst minerals is shown in multielemental diagrams (Fig. 13) and REE patterns (Fig. 14). The anorthoclase contains practically no admixtures, except Ba and Sr, in all of the samples. The fayalite, hedenbergite and glasses have negative Eu anomalies. The fayalite is enriched in HREE, but their concentrations are much lower than in the matrix glasses. Only the hedenbergite is richer in

Table 8. Composition (wt %) of rocks and matrix glasses

Component	NR-7	G(58)	XE1	XE2	XE3	G(3)	NR-23	G(21)	NR-1	G(11)	NR-2	G(12)
SiO_2	72.18	72.12	74.51	69.91	69.87	72.50	73.63	74.43	74.65	76.38	75.11	76.70
TiO_2	0.40	0.40	0.22	0.44	0.33	0.7	0.26	0.25	0.14	0.03	0.14	0.02
Al_2O_3	9.67	9.72	10.60	13.85	14.19	10.88	11.41	10.77	12.51	11.99	12.31	11.84
FeO*	6.51	6.45	4.22	4.66	4.13	6.09	4.37	4.20	2.33	1.92	2.33	1.90
MnO	0.17	0.23				0.17	0.11		0.05	0.00	0.05	0.00
MgO	0.05					0	0.06		0.06	0.00	0.05	0.00
CaO	0.47	0.32	0.30	0.82	0.76	0.58	0.36	0.22	0.47	0.21	0.44	0.21
Na_2O	6.11	6.29	5.47	6.47	6.90	4.54	5.47	5.53	5.26	4.97	5.09	4.83
K_2O	4.40	4.36	4.57	3.84	3.81	4.55	4.30	4.50	4.48	4.44	4.45	4.44
P_2O_5	0.04						0.03	0.00	0.05	0.00	0.04	0.00
Cl		0.15	0.14					0.13		0.09		0.09
Total	98.89	99.92	94.83	101.84	97.41	98.16	98.93	98.90	98.88	100.09	98.69	99.74
NK/A	1.53	1.55	1.32	1.07	1.09	1.14	1.20	1.30	1.08	1.08	1.07	1.08
Na/K	1.39	1.44	1.20	1.68	1.81	0.99	1.27	1.23	1.17	1.12	1.14	1.09
Component	NR-5	G(10)	NR-8	G(17)	NR-16	G(13)	NR-18	G(15)	NR-19	G(9)	NR-20	G(25)
SiO_2	75.13	76.43	75.58	75.68	74.87	76.86	74.82	76.84	74.50	75.79	74.17	75.97
TiO_2	0.15	0.06	0.13	0.00	0.14	0.17	0.14	0.00	0.14	0.00	0.14	0.00
Al_2O_3	12.18	11.98	12.02	12.31	12.81	11.75	12.85	11.84	13.31	12.45	13.23	12.38
FeO	2.31	1.85	2.14	1.85	2.37	1.83	2.30	1.80	2.17	1.79	2.34	1.65
MnO	0.05	0.00	0.05	0.00	0.05	0.00	0.05	0.00	0.05	0.00	0.05	0.00
MgO	0.05	0.00	0.05	0.00	0.05	0.00	0.05	0.00	0.05	0.00	0.06	0.00
CaO	0.41	0.22	0.41	0.24	0.40	0.06	0.38	0.17	0.53	0.27	0.46	0.14
Na_2O	5.16	5.02	4.98	4.32	4.77	4.73	4.86	4.83	4.80	5.10	5.00	4.32
K_2O	4.54	4.38	4.61	5.61	4.51	4.52	4.52	4.43	4.42	4.52	4.52	5.54
P_2O_5	0.02	0.00	0.03	0.00	0.03	0.00	0.03	0.00	0.04	0.00	0.04	0.00
Cl		0.09		0.00		0.10		0.12		0.11		
Total	98.97	102.28	99.03	98.70	98.79	99.35	98.80	98.67	99.05	101.34	99.21	99.02
NK/A	1.10	1.08	1.10	1.07	0.99	1.08	1.00	1.08	0.95	1.07	0.99	1.06
Na/K	1.14	1.15	1.08	0.77	1.06	1.04	1.07	1.09	1.09	1.13	1.11	0.78

G—matrix glass (numerals in parentheses show the number of analyses); XE1, XE2, XE3 are enclaves (Fig. 3) in pantellerite NR-7. Concentrations of oxides in glasses and rocks are normalized to 100 wt %. Totals are the unnormalized totals of major oxides; FeO* is total Fe; NK/A is the agpaitic index, Na/K is the Na_2O/K_2O ratio.

REE and trace elements than the rocks and matrix glasses and typically has convex REE patterns from La to Sm and concave patterns from Gd to Lu (Fig. 14). Note that the configuration of the normalized REE patterns of the fayalite and hedenbergite is analogous to those of these minerals in comendites from the Olkaria Complex (Marshall et al., 2009). The glasses are richer than rocks in Cs, Th, U, Ta, REE, Y, Pb, and Hf and poorer in Rb, Nb, and Zr. The glasses have deeper negative Y anomalies (Fig. 13). The glasses of pantellerite NR-7 and high-Fe comendite NR-23 are the richest in Li (90–109 ppm) and B (84–86 ppm).

MELT INCLUSIONS

Phenocrysts of various minerals often contain MI (Fig. 15), and no fluid inclusions have been found so far in any of these phenocrysts. MI are the most abun-

dant in anorthoclase and fayalite. MI in the anorthoclase are relatively large (20–70 μm), equant or elongate. These inclusions are filled with primary quenched glass with a single or a number of shrinkage bubbles (Figs. 2f, 15a). MI sometimes contain feldspar, clinopyroxene and titanomagnetite microlites (Figs. 15b, 15c). Anorthoclase phenocrysts from pantellerite NR-7 typically contain variably recrystallized MI bearing feldspar–quartz symplectite with phenocrysts of aegirine-augite and Fe–Ti oxides (Fig. 2d). Several MI in the anorthoclase are cut by cracks, which precludes thermometric study of these inclusions. It is impossible to monitor the glass of MI at high temperatures in transparent yellow fayalite crystals because of iron oxidation and blackening of the host mineral (we have not conducted experiments in an atmosphere of an inert gas). We have examined the thermometric characteristics of a number of MI in anorthoclase without discernible crosscutting cracks. Bubbles in these MI became round at heating to temperatures of 400–500°C. Further heating to 750–800°C resulted in insignificant shrinkage of the bubbles. Homogenization was detected only in small (no larger than 10 μm) MI at 950–1000°C. Large MI reserved their bubbles even upon heating to 1100–1200°C and holding at these temperatures for 7–9 h. Some MI increased their volume for 20–30 vol % during the experiments because of the dissolution of the wall of the host crystal (anorthoclase). Rapid dissolution of the anorthoclase occurred in the course of early heating to 500–700°C for 2–3 h, and the further temperature increase to 800–1000°C and long exposures (7–9 h) was associated with progressively slower dissolution.

We have analyzed glasses and crystalline phases of several exposed MI, which were studied mostly in anorthoclase phenocrysts. The glasses of MI contained daughter phases (microlites) of sanidine that was much richer in K than the host anorthoclase (Fig. 5b). In contrast to hedenbergite phenocrysts in the matrix of the rocks, clinopyroxene microlites in the glasses of MI are aegirine-augite in composition (Fig. 6c), and the titanomagnetite is richer than in the rocks and contains 5–10 wt % TiO_2. The recrystallization products of the glasses of certain MI in anorthoclase, hedenbergite and fayalite contain quartz grains.

The composition of the primary quenched glasses of MI are shown in Fig. 11. The compositions were recalculated to anhydrous basis (normalized to 100 wt %). In all instances, the quality of analyses of the glasses was controlled using the composition of the host anorthoclase, whose analytical total should have been close to 100 wt %. We have analyzed glasses in more than fifty MI in anorthoclase phenocrysts from the low-Fe comendite. The glasses can be classified into two groups. The glasses of one of them have proportions of elements close to those in the matrix glass (Fig. 11). Such MI are usually hosted in the margins of phenocrysts, which likely entrapped portions of the melt from which the phenocrysts grew before the eruptions. The glasses of the second group are richer in silica and contain up 85–87 wt % SiO_2, less alkalis ($Na_2O + K_2O$) and Al_2O_3, and more FeO (Fig. 11). These MI are hosted in the central portions of phenocrysts and their intermediate zones (i.e., are older). Note that the phenocrysts do not show any significant compositional variations from their cores to peripheries. Obviously, anorthoclase crystallized on the walls of these MI (which are older than MI of the first group) from the entrapped melt. This has significantly modified the composition of the residual melt in MI and resulted in an increase in its alkalinity (NK/A increases from 1.1 to 1.7, and some of the Fe richest compositions plot within the pantelleritic field, Fig. 11c). Thereby the analytical totals show the greatest dispersion and most significantly ingdeviate from 100 wt % (by as much as 8–9 wt %) likely because of variations in the water content of the glasses (Fig. 12a). With rare exceptions, the deficit of the analytical totals increases with increasing silicity of the glasses. This is also a consequence of the crystallization of anhydrous anorthoclase on the walls of MI and the resultant enrichment of the residual melt in water. Relatively anhydrous glasses with analytical totals deficient for no more than 2 wt % and containing 83–84 wt % SiO_2 (Fig. 12a) were found in a few MI of the second group. These MI are intersected by cracks and have likely partly lost their water via leaking. We observed rapid dissolution of anorthoclase in thermometric experiments in MI of the second group.

This anomalous behavior of MI is explained by the elevated alkalinity of the residual melt and its high water content during the initial heating of the inclusions. After the rapid dissolution of the host-mineral walls of the inclusions, the melt became less alkaline and contained less water. The compositions of the anomalous glasses in the second-group MI does not correspond to the composition of the parental comenditic melt. Data on these glasses can be utilized only upon correcting their composition with regard for the crystallization of the host anorthoclase on the walls of MI.

Fig. 11. Composition of matrix glasses in rocks and primary quenched glasses in melt inclusions in mineral phenocrysts. The dashed line connects the composition points of matrix glasses of the rocks, and the dotted line with an arrowhead connects composition points of glasses in melt inclusions in anorthoclase phenocrysts. (a) TAS diagram; (b) relations between the SiO_2 and Al_2O_3 concentrations of the glasses; (c) classification diagram (Macdonald, 1974). Matrix glasses of rocks: (1) pantellerite NR-7; (2) high-Fe comendite NR-23; (3) low-Fe comendites. Glasses in melt inclusions in phenocrysts: (4) anorthoclase, sample NR-7; (5) hedenbergite, sample NR-7; (6) anorthoclase, sample NR-23; (7) hedenbergite, sample NR-23; (8) anorthoclase form low-Fe comendites; (9) pantelleritic glass in enclave XE3 of comenditic trachyte (Fig. 3d), sample NR-7.

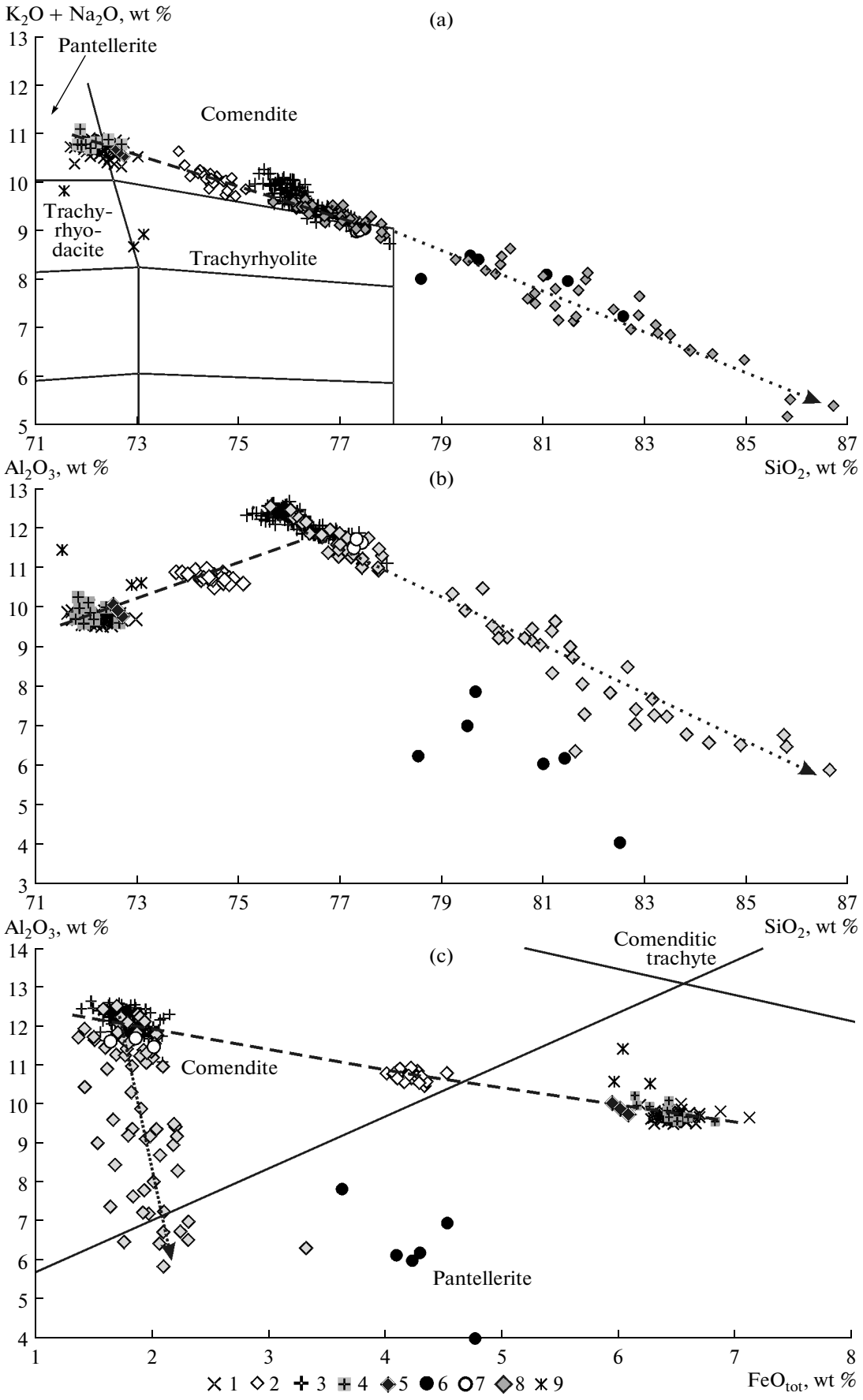
(a)
$K_2O + Na_2O$, wt %
Pantellerite
Comendite
Trachy-
rhyo-
dacite
Trachyrhyolite
SiO_2, wt %
(b)
Al_2O_3, wt %
SiO_2, wt %
(c)
Al_2O_3, wt %
Comenditic
trachyte
Comendite
Pantellerite
FeO_{tot}, wt %
1 2 3 4 5 6 7 8 9

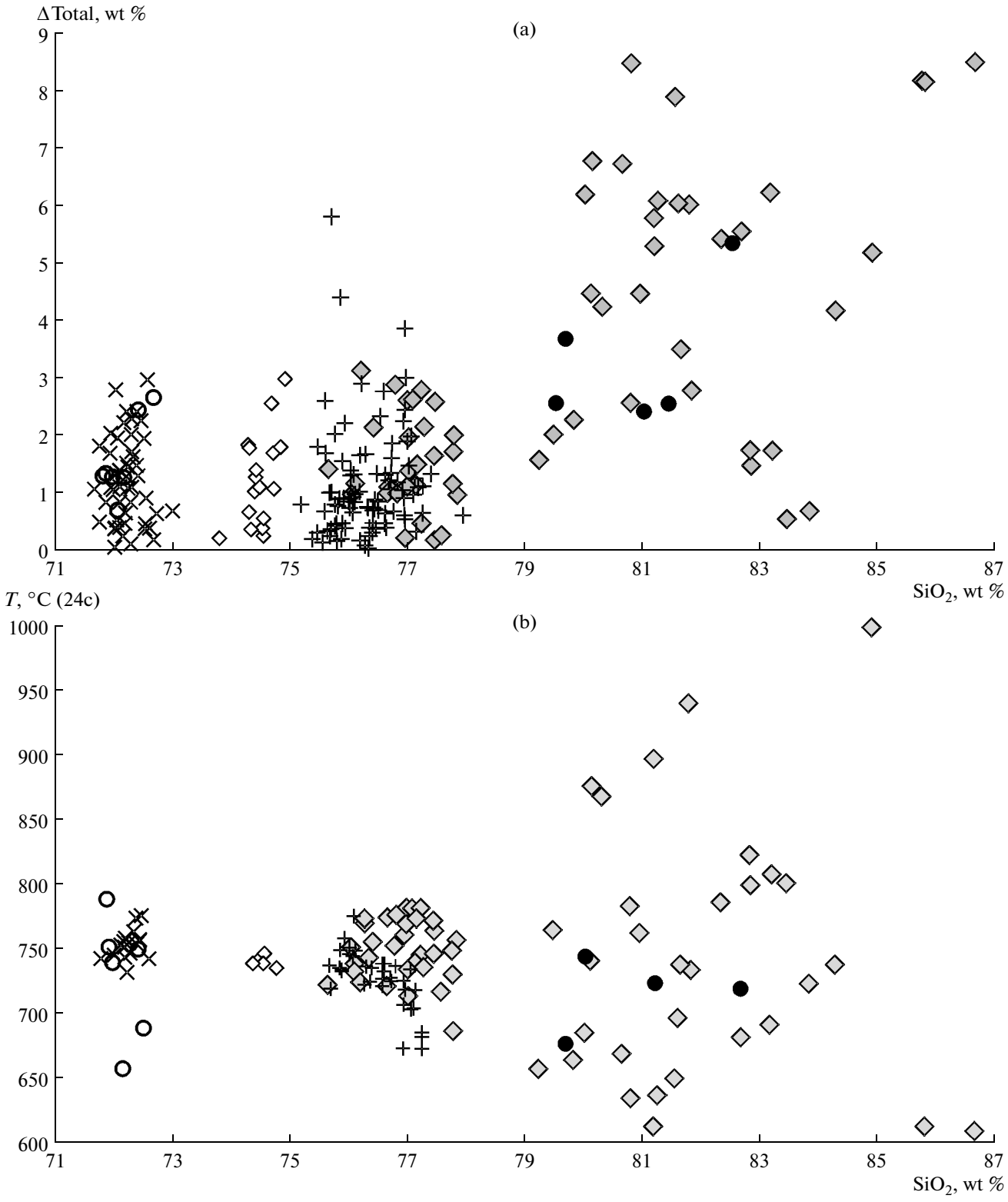

Fig. 12. Relations between: (a) SiO_2 concentrations and deficiencies of analytical totals, and (b) crystallization temperature of anorthoclase phenocrysts in glasses of the rock matrix and melt inclusions in anorthoclase from comendites and pantellerites. ΔTotal is the difference between 100 wt % and the actual analytical totals of oxides. *T*,°C (24c) is the equilibrium crystallization temperature of anorthoclase phenocrysts and microlites in melts calculated by Eq. (24c) in (Putirka, 2008). See Fig. 11 for symbol explanations.

Table 9. LA-ICP-MS analyses of matrix glasses and anorthoclase, fayalite, hedenbergite phenocrysts

Element	Glass				Anorthoclase				Fayalite			Hedenbergite			
	NR-7 (6)	NR-23 (4)	NR-1 (4)	NR-5 (4)	NR-7 (4)	NR-23 (3)	NR-1 (5)	NR-5 (2)	NR-23 (1)	NR-1 (2)	NR-5 (1)	NR-7 (1)	NR-23 (1)	NR-1 (1)	NR-5 (2)
Mg	63	17	27	126	8.0	2.2	2.3	148	559	1311	2427	2297	593	6628	10784
P	205	97	44	83	23		37	63	159	160	153	51	25	653	56
Ti	1968	1158	522	488	60	285	35	41	70	71	56	2134	970	1025	1076
B	84	86	69	62	4.9	6.6	4.2	4.5	3.83	3.20	3.47	3.00	18	7.02	4.83
Li	109	90	78	73	1.3	4.9	6.4	7.3	41	27	27	33	36	25	21
Rb	151	155	127	135	31	40	30	28			0.05		53	0.16	0.52
Cs	19	15	15	15	0.05	0.09	0.03	0.08	0.01			0.07	4.42	0.14	0.22
Ba	7.4	1.5	4.9	15.3	12	6.4	151	94	0.02		0.02	0.04	0.42	0.58	0.03
Sr	0.8	0.21	0.20	3.21	0.89	0.74	6.7	5.9	0.11	0.02	0.03	0.91	0.48	0.85	1.55
Zr	1496	1304	558	620	2.4	0.64	0.09	0.19	0.24	0.17	356	524	551	3037	126
Hf	46	35	21	23	0.01	0.04	0.01	0.01	0.03		13	22	16	83	
Ta	8.4	6.9	6.5	6.1	0.01	0.05	0.05	0.05			0.09	0.03	2.30	0.04	0.30
Nb	84	82	62	59	0.21	1.78		0.06			0.32	0.43	24	0.44	1.2
Sc	2.0	2.2	1.7	1.5	0.52	1.58	0.90	0.78	1.37	3.98	3.59	47	10	112	134
V	0.03	0.13	0.06	1.67	0.04		0.11	0.61		0.05	0.21	3.3	2.1	4.9	8.0
Cr		18	10	22	4.8			3.9		26		8.5			
Ni	1.4	0.4	0.2		0.43	0.93	0.13	1.84	2.1	2.5	2.9	4.5	1.9	2.0	3.2
Cu	5.4	7.3	4.0	8.9	2.3	2.4	2.0	3.8	0.30		9.0	1.0	2.4	1.2	5.2
Pb	66	55	45	61	1.0	1.3	8.1	4.6	0.08			1.6	17.5	2.0	2.3
Th	59	49	42	45	0.06						2.31	0.03	12.16	4.0	
U	17	15	14	15	0.02	0.04	0.01	0.01			1.49	0.06	4.2	5.0	
Y	167	128	103	112	0.25	0.01	0.01	0.01	25	32	42	179	130	370	351
La	180	138	73	80	0.37	0.11	0.89	0.66	0.05	0.02	0.58	143	126	150	114
Ce	374	294	161	173	0.37	0.17	0.72	1.2	0.10	0.02	1.3	446	359	526	404
Pr	39	30	17	17	0.07	0.01	0.03		0.02	0.02	0.16	70	50	89	64
Nd	151	116	62	60	0.47	0.04	0.05		0.32	0.13	1.3	365	215	468	322
Sm	35	25	17	16	0.04	0.06	0.01	0.02	0.41	0.33	0.68	87	48	129	100
Eu	2.1	0.89	0.34	0.29	0.14	0.16	0.78	0.58		0.03	0.04	5.0	1.9	2.2	1.8
Gd	32	22	16	18	0.06	0.02			0.59	0.78	1.86	64	41	112	77
Tb	5.9	4.2	3.1	3.6	0.01				0.28	0.36	0.31	9.5	6.0	17	14
Dy	39	28	24	25	0.04		0.02		3.8	5.4	6.7	58	35	123	95
Ho	7.9	5.9	4.7	4.6	0.01				1.2	1.8	2.2	11	7.4	24	21
Er	25	18	15	14	0.04	0.02			5.7	9.0	10	34	23	57	71
Tm	3.8	2.6	2.3	2.3					1.0	2.2	1.9	6.1	3.7	10	12
Yb	24	17	15	15	0.04	0.01			10	17	23	55	32	90	93
Lu	3.6	2.5	2.2	2.4					2.2	3.5	4.6	12	6.9	20	18

The absence of data corresponds to concentrations below the detection limits, numerals in parentheses show the numbers of analyses.

Table 10. Phase/glass distribution coefficients of elements based on LA-ICP-MS analyses

Element	Glass		Anorthoclase				Fayalite			Hedenbergite			
	G7/G1	G7/G5	NR-7	NR-23	NR-1	NR-5	NR-23	NR-1	NR-5	NR-7	NR-23	NR-1	NR-5
Mg	2.37	0.50	0.13	0.13	0.09	1.17	32.9	49.3	19.3	36.4	34.9	249.3	85.6
P	4.69	2.45	0.11		0.84	0.76	1.64	3.66	1.84	0.25	0.26	14.98	0.67
Ti	3.77	4.03	0.03	0.25	0.07	0.08	0.06	0.14	0.11	1.08	0.84	1.96	2.20
B	1.21	1.34	0.06	0.08	0.06	0.07	0.04	0.05	0.06	0.04	0.21	0.10	0.08
Li	1.40	1.50	0.01	0.05	0.08	0.10	0.45	0.34	0.38	0.30	0.40	0.32	0.29
Rb	1.19	1.12	0.20	0.25	0.24	0.21			0.00	0.00	0.34	0.00	0.00
Cs	1.22	1.22	0.00	0.01	0.00	0.01	0.00			0.00	0.29	0.01	0.01
Ba	1.53	0.49	1.67	4.19	31.0	6.15	0.02		0.00	0.01	0.27	0.12	0.00
Sr	3.93	0.24	1.16	3.58	34.3	1.83	0.53	0.08	0.01	1.18	2.30	4.36	0.48
Zr	2.68	2.41	0.00	0.00	0.00	0.00	0.00	0.00	0.57	0.35	0.42	5.44	0.20
Hf	2.14	1.97	0.00	0.00	0.00	0.00	0.00		0.57	0.47	0.46	3.90	0.00
Ta	1.29	1.38	0.00	0.01	0.01	0.01			0.01	0.00	0.33	0.01	0.05
Nb	1.34	1.42	0.00	0.02		0.00			0.01	0.01	0.29	0.01	0.02
Sc	1.17	1.32	0.26	0.72	0.53	0.52	0.62	2.35	2.38	24	4.7	66	89
V	0.49	0.02	1.53		1.81	0.37		0.88	0.13	116	16	83	4.80
Cr						0.18		2.59					
Ni	6.17		0.30	2.45	0.57		5.46	10.8		3.13	4.93	8.75	
Cu	1.33	0.60	0.43	0.33	0.49	0.42	0.04		1.01	0.19	0.33	0.31	0.58
Pb	1.46	1.08	0.02	0.02	0.18	0.08	0.00		0.00	0.02	0.32	0.04	0.04
Th	1.39	1.32	0.00						0.05	0.00	0.25	0.09	0.00
U	1.23	1.17	0.00	0.00	0.00	0.00			0.10	0.00	0.28	0.35	0.00
Y	1.62	1.49	0.00	0.00	0.00	0.00	0.20	0.31	0.37	1.07	1.02	3.59	3.14
La	2.47	2.24	0.00	0.00	0.01	0.01	0.00	0.00	0.01	0.79	0.92	2.05	1.42
Ce	2.32	2.16	0.00	0.00	0.00	0.01	0.00	0.00	0.01	1.19	1.22	3.26	2.33
Pr	2.32	2.26	0.00	0.00	0.00		0.00	0.00	0.01	1.77	1.65	5.30	3.69
Nd	2.44	2.51	0.00	0.00	0.00		0.00	0.00	0.02	2.41	1.84	7.57	5.34
Sm	2.00	2.14	0.00	0.00	0.00	0.00	0.02	0.02	0.04	2.50	1.91	7.41	6.15
Eu	6.22	7.30	0.07	0.18	2.31	2.03		0.08	0.14	2.40	2.15	6.39	6.11
Gd	2.02	1.81	0.00	0.00			0.03	0.05	0.11	2.00	1.85	7.11	4.36
Tb	1.90	1.64	0.00				0.07	0.12	0.09	1.60	1.43	5.36	3.80
Dy	1.66	1.60	0.00		0.00		0.14	0.23	0.27	1.48	1.26	5.17	3.87
Ho	1.68	1.71	0.00				0.21	0.38	0.48	1.35	1.25	5.13	4.56
Er	1.68	1.76	0.00	0.00			0.31	0.61	0.71	1.37	1.28	3.84	5.03
Tm	1.66	1.66					0.39	0.94	0.81	1.59	1.43	4.27	5.08
Yb	1.63	1.55	0.00	0.00			0.61	1.16	1.49	2.30	1.95	6.14	6.00
Lu	1.66	1.52					0.86	1.64	1.96	3.39	2.77	9.40	7.84

The absence of data corresponds to concentrations below the detection limits of LA-ICP-MS analysis, G7/G1 and G7/G5 is the ratios of element concentrations in glass from pantellerite NR-7 to those in glasses in low-Fe comendites NR-1 and NR-5.

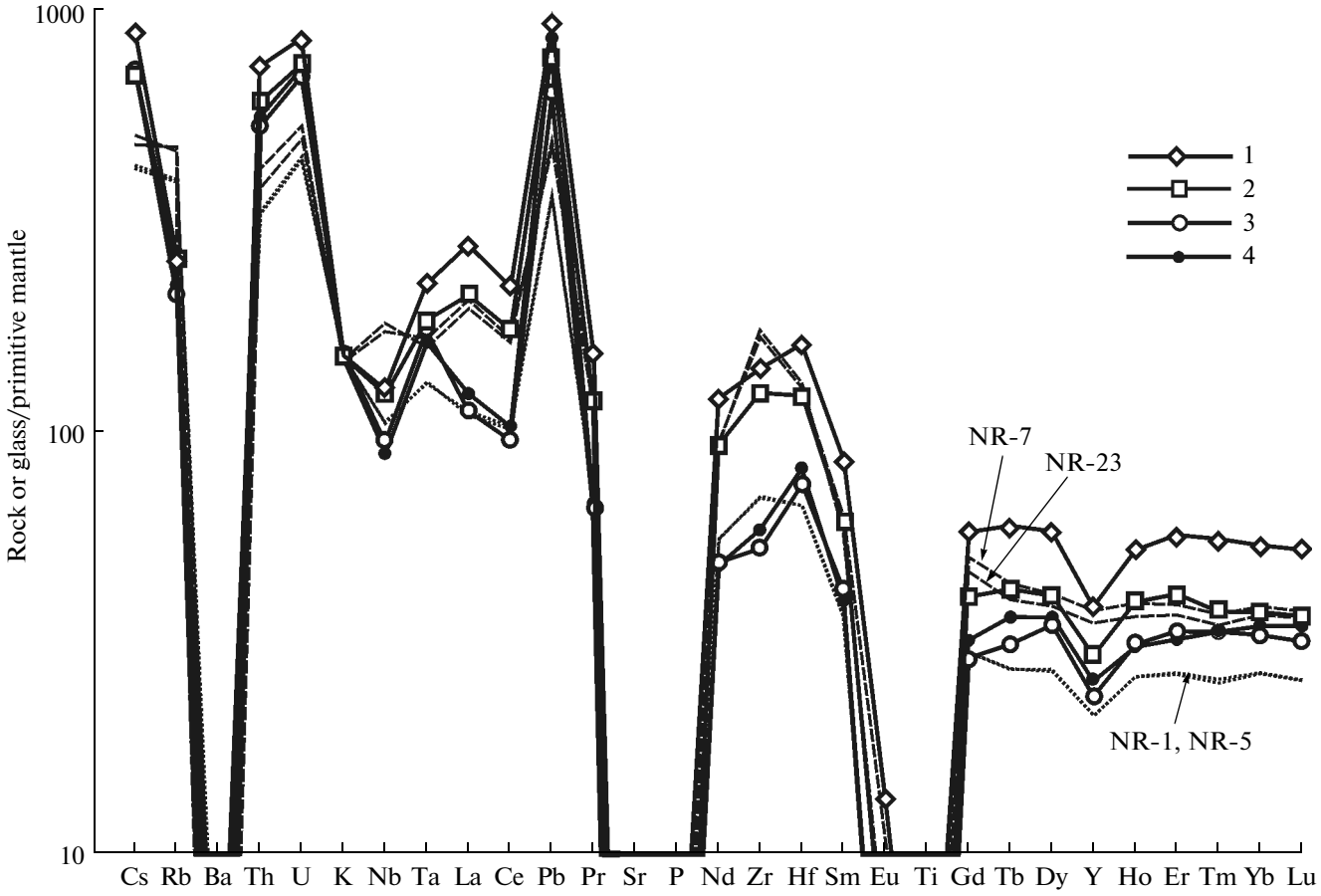

Fig. 13. Primitive mantle-normalized (McDonough and Sun, 1995) multielemental patterns of pantellerite NR-7, comendites NR-23, NR-1, NR-5 and matrix glasses of these rocks (LA-ICP-MS analyses). Based on data from Table 7 for rock compositions and Table 9 for glass compositions. (1) Glass in NR-7; (2) glass in NR-23; (3) glass in NR-1; (4) glass in NR-5.

In sample NR-23 of high-Fe comendite, all MI in anorthoclase are anomalous and have analytical Δ totals about 3 wt %. The compositions of glasses in MI from anorthoclase in pantellerite NR-2 are close to the composition of the matrix (Fig. 12a). Except the second-group anomalous MI, most analyses of glasses in our samples are Δ total 1–3 wt %. This range likely corresponds to the range of water contents in the melts from which the phenocrysts crystallized. The glasses of MI in anorthoclase in all of our samples contain 0.1–0.2 wt % Cl, and their F concentrations are below the detection limit (<0.2–0.3 wt %) by SEM EDS. The composition of the glasses of MI exposed in a few hedenbergite and fayalite phenocrysts from samples NR-23 and NR-7 correspond to the compositions of the matrix glasses (Fig. 12a).

CRYSTALLIZATION PARAMETERS OF MINERALS

We made use of expression 24c from (Putirka, 2008) to calculate the temperature of equilibrium between melt in inclusions and their host anorthoclase phenocryst, with regard for the probable water content of the melts (estimated from the differences of the analytical totals and 100 wt % for the glasses) (Fig. 12a). For the low-Fe comendites without anomalous MI of the second group, this temperature lies within the range of 720–780°C at an average of about 750°C (Fig. 12b). In sample NR-7, four MI have equilibrium temperature within this range and the other two MI have temperatures of 655 and 686°C, which can be explained by the relatively low crystallization temperature of anorthoclase in the pantelleritic melt. The lowest temperatures are typical of microlites in MI and matrix glass of the comendites. The decrease in the crystallization temperature of the anorthoclase microlites is correlated with the increase in their Fe concentration from 0.6–1 wt % Fe_2O_3 in the matrix to 3–4 wt % Fe_2O_3 in MI.

Ilmenite and titanomagnetite have never been found in aggregates in the low-Fe comendites. If these minerals crystallized roughly simultaneously from the low-Fe comenditic melt, then two pairs of ilmenite and titanomagnetite microlite containing 17–20% of the ulvospinel end member in samples NR-18 and

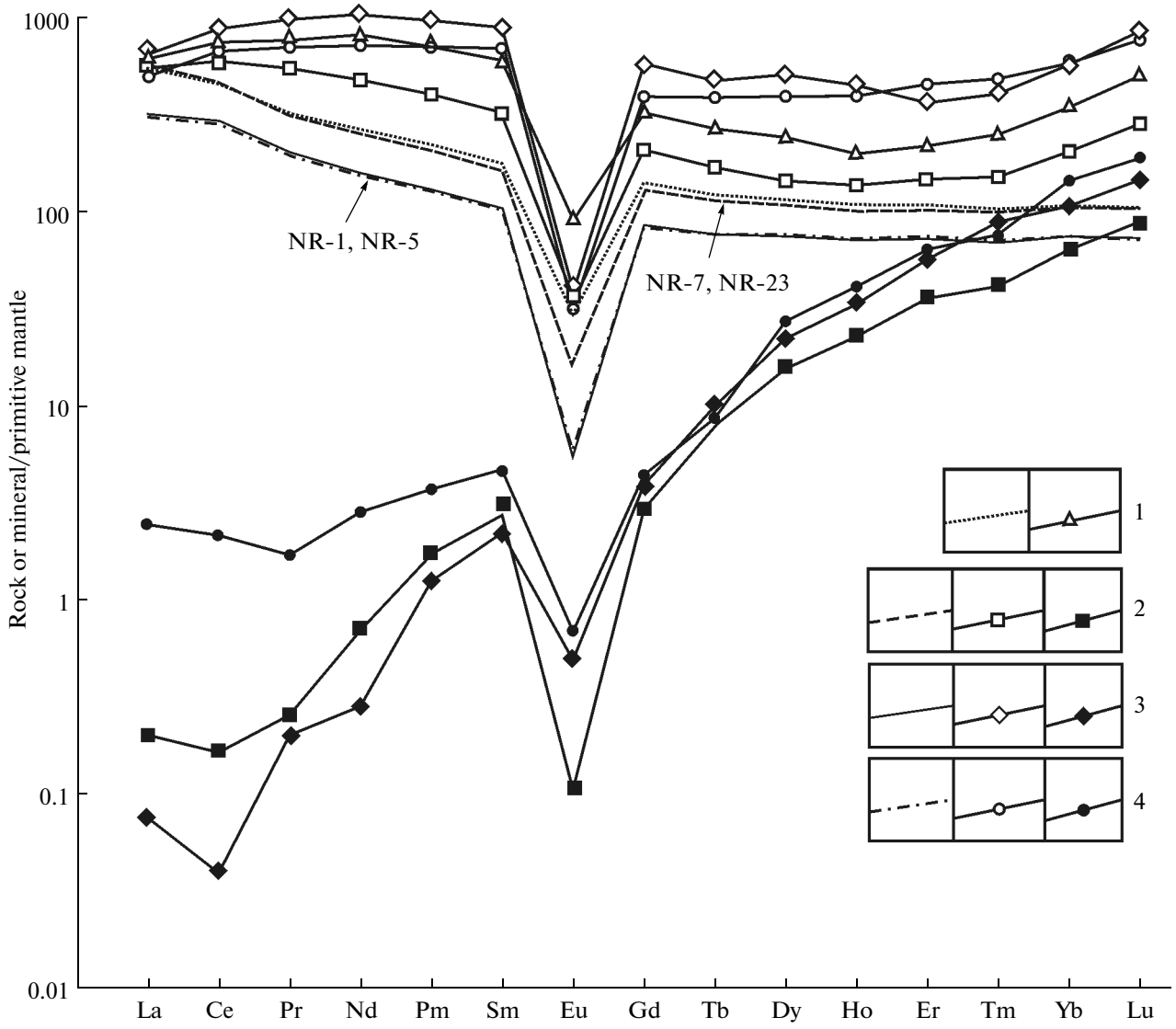

Fig. 14. Primitive mantle-normalized (McDonough and Sun, 1995) REE patterns of rocks and hedenbergite, fayalite phenocrysts. (1) Pantellerite NR-7: rock and hedenbergite; (2) comendite NR-23: rock, hedenbergite, fayalite; (3) comendite NR-1: rock, hedenbergite, fayalite; (4) comendite NR-1: rock, hedenbergite, fayalite. Arrows point to REE patterns of rocks NR-1, NR-5, NR-23, NR-7.

NR-20 yield the following crystallization parameters, which were calculated by the thermometer and oxybarometer in (Ghiorso and Evans, 2008): 688°C, ΔNNO (Ni–NiO buffer) = –2.63; 731°C, ΔNNO = –2.59.

The QUILF-95 program (Andersen et al., 1993) is used to calculate mineral equilibria and estimate conditions under which various rocks, including volcanics, were formed (Ren et al., 2006; White et al., 2005, 2009; LeMasurier et al., 2001; and others). The fact that the comendites and pantellerites contain association of clinopyroxene, fayalite and ilmenite phenocrysts makes it possible to calculate their crystallization parameters: temperature, pressure, oxygen fugacity (fO_2) depending on the composition of the minerals and on quartz activity a_{SiO_2}. Silica activity a_{SiO_2} is equal to one if quartz crystallizes (i.e., the melt is saturated with respect to this mineral) and is lower than one in the absence of silica minerals quartz in the melt. Depending on the pressure and a_{SiO_2}, the temperature was evaluated by the Fe–Mg–Ca proportions in the clinopyroxene and olivine, and the oxygen fugacity fO_2 was estimated from the concentrations of the hematite end member in the ilmenite. Inasmuch as the rocks contain no quartz phenocrysts, we calculated all parameters for $a_{SiO_2} \leq 1$ (1.0, 0.9, 0.8). The results of the QUILF calculations depend on the Mg concentra-

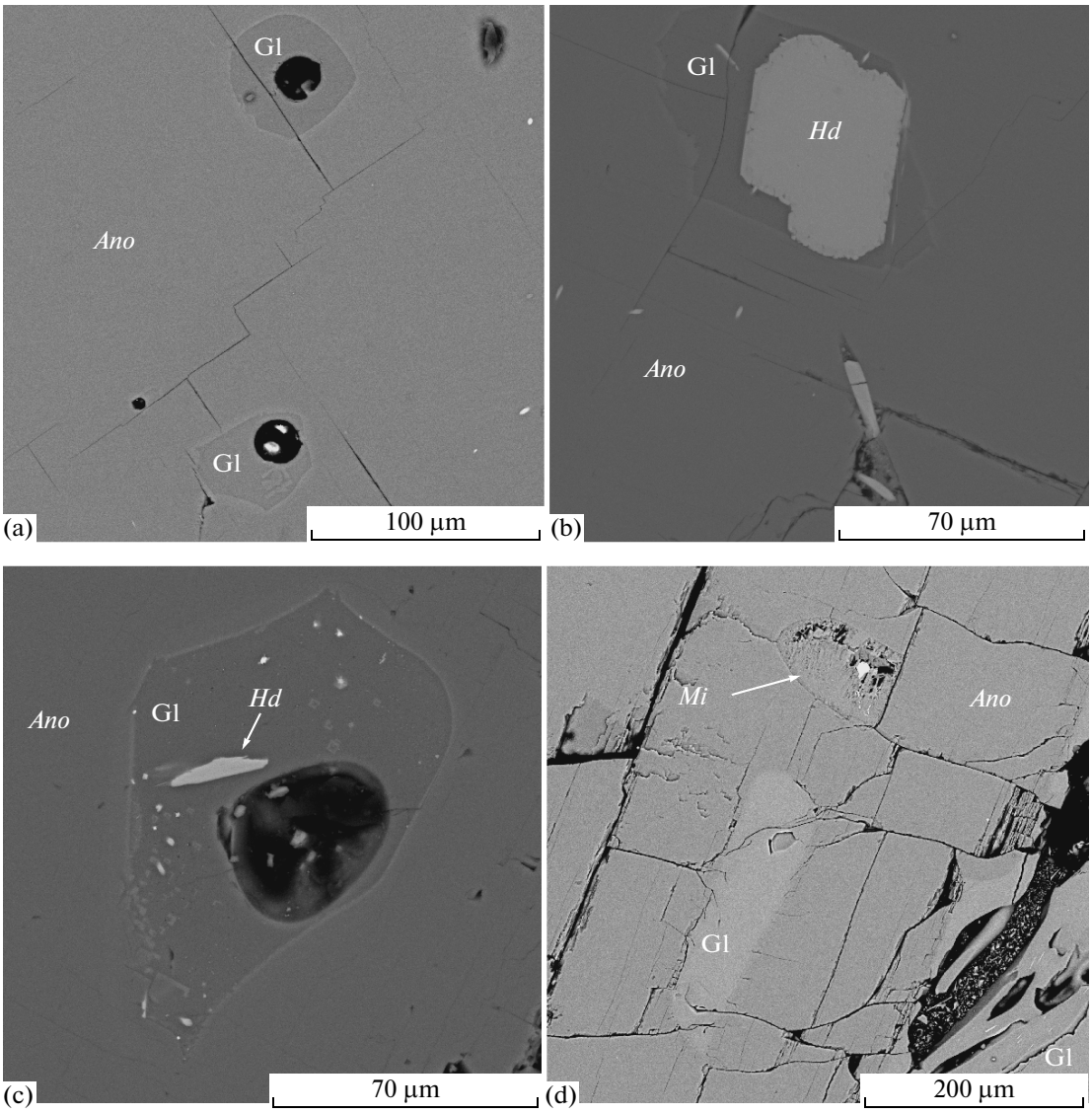

Fig. 15. BSE images of melt inclusions in anorthoclase phenocrysts. (a) MI with primary quenched glass and exposed contraction bubbles, the glass of one MI hosts an anorthoclase microcline, sample NR-18; (b) MI with xenogenic hedenbergite in the glass, sample NR-5; (c) MI with a xenogenic hedenbergite daughter phase and with submicrometer-sized anorthoclase and titanomagnetite grains, sample NR-1; (d) MI with primary quenched glass and quartz-feldspathic symplectite, sample NR-18. See Fig. 2 for symbol explanations.

tion in the minerals. The hedenbergite contains 0.2–0.6 wt % MgO (Table 11), and these values persistently occur in SEM-EDS analyses of the mineral. The ilmenite and fayalite often contain MgO concentrations lower than the detection limits of SEM-EDS (0.2–0.3 wt %) or close to this threshold. LA-ICP-MS analysis of a fayalite phenocryst from sample NR-23 yielded 560 ppm Mg (Table 9). Because of this and with regard for the uncertainties in the Mg concentrations of the minerals, the concentrations of the Gk ($MgTiO_3$) end member of ilmenite and the Fo (Mg_2SiO_4) end member of olivine were assumed in the calculations as variables. The results of these calculations are summarized in Table 12. At a silica activity $a_{SiO_2} = 1$, the minimum temperature of 715°C at a maximum pressure of 3.3–3.7 kbar was calculated for the average compositions of equilibrium ilmenite, hedenbergite and fayalite in pantellerite NR-7 and for the mineral aggregate (domain 15) shown in Fig. 2c. If the silica activity is decreased to 0.8 (no quartz in the melt), the temperature is only insignificantly higher, 743–746°C, but the pressure increases to 7.4–7.9 kbar. According to calculation data, phenocrysts in the mineral aggregate of domain 4 in sample NR-23

Table 11. Composition (wt %) of minerals in comendites and pantellerite used in QUILF calculations

Oxide	NR-23, spot 4			NR-7, spot 15		NR-7 average		Average comendite		
	Cpx	*Ilm*	*Fa*	*Cpx*	*Fa*	*Cpx*	*Fa*	*Cpx*	*Ilm*	*Fa*
SiO_2	48.37		29.35	48.16	29.30	48.58	29.50	48.97		29.58
TiO_2	0.23	50.46		0.24		0.46		0.31	50.46	
Al_2O_3	0.26			0.47		0.22		0.35		
FeO	30.1	47.02	65.38	30.65	66.82	30.60	66.94	29.72	47.02	66.20
MnO	1.23	1.56	3.53	1.30	3.38	1.29	3.46	1.31	1.56	3.10
MgO	0.2	0.03	0.2	0.34		0.30	0.10	0.64	0.03	0.78
CaO	17.63		0.39	16.58	0.28	16.87	0.29	18.15		0.23
Na_2O	1.33			1.88		1.85		0.79		
Total	99.35	99.07	98.85	99.62	99.78	100.17	100.29	100.24	99.07	99.89

Cpx—clinopyroxene, *Ilm*—ilmenite, *Fa*—fayalite.

(Fig. 2b) could crystallize at 763–798°C and 3–7.3 kbar; phenocrysts in the low-Fe comendites could crystallize at similar temperatures of 748–783°C (according to the average compositions of the minerals) but at lower pressures of 2.3–6.7 kbar. In all instances, the calculated oxygen fugacity fO_2 was lower than the FMQ buffer, with ΔFMQ increasing from −1.08 to 1.75 at $a_{SiO_2} \leq 1$.

It should be stressed that the differences in the crystallization temperatures, pressures, and ΔFMQ are controlled first of all by the variations in the Mg concentration in the minerals. The ilmenite has a practically unchanging composition in all of the rocks. Fayalite in samples NR-23 and NR-7 is identical in composition and is more magnesian in the low-Fe comendites. The greatest variations in the Mg concentration are typical of the hedenbergite. It follows from calculation results that the crystallization parameters of the phenocrysts in the absence of quartz in the melts (minimum $a_{SiO_2} \leq 1$) are 715–763°C, 2.3–3.7 kbar, ΔFMQ from −1.08 to −1.27.

The QUILF crystallization temperatures of the hedenbergite, fayalite, ilmenite are close to the estimates based on the temperatures (approximately 750°C) of equilibrium between the matrix glass, anorthoclase phenocrysts and between MI glasses and anorthoclase in the low-Fe comendites (Fig. 12b). This temperature (715°C) is much lower than the average equilibrium temperature (750°C) calculated by the thermometer (Putirka, 2008) for equilibrium anorthoclase and glass pairs in pantellerite NR-7 (Fig. 12b). This may be explained by the absence of consistent experimental data for the calibration of the thermometer on equilibrium between feldspars and alkali melts. In this connection, it is also pertinent to mention that calculation by the thermometer (Hanchar and Watson, 2003) of the saturation temperature of alkali melts with Zr yield unrealistically high values: 902–944°C for low-Fe comendites, 1007°C for high-Fe comendite NR-23, and 944°C for pantellerite NR-7. Equally significant temperature discrepancies are reported in (Marshall et al., 2009) for comendites from the Olkaria Complex. The Zr thermometer (Hanchar and Watson, 2003) seems to be inapplicable to comenditic and pantelleritic melts.

DISCUSSION

It is interesting to compare comendites and pantellerites of Nemrut volcano with mineralogically and geochemically similar rocks elsewhere. The pre-caldera high-Fe comendites of Nemrut volcano have major-component compositions and trace-element patterns similar to those of comendites from Pektusan volcano (Fig. 16) in a rift zone at the boundary between China and North Korea (Horn and Schmincke, 2000; Popov et al., 2005, 2008; Fan et al., 2006; Sakhno, 2007b, Andreeva et al., 2014). High-Fe comendites and pantellerites from several volcanic centers in the East African (Kenya, Ethiopian, Afar) Rift also have composition similar to those of rocks from Nemrut (Figs. 16, 17). These are pantellerites from Dabbahu volcano in the Afar Rift (Field et al., 2012, 2013), pantellerites of the pre-caldera stage of Gedemsa volcano in the Ethiopian Rift (Peccerillo et al., 2003), comendites with variable Fe concentra-

Table 12. Results of QUILF calculations of the clinopyroxene–fayalite–ilmenite mineral equilibrium for comendites and pantellerite samples

Mineral/end member	NR-23, spot 4		NR-7, spot 15		NR-7 average		Average comendite			
	Input	Calc	Input	Calc	Input	Calc	Intut	Calc	Input	Calc
Ilmenite										
Hem	0.0348	0.035	0.0348	0.035	0.0348	0.035	0.0349	0.035	0.0349	0.035
Gk	**0.0011**	0.000	**0.0011**	0.001	**0.0011**	0.001	**0.0011**	0.002	**0.0011**	0.002
Py	0.0342	0.034	0.0342	0.034	0.0342	0.034	0.0336	0.034	0.0336	0.034
Olivine										
Fo	**0.0054**	0.004	**0.0053**	0.006	**0.0053**	0.005	0.0205	0.021	0.0205	0.021
La	0.0075	0.007	0.0053	0.005	0.0055	0.005	0.0043	0.004	0.0043	0.004
Augite										
En	0.0072	0.007	0.0128	0.013	0.0111	0.011	0.0205	0.011	0.0205	0.011
Wo	0.4314	0.431	0.4366	0.437	0.4395	0.440	0.4395	0.440	0.4395	0.440
$a_{SiO_2(Qz)}$	1.0		1.0		1.0		1.0		**1.0**	1.0
P, bar		2963		3756		3335		2296		2380
T, °C		763		715		715		748		748
$\log fO_2$		−16.39		−17.27		−17.27		−16.71		−16.70
DFMQ		−1.27		−1.08		−1.08		−1.16		−1.16
$a_{SiO_2(Qz)}$	0.9		0.9		0.9		0.9		**0.9**	0.9
P, bar		4971		5626		5187		4342		4400
T, °C		779		729		726		764		765
$\log fO_2$		−16.03		−16.93		−17.02		−16.33		−16.32
DFMQ		−1.50		−1.30		−1.28		−1.39		−1.39
$a_{SiO_2(Qz)}$	0.8		0.8		0.8		0.8		**0.8**	0.8
P, bar		7262		7887		7392		6705		6740
T, °C		798		746		743		783		784
$\log fO_2$		−15.63		−16.53		−16.63		−15.90		−15.90
DFMQ		−1.75		−1.55		−1.52		−1.64		−1.65

Notation from the QUILF-95 program (Andersen et al., 1993): *Hem*, *Gk*, and *Py*-end members of ilmenite; *Fo* and *La*-end members of olivine; *En* and *Wo*-end members of clinopyroxene; $a_{SiO_2(Qz)}$ -quartz activity coefficients; $\log fO_2$—oxygen fugacity; ΔFMR—oxygen fugacity relative to the FMQ (fayalite–magnetite–quartz) buffer. Variables (Input) are printed in bold font, the column Calc presents calculation results (see text for explanations).

tions, and pantellerites at volcanic centers of the Olkaria Complex in the Kenya Rift (Macdonald et al., 1987; Marshall et al., 2009). Mildly alkaline low-Fe comendites is rare, and as far as we know, this rock is widespread elsewhere only in the Oklaria Complex (Marshall et al., 2009). Trachyrhyolites of similar major-component and mineralogical composition with NA/K = 0.93–0.99 make up the lava dome of Alid volcano in Eritrea (Lowenstern et al., 2006). Pantellerites on Pantelleria Island (White et al., 2009), post-caldera pantellerites of Gedemsa volcano (Peccerillo et al., 2003), pantellerites of the Boseti Complex in the Main Ethiopian Rift (Ronga et al., 2010) and pantellerites in the West Antarctic Rift (LeMasurier et al., 2011) differ from Nemrut pantellerites in being richer in Fe and alkalis and poorer in Al_2O_3 and SiO_2 (Fig. 17).

Comendites and pantellerites often compose lava flows and domes and occasionally occur as products of explosion eruptions, such as pumice, ignimbrite, and tuff, as at Pektusan (Sakhno, 2007a, 2007b) and Dabbahu (Field et al., 2013) volcanoes. The catastrophic eruption of Pektusan in the past millennium (939–946) was triggered by the ejection of a vast amount of high-Fe pyroclastic comenditic material (Horn and Schmincke, 2000). The comendites and pantellerites of vitreous lavas (obsidian) only rarely contain more

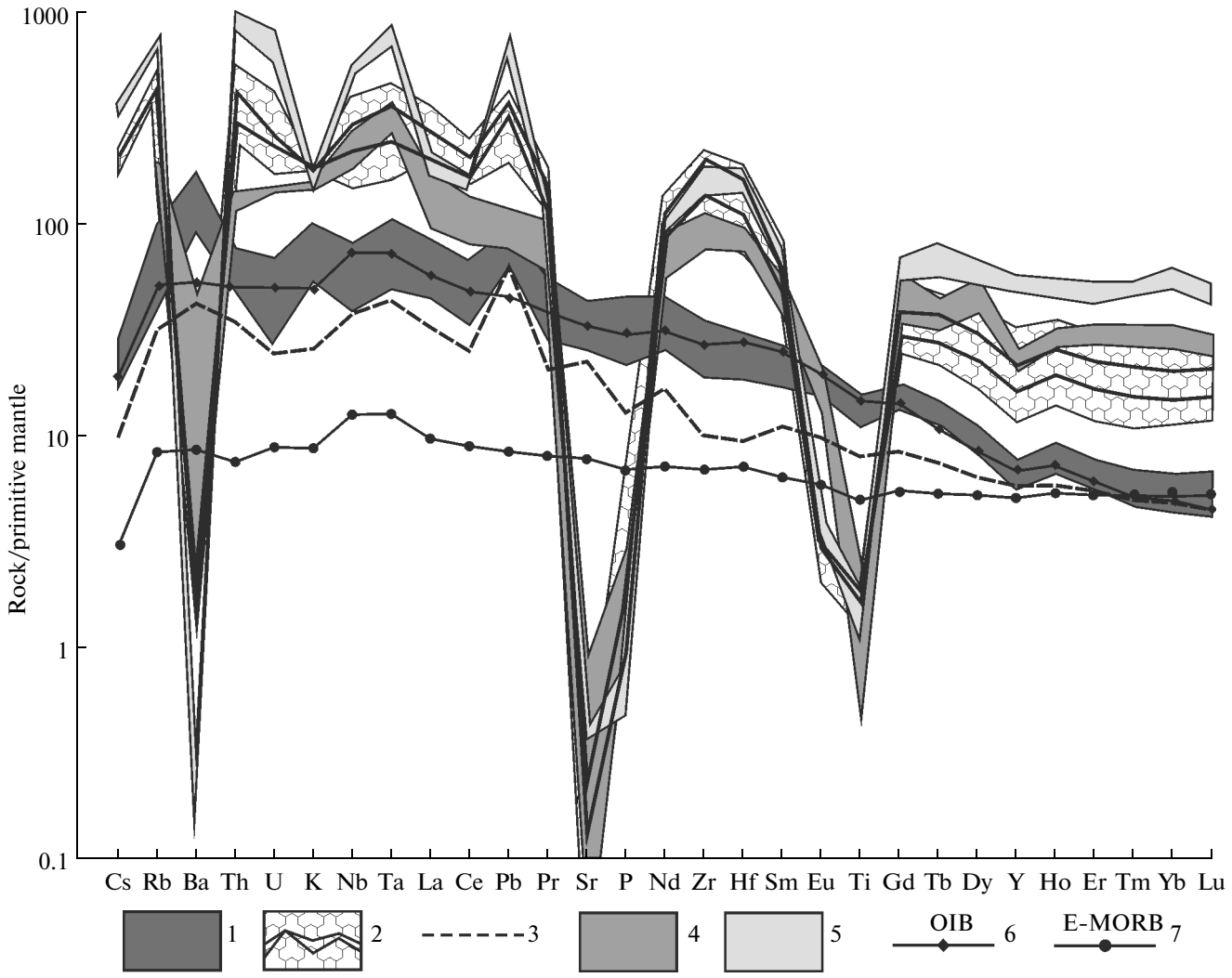

Fig. 16. Primitive mantle-normalized (McDonough and Sun, 1995) multielemental patterns of rocks from Pektusan volcano (Fan et al., 2006; Andreeva et al., 2014), Olkaria Complex (Macdonald et al., 1987, 2008) and Dabbahu volcano (Field et al., 2013). Pektusan volcano: (1) trachybasalts; (2) high-Fe comendites and pantellerites. Olkaria Complex: (3) trachybasalts; (4) high-Fe comendites. Dabbahu volcano: (5) pantellerites, (6, 7) OIB and E-MORB basalts.

than 10 vol % phenocrysts. The latter are dominated by anorthoclase, which shows insignificant variations in the concentration of the albite end member and almost devoid of Ca. Other phenocryst minerals, which are contained in subordinate amounts in the rocks, are hedenbergite, fayalite, ilmenite, sometimes together with titanomagnetite. The accessory minerals, which are not necessarily contained in all of the complexes, are aenigmatite, chevkinite, amphibole (ferrorichterite), aegirine-augite, fluorapatite, pyrrhotite, zircon, and very rare fluorite. Several comendites and pantellerites varieties contain quartz as phenocrysts and as a devitrification product of the matrix glass. Some varieties are very poor in quartz phenocrysts. For example, these phenocrysts were identified only in a single sample of pantellerite from Dabbahu volcano (Field et al., 2013). Note that none of the comendites and pantellerites samples from Nemrut volcano contains quartz phenocrysts.

Detailed data are now available on the mineralogy, isotopic geochemistry and crystallization processes of comendites from the Olkaria Complex (Macdonald et al., 1987, 2008; Heumann and Davies, 2002; Marshall et al., 2009). Similar to what is typical of Nemrut, an increase in the alkalinity of the rocks (NK/A increases from 1 to 1.55) and their Fe concentration (from 2–3 to 3–4.5 wt % FeO) are coupled with their significant enrichment in Zr, Nb, Rb, Th, REE and depletion in Ba, Sr, P, Eu, Ti (Table 7, Figs. 10 and 16). To simulate the crystallization of the alkaline melts, experiments were conducted with comendite from the Olkaria Complex and pantellerite from the nearby Eburru Complex in the Kenya Rift (Scaillet and Macdonald, 2001, 2003, 2006).

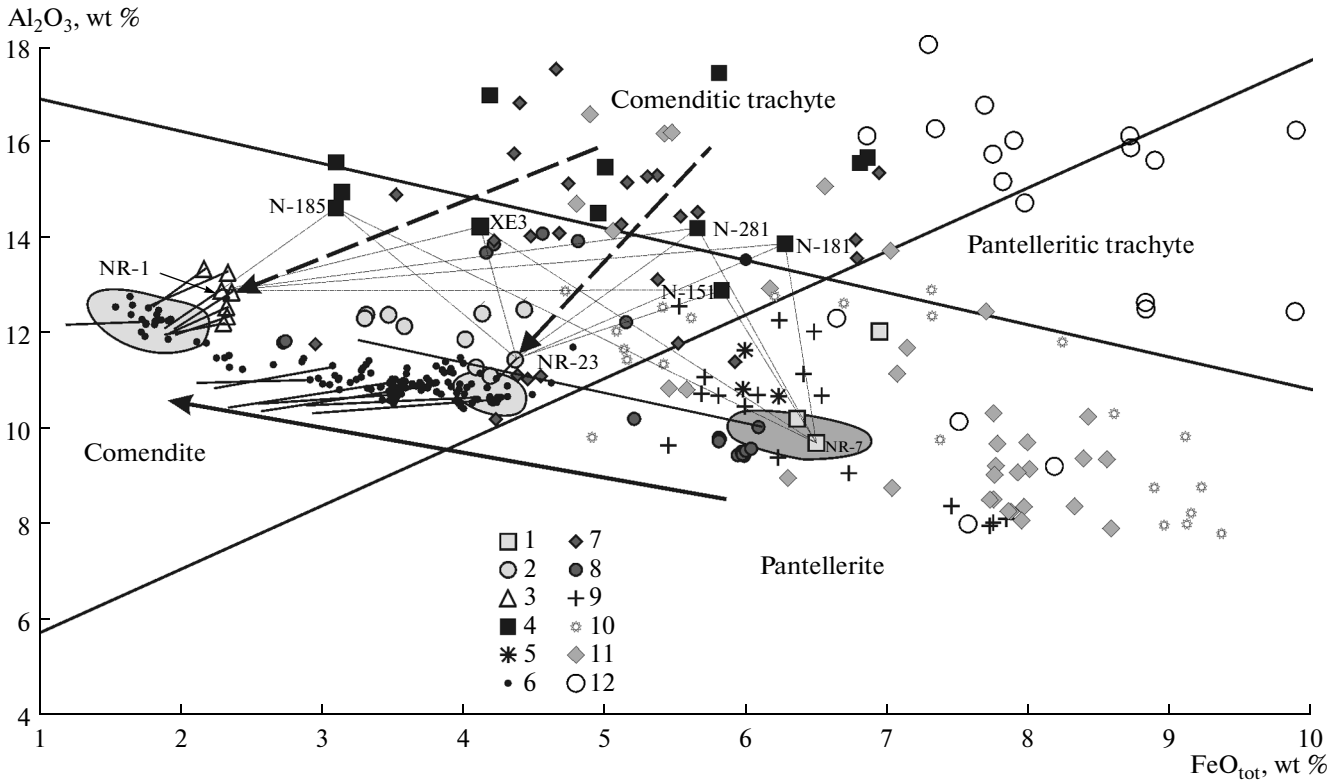

Fig. 17. Al_2O_3–FeO_{tot} diagram for alkaline rocks in areas with comenditic and pantelleritic volcanism. Thin dashed lines extending from the composition points of XE3, N-151, N-181, N-185, and N-281 toward pantellerite NR-7, comendites NR-23, NR-1 are calculated in mass-balance models (Table 15, Figs. 19, 20). Contoured fields correspond to the matrix glasses of pantellerite NR-7, high-Fe comendite NR-23 and low-Fe comendites. The diagram shows passing vectors from the composition points of rocks toward their matrix glasses. Heavy dashed lines with arrowheads show the hypothetical compositional evolution of the melts from the comenditic trachyte field (they are continuations of the evolutionary vectors from rocks to glasses). The heavy line with an arrowhead indicates the compositional evolution of melts produced via mixing comenditic–comenditic (Olkaria Complex) and pantelleritic–comenditic (Dabbahu volcano) melts. Nemrut: (1) pantellerites; (2) high-Fe comendites (Table 7; data from Çubukçu et al., 2012); (3) low-Fe comendites (Table 7); (4) trachytes and comenditic trachytes (Çubukçu et al., 2012); (5) pantelleritic glass in enclave XE3 (Table 8, Fig. 3c); (6) Olkaria Complex (Marshall et al., 2009). (7) Pektusan (Popov et al., 2005, 2008; Fan et al., 2006; Andreeva et al., 2004). (8) Dabbahu volcano (Field et al., 2012, 2013). (9) Gedemsa volcano (Peccerillo et al., 2003). (10) Boseti Complex (Ronga et al., 2010). (11) Pantelleria Island (White et al., 2009). (12) Antarctica (LeMasurier et al., 2011).

Data obtained on the Olkaria Complex led Macdonald et al. (1987) to hypothesize that the fractional crystallization of low-Fe comenditic melt can give rise to more alkaline and Fe richer comenditic and pantelleritic melts. According to mass balance simulations, the crystallization of approximately 75–82 wt % of a quartz and anorthoclase mixture from low-Fe comenditic melt results in a more alkaline high-Fe comenditic melt (Macdonald et al., 1987; Marshall et al., 2009). Also, according to experimental data, low-temperature (liquidus below 700°C) residual pantelleritic melt, including extremely alkaline one, whose NK/A > 2 and whose FeO concentration up to >12 wt %, can be obtained via >25% crystallization of a mixture of quartz and anorthoclase from high-Fe comenditic melt. The results of the mass balance calculations are consistent with experimental data (Scaillet and Macdonald, 2001, 2003, 2006). The model of fractional crystallization of comenditic melt from which a mixture of quartz and anorthoclase is removed was applied to analyze the magma evolution of the Olkaria Complex (Macdonald et al., 2008; Marshall et al., 2009) and Eburru Complex (Ren et al., 2006).

In the Al_2O_3–FeO_{tot} classification diagram, the composition points of comendite–pantelleritic series in various complexes, including Nemrut volcano, define a linear trend from low-Fe comendites to pantellerites (Figs. 8, 11, 17; Table 13). In this context, it would be logical to hypothesize that Nemrut comendites and pantellerites could be produced via fractional crystallization of low-Fe comenditic melt, similar to what took place in the Olkaria Complex in the Kenya Rift. However, arguments presented below completely invalidate this hypothesis.

First of all, this model is inconsistent with data on the age of the rocks and the eruption sequence of the volcano. The trachytic, comendite trachytic, pantelleritic, and high-Fe comenditic lavas of the precaldera stage in the evolution of the stratovolcano were dated at 1 Ma to 89 ka (Çubukçu et al., 2012). The fol-

Table 13. Composition (wt %) of rocks and minerals used in mass balance calculations

Component	NR-7	G7	NR-23	G23	A23	P23	F23	NR-1	G1	A1	P1	F1	NR-5	G5
SiO_2	72.18	72.12	73.63	74.43	67.47	48.59	29.77	74.65	76.38	67.52	48.62	29.68	75.13	76.43
TiO_2	0.40	0.40	0.26	0.25		0.27		0.14	0.03		1.19		0.15	0.06
Al_2O_3	9.67	9.72	11.41	10.77	18.49	0.13		12.51	11.99	18.76	0.57		12.18	11.98
FeO	6.51	6.45	4.37	4.20	0.60	30.53	66.49	2.33	1.92	0.09	27.99	66.67	2.31	1.85
MnO	0.17	0.23	0.11			1.26	3.49	0.05	0.00		1.86	3.05	0.05	0.00
MgO	0.05		0.06			0.24		0.06	0.00		0.65	0.35	0.05	0.00
CaO	0.47	0.32	0.36	0.22		17.66	0.24	0.47	0.21	0.11	16.66	0.25	0.41	0.22
Na_2O	6.11	6.29	5.47	5.53	7.78	1.32		5.26	4.97	7.30	2.47		5.16	5.02
K_2O	4.40	4.36	4.30	4.50	5.55			4.48	4.44	6.23			4.54	4.38
P_2O_5	0.04		0.03					0.05					0.02	

Component	XE3	GXE3	A_{XE3}	$A1_{XE3}$	N-151	N-181	N-185	N-281	IM	MT	AP
SiO_2	69.87	72.50	66.66	67.75	69.48	66.81	70.02	67.43		0.40	1.98
TiO_2	0.33	0.7		0.23	0.52	0.43	0.24	0.49	50.46	19.69	
Al_2O_3	14.19	10.88	19.01	17.78	12.84	13.84	14.58	14.17		0.33	
FeO	4.13	6.09	0.62	1.51	5.83	6.28	3.10	5.66	47.02	73.40	0.78
MnO		0.17			0.13	0.23	0.08	0.21	1.56	1.03	
MgO		0	0.31	0.37	0.02	0.06	0.04	0.14	0.03		
CaO	0.76	0.58	7.52	8.73	0.48	1.07	1.31	1.26			55.71
Na_2O	6.90	4.54	5.88	3.64	5.81	6.21	5.39	5.40			
K_2O	3.81	4.55			4.80	5.02	5.20	5.17			
P_2O_5					0.05	0.06	0.03	0.06			39.52

Rock analyses are normalized to 100 wt %, G—matrix glass, A—anorthoclase, P—clinopyroxene, F—fayalite (numerals after symbols correspond to the numbers of rock samples); XE3—enclave (Fig. 3c) from NR-7; GXE3 is pantelleritic glass in enclave XE3; A_{XE3} and $A1_{XE3}$ are anorthoclase in enclave XE3; N-151, N-181, N-185, N-281 are comenditic trachyte from (Çubukçu et al., 2012); IM—ilmenite, MT—titanomagnetite, AP—fluorapatite.

lowing K–Ar ages (ka) were obtained: 1010 ± 40, 384 ± 23 for the trachytes, 333 ± 41, 264 ± 6, 89 ± 2 for the comenditic trachytes, 567 ± 23, 384 ± 23, 99 ± 3 for the pantellerites, and 310 ± 100, 242 ± 15, 158 ± 4, <89 ± 2 for the high-Fe comendites. The low-Fe comenditic magma was erupted in the caldera after the collapse of the stratovolcano (Fig. 1). This magma produced post-caldera low-Fe comendite dated at 30 ± 2, 24 ± 1, 15 ± 1, 8 ± 3 ka. The low-Fe comendites of analogous major- and trace-element composition were formed in the "rift" zone at about 500 years ago. Thus, data on the volcanostratigraphy of Nemrut provide absolutely no grounds to suggest that the youngest post-caldera low-Fe comenditic melt could give rise to high-Fe comenditic magma.

Mass Balance Simulations

The pre- and post-caldera comendites have remarkably different major- and trace-element compositions (Table 7, Figs. 8, 10). The pre-caldera high-Fe comendites is usually more alkaline (NK/A = 1.1–1.2) than the post-caldera one (NK/A = 0.95–1.17) and the ranges of their Fe concentrations do not overlap (Figs. 8, 11). Comendites and pantellerites of Nemrut volcano not contain of quartz phenocrysts. This is the most conspicuous difference of the mineralogy of the rocks from those in the Kenya Rift. Minute segregations and patches of quartz and anorthoclase in devitrified glass (Figs. 2a, 4g–4i) in some comendite samples from Nemrut were formed after the melt solidified into glass and were not anyhow related to the process of magmatic crystallization. Hence, quartz was not involved in the fractionation of the comenditic and pantelleritic melts. Mass balance simulations demonstrate, for example, for samples NR-1 and NR-5 that no consistent model can be suggested for the fractionation of high-Fe comenditic melt without quartz as a crystallizing mineral (Table 14, models 1 and 2). Any increase in the Fe concentration in the residual melt can result from the crystallization of Fe-free minerals alone (a mixture of anorthoclase and

Table 14. Mass balance models for crystallization of comenditic and pantelleritic melts

Material	1*	2	3	4	5	6	7	8
	NR-1**	NR-5	NR-1	NR-5	NR-23	NR-23	NR-23	NR-23
	Residual melt, wt %							
NR-23	85.62	89.51	40.32	46.41				
NR-1					96.94			
NR-5						96.61		
G1							60.41	
G5								62.18
G7							31.61	30.29
	Crystallizing phases, wt %							
A1	16.87	13.31	42.18	36.89				
P1	0	0	1.22	0.84				
F1	0	0	0.16	0				
MT	0	0	0.11	0	0	0	0	0
IM	0	0	0	0.04	0.16	0.20	0.23	0.20
AP	0.18	0.07	0.13	0.08	0	0	0.02	0.13
Qz			15.82	15.64				
A23					0	0	5.90	5.40
P23					0.68	0.30	0.75	0.24
F23					2.81	2.96	1.20	1.60
Total	102.67	102.88	99.93	99.90	100.59	100.06	100.13	100.04
ΣX^2	2.765	3.465	0.019	0.073	0.713	0.379	0.013	0.008

ΣX^2 is the sum of squared deficiencies (differences between the original and calculated values) for oxide concentrations. See Table 13 for phase symbols.

* Model number; ** Parental melt.

quartz) from the melt. The removal of anorthoclase alone from the low-Fe comenditic melt does not produce a residual melt corresponding to the high-Fe comendite in composition.

Table 14 presents models 2 and 3, in which the fractionation of the low-Fe comenditic melt involves hypothetical quartz. In these models, the minimum deficiencies ($\Sigma X^2 = 0.019–0.073$) are close to the estimates obtained by the crystallization differentiation of the low-Fe comenditic melt from the Olkaria Complex (Macdonald et al., 2008; Marshall et al., 2009), i.e., the total of quartz, anorthoclase, and Fe-bearing phases is close to 60 wt %. However, these models are inapplicable to Nemrut volcano because quartz did nor crystallize from the comenditic and pantelleritic melts.

The arguments presented above are sufficient to demonstrate that the model of the derivation of high-Fe comenditic melt from low-Fe comenditic one is inapplicable to Nemrut. Mass balance simulations demonstrate that a more realistic model is the fractionation of comenditic melt associated with a decrease in its Fe concentration mostly as a consequence of the preferential crystallization of hedenbergite, titanomagnetite and ilmenite. These models are calculated with great deficiencies ($\Sigma X^2 = 0.38–0.71$) using oxide concentrations (Table 14, models 5–6). The model can be tested using trace elements and the distribution coefficients of elements (Table 10) between anorthoclase, hedenbergite, fayalite and matrix glasses of the comendites. Note that the low-Fe comendites typically shows relatively small variations in and lower concentrations of trace elements than in the high-Fe comendites and pantellerites (Table 7, Fig. 10). Mass balance models led us to an unambiguous conclusion: the removal of minor fayalite, hedenbergite and titanomagnetite amounts (3.5–3.7 wt % in total for models 5, 6, Table 14) from the high-Fe comenditic melt cannot any significantly diminish the concentrations of trace elements in the residual low-Fe comenditic melt. Thus, the fractional crystallization of anorthoclase, hedenbergite, titanomagnetite and ilmenite from comenditic melt, in the absence of quartz, cannot yield (according to mass balance calculations) consistent compositional trends of the rocks from either low- to high-Fe comendites and pantellerites or high- to low-Fe comendites.

This led us to analyze other, hopefully more plausible, models for the origin of Nemrut comendites and pantellerites. One of the models is underlain by the assumption of the onset of liquid immiscibility of the high-Fe comenditic melt and its exsolution into low-Fe comenditic and pantelleritic melts. According to the other model, the comenditic and pantelleritic melts are residual melts after the fractional crystallization of the pre-caldera trachytic and trachyte-comenditic magmas.

According to the former model, the geochemical specifics of the derivative residual melts was controlled by the redistribution of elements in the parental comenditic melt in response to gradual changes in its trace-element composition or because of the onset of liquid immiscibility and exsolution into compositionally contrasting liquids. The composition of melt in a chamber can be modified by convection flows, diffusion of components, and fluid–melt interaction, which is facilitated by the fluid phase released during melt degassing. Such process can take place, for example, in the magmatic chambers of rare-metal granitoid melts, with volatile and trace elements accumulated in the apical zone. In evaluating the *P-T-X* parameters, one should take into account possible liquid immiscibility of silicate melts, including acid agpaitic ones, and their exsolution into compositionally contrasting liquids (silicate, silicate–salt, halide, and carbonatite ones). For example, extremely alkaline and Fe-rich (9–17 wt % FeO_{tot}) pantellerites of the Boseti Complex in the Ethiopian Rift contains glasses of different alkalinity, with contrastingly different concentrations of Fe, Al and other elements (Ronga et al., 2010; Macdonald et al., 2012). According to this model, the high-Fe comenditic melt in the chamber exsolved into low-Fe comenditic and pantelleritic melts. The comenditic melt was accumulated in the upper part of the magmatic chamber, whereas the pantelleritic liquid resided in its bottom portion. This follows from the difference between the densities of these melts, which amounts to approximately 0.1 g/cm^3 at a given temperature. The densities of melts of different composition were estimated, depending on temperature, from analyses of the glasses, using numerical techniques discussed in (Peretyazhko, 2010).

This model is consistent with the major- and trace-element composition of the rocks. The composition of the high-Fe comenditic melt (NR-23) was calculated with the minimum deficiencies of oxide concentrations ($\Sigma X^2 = 0.013–0.008$) as a mixture of two melts: one corresponding to the matrix glass and the other being pantellerite NR-7 and comendite NR-1 or NR-5, with a minor admixture (7.3–7.6 wt %) of crystalline phases, first and foremost, anorthoclase (Table 14, models 7, 8). The mass balance calculations were carried out with trace-element distribution coefficients between the melts (glasses from NR-7 and NR-1, NR-5), anorthoclase, hedenbergite, fayalite, and glass (Table 10). The model also took into account zircon fractionation (up to 0.08 wt %) that contained about 1 wt % HfO_2 and ilmenite that contained up to 0.7 wt % Nb_2O_5. The distribution coefficients of trace elements for these minerals were borrowed from (Marshall et al., 2009). Calculation data indicate that the removal of pantelleritic liquid from the high-Fe comenditic melt (for example, as a consequence of liquid immiscibility of this melt) should lead to a residual low-Fe melt with a distribution of trace elements as in the low-Fe comendites (Fig. 18). This model is able to explain the significant decrease in the La, Ce, Zr, and Hf concentrations in the residual low-Fe comenditic melt (Fig. 18a). Discrepancies between the calculated and residual compositions were detected for U, Th, Y and can be explained by redistribution of accessory phase containing these elements between the melts. A disadvantage of this model is the absence of obvious evidence of liquid immiscibility in the comenditic glasses. Fluidal textures with a pronounced boundary between pale and dark glass layers was detected only in sample NR-7. Having similar major-component composition, the dark glass of sample NR-7 is, for example, 200–400 ppm richer in Zr than the pale glass (LA-ICP-MS data). It should also be mentioned that some varieties of the pre-caldera comendites bear lower Fe concentrations (no higher than 3 wt % FeO_{tot}; Fig. 8). These rocks could have been produced by relatively low-Fe comenditic magma that was pooled in the upper parts of magmatic chambers during various evolutionary stages of Nemrut volcano.

A fact of paramount importance for the alternative model of the origin of the residual comenditic and pantelleritic melts is that pantellerite in sample NR-7 contains enclaves (XE3, Fig. 3c) with glass in interstices of anorthoclase microlites (Figs. 3d, 3e). Mass balance calculations indicate that the matrix of enclaves contains approximately 50 wt % of such glass. The bulk composition of enclave XE3 was analyzed by SEM-EDS rastering portions of its matrix (Table 8), and the fact that it contains hedenbergite phenocrysts (Table 2, analysis 4) with inclusions of ilmenite (Table 4) and fluorapatite (Table 5, analysis 4) suggests that this enclave is a relic of comenditic trachyte. At Nemrut volcano, these rocks of various age (333 ± 41, 264 ± 6, 89 ± 2 ka) occur in association with high-Fe comendites and pantellerites. The pantelleritic residual melt was formed as a result of mass anorthoclase crystallization in the trachyte-comenditic magma. The settling of the trachyte-comenditic mush and the pooling of the melt could form a pantelleritic layer in the bottom parts of the magmatic chambers during the pre-caldera stage of the evolution of the volcano.

It is logical to assume that the trachyte-comenditic magma could generate not only pantelleritic but also comenditic melts with various Fe concentrations. This assumption can be tested by mass balance models: how much the mass balance simulations of the composition of the comenditic (NR-23 and NR-1) and

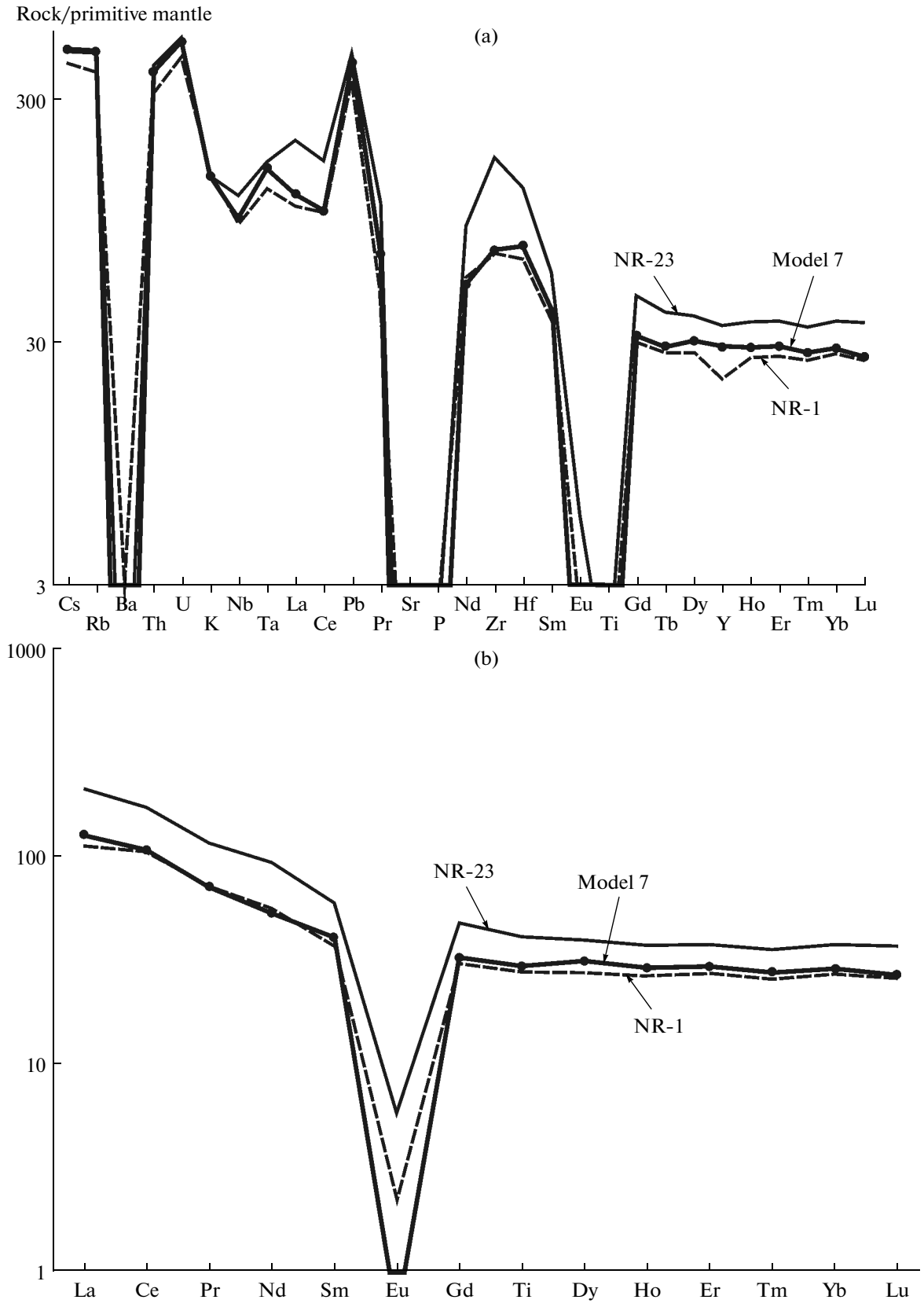

Fig. 18. Results of mass balance simulations of the partition of high-Fe comenditic melt into pantelleritic and low-Fe comenditic melts according to model 7 in Table 14. Concentrations of elements are normalized to the primitive mantle (McDonough and Sun, 1995). (a) Multielemenal and (b) REE patterns.

Table 15. Mass balance models for the fractional crystallization of trachyte comenditic melts

Material	1*	2	3	4	5	6	7	8	9	10	11	12	13	14	15
	Enclave XE3**			N-151			N-181			N-185			N-281		
	Residual melt, wt %														
NR-7	44.77			62.54			41.08			49.39			39.91		
NR-23		48.66			69.92			45.71			54.73			45.14	
NR-1			49.62			72.59			47.07			55.47			49.29
	Crystallizing phases, wt %														
A_{XE3}	8.36	0.00	0.00	35.25	26.05	20.02	51.80	46.05	43.07	51.30	43.14	39.57	53.43	46.97	41.90
Al_{XE3}	45.87	48.50	45.81	0.00	0.00	1.08	0.00	0.00	0.00	0.00	0.00	0.00	0.00	0.00	0.00
F23	0.00	0.32	2.17	1.72	1.84	3.37	2.95	2.58	3.53	0.00	0.00	0.00	1.33	2.62	2.13
P23	1.76	2.23	2.31	0.58	0.18	0.44	3.56	3.51	3.93	0.00	1.90	4.59	5.24	4.32	4.26
MT	0.00	0.50	0.00	0.00	1.81	2.21	0.00	1.63	1.85	0.00	0.00	0.04	0.00	0.00	2.10
IM	0.00	0.00	0.29	0.50	0.00	0.00	0.50	0.00	0.00	0.00	0.00	0.28	0.58	0.71	0.00
AP	0.04	0.00	0.00	0.00	0.17	0.00	0.14	0.21	0.05	1.14	0.80	0.15	0.02	0.27	0.21
Total	100.79	100.21	100.20	100.59	99.96	99.70	100.03	99.68	99.51	101.82	100.58	100.08	100.50	100.03	99.87
ΣX^2	0.378	0.014	0.125	0.471	0.077	0.311	0.088	0.185	0.402	2.725	1.052	0.486	1.381	0.675	0.424

ΣX^2 is the sum of squared deficiencies (differences between the original and calculated values) for oxide concentrations. See Table 13 for phase symbols.

* Model number; ** Parental melt.

pantelleritic (NR-7) melts are consistent with the composition of the comenditic trachyte (enclave XE3 and samples N-151, N-181, N-185, N-281 from Çubukçu et al., 2012) at fractional crystallization of anorthoclase, hedenbergite, fayalite, titanomagnetite, ilmenite, fluorapatite from the parental melts. In these models, we assumed the composition of the anorthoclase with various Fe concentrations as in enclave XE3; hedenbergite, fayalite and ilmenite as in pantellerite NR-7 and the pre-caldera (NR-23) and post-caldera (NR-1, NR-5) comendites (Table 13). According to the simulated models, the residual melts with compositional variations from low-Fe comendites to pantellerites can be obtained via the fractional crystallization of phenocrysts in the parental trachyte-comenditic magmas (Table 15). The process yields 41 to 73 wt % residual melts with various Fe concentrations. The trachyte-comenditic melt can yield the smallest amount (41–63 wt %) of pantelleritic melt and the greatest amount of low-Fe comenditic melt (47–73 wt %). In all models, the dominant fractionated phase is anorthoclase (20–52 wt %). The transition from pantelleritic to low-Fe comenditic melt is coupled with a decrease in the anorthoclase proportion among the crystallizing phases and an increase in the proportions of hedenbergite and fayalite. The results of mass balance simulations are consistent with the composition of the rocks. Mass balance simulations (Table 15, models 1–2, 4–5, 7–8, 10–11, 13–14) can explain why the concentrations of trace elements in pantellerite NR-7 and high-Fe comendite NR-23 are similar (Table 7) and why the multielemental patterns of the rocks (Fig. 10) show the deepest Ba and Sr anomalies. The reasons for these features is that insignificant variations in the weight percentage of the residual melt (an increase by 3–5 wt %) and anorthoclase (decrease by 5–9 wt %) do not any significantly modify the geochemistry of the pantelleritic and high-Fe comenditic residual melts (Figs. 19, 20). Crystallization of anorthoclase with elevated Ba and Sr concentrations from the parental trachyte-comenditic melts in the practically absolute absence of other minor elements in this minerals (Table 9) results in comenditic and pantelleritic residual melts with anomalously low Ba (2–13 ppm) and Sr (0.5–3 ppm) concentrations and in the very strong enrichment of other minor elements in these melts. An anomalously strong decrease in the Sr concentration in the residual melts can also be enhanced by the crystallization of fluorapatite, which contains up to 1 wt % SrO (Table 5, analysis 4). The higher Ba concentrations (up to 30 ppm) in the low-Fe comendite is explained by a decrease in the weight percentage of anorthoclase during the crystallization of the trachyte-comenditic melt (Table 15, models 3, 6, 9, 12, 15).

According to (Çubukçu et al., 2012), the dominant pre-caldera volcanic rocks of Nemrut volcano are trachytes, comenditic trachytes, and high-Fe comendites (Fig. 1). Pantellerites was also erupted during various pre-caldera evolutionary stages of the volcano (at 567 ± 23, 384 ± 23, 99 ± 3 ka) but is found rarely. The trachyte-comenditic magma likely more significantly evolved toward residual high-Fe comenditic than toward pantelleritic compositions. In the trachyte-

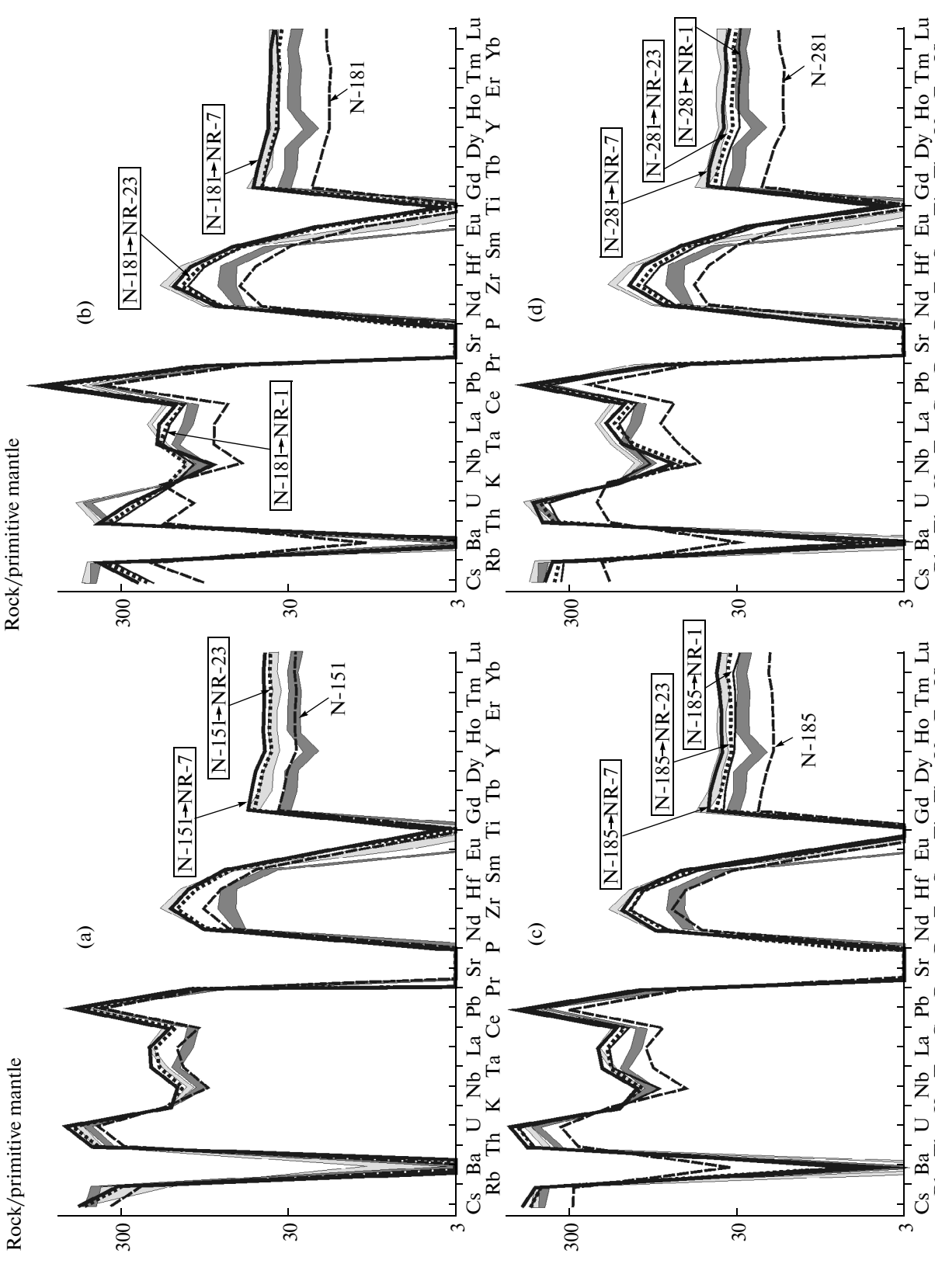

Fig. 19. Primitive mantle–normalized (McDonough and Sun, 1995) multielemental patterns simulated with mass-balance models for the fractional crystallization of trachyte-comenditic melts. Simulated models in Table 15: (a) models 4 and 5; (b) models 7–9; (c) models 10–12; (d) models 13–14.

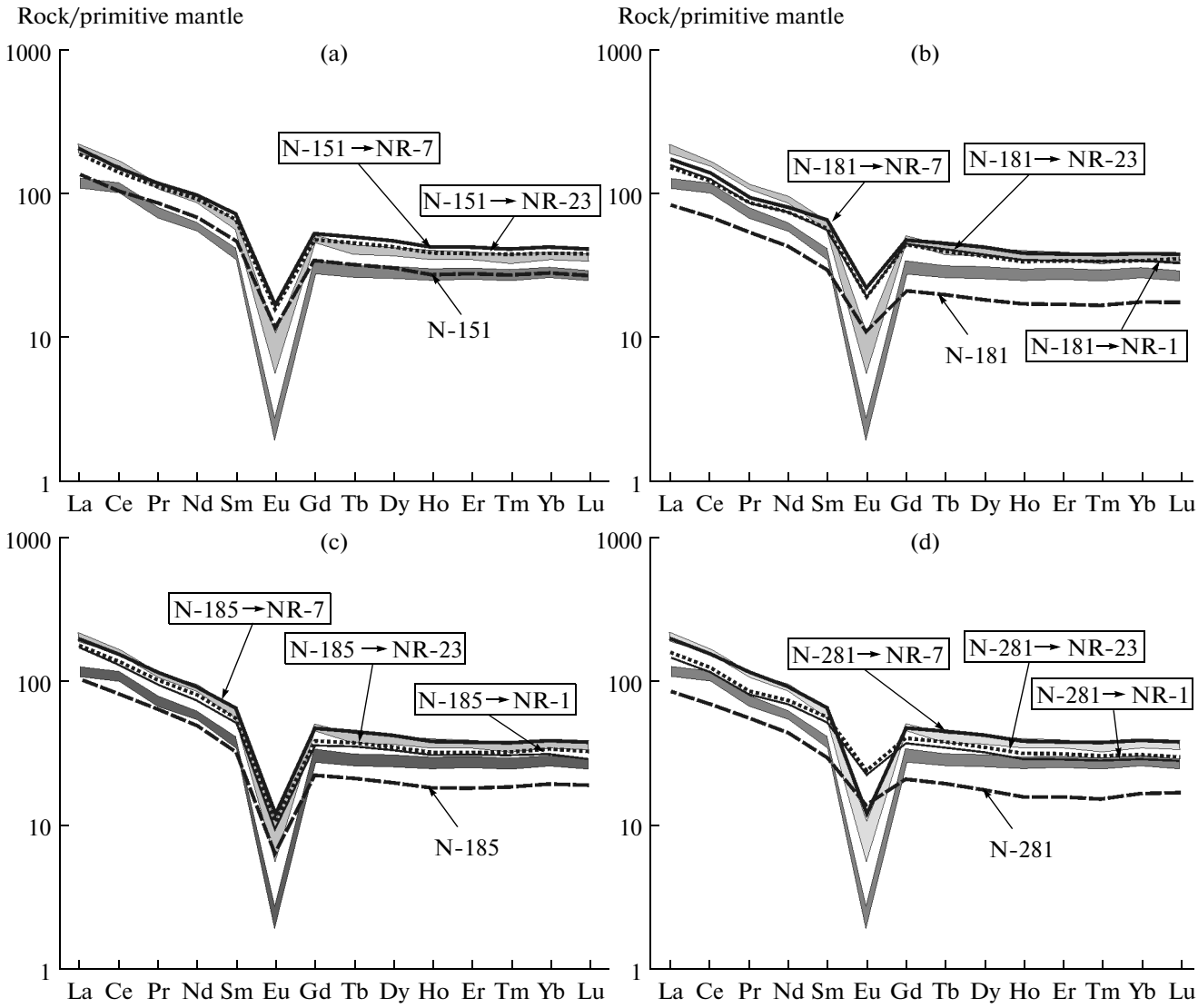

Fig. 20. Primitive mantle-normalized (McDonough and Sun, 1995) REE patterns simulated with mass-balance models for the fractional crystallization of trachyte-comenditic melts. Simulated models in Table 15: (a) models 4 and 5; (b) models 7–9; (c) models 10–12; (d) models 13–14.

comenditic magmatic mush, residual high-Fe comenditic melts likely have got similar Fe concentrations and higher alkalinity than in the parental melt because of an increase in the percentage of crystallizing Fe-bearing minerals (hedenbergite, fayalite, Fe and Ti oxides) relative to anorthoclase. At the magmatic evolution toward pantelleritic melt, the dominant crystallizing mineral was anorthoclase, and the residual melt was enriched in Fe and alkalis relative to the parental trachyte-comenditic one (Table 15, models 1, 4, 7, 10, 13).

Mass balance simulations indicate that the trachyte-comenditic melts can also yield residual high-Fe comenditic melt (Table 15, models 3, 6, 9, 12, and 15). These melts contain less Fe because of an increase in the percentage of crystallizing clinopyroxene and fayalite relative to anorthoclase. Only the fractional crystallization of the trachyte-comenditic melt whose composition corresponds to comenditic trachyte N-281 yields concentrations of trace elements approaching those in the low-Fe comendites (Table 15, Figs. 19d, 20d). The reason for this is that the post-caldera low-Fe comenditic melts with little varying geochemical characteristics (Table 7) could be formed from a single source of trachyte-comenditic magma of composition close to that of comenditic trachyte N-281.

In Fig. 17, dashed lines show the trends of the Al_2O_3 and FeO_{tot} concentrations of the rocks (XE3, N-185, N-151, N-281, and N-181) and their matrix glasses in samples NR-1, NR-23, NR-7. The trends are directed similarly, and at similar angles, to the lines connecting the composition points of the rocks and

matrix glasses, and this is consistent with the model of fractional crystallization (Table 15). If the pantelleritic and comenditic melts were produced by magmas of similar composition, then the intersections of the continuations of the evolutionary trends (rock–glass tie lines) should correspond to the original composition of this common parental magma. The intersections of the trends for Nemrut lie in the field of comenditic trachyte (Fig. 17), and this proves the plausibility of the model of fractionation of parental trachyte comenditic magma.

Note that the directions of the evolutionary trends of the melts drawn from the composition points of the rocks to matrix glasses are different for comendites from Nemrut and the Olkaria Complex (Fig. 17). The trends for comendite in the Kenya Rift lie within the field of the linear trend from high- to low-Fe varieties, which is in conflict with the model (Macdonald et al., 1987; Marshall et al., 2009; Scaillet and Macdonald, 2001, 2003, 2006) of fractionation of low-Fe comenditic melt and its evolution toward Fe richer comenditic and pantelleritic melts. Mass balance models (our unpublished data) indicate that such trends for rocks from the Olkaria Complex likely resulted from the mixing of comenditic magmas with variable concentrations of Fe and trace elements. Evidence of mixing between pantelleritic and comenditic magmas at Dabbahu volcano is presented in (Field et al., 2013). As an illustrative example, Fig. 17 shows such a trend for pantellerite whose matrix contains high-Fe comenditic glass.

Crystallization of Comenditic and Pantelleritic Magmas

It is interesting to analyze parameters that can affect proportions of phases crystallizing from comenditic and pantelleritic melts. Below we employ experimental data on the stability fields of the minerals at various redox and P–T parameters. This information was obtained for comendites from the Olkaria Complex (Scaillet and Macdonald, 2001, 2003), pantellerites from the Eburru Complex (Scaillet and Macdonald, 2006), and Pantelleria Island (Di Carlo et al., 2010). The crystallization of comenditic and pantelleritic melts was studied within the temperature range of 660–800°C, pressures of 0.25–1.5 kbar, and oxygen fugacity below the Ni–NiO buffer. The experiments have determined the composition of the residual glasses and minerals and delineated the crystallization fields of anorthoclase, quartz, Fe and Ti oxides, hedenbergite, fayalite, amphibole, chevkinite, aenigmatite, biotite, and fluorite depending on P-T conditions, oxygen fugacity, and the contents of water dissolved in the melt.

All comendite and pantellerite varieties from Nemrut volcano typically contain similar associations of phenocryst minerals (anorthoclase, hedenbergite, fayalite, ilmenite ± titanomagnetite), with little varying compositions of the minerals (Tables 1–4, Figs. 5, 6). According to (Scaillet and Macdonald, 2001, 2003), the phenocrysts crystallized from mildly alkaline (NA/A = 1.05) comenditic melt under pressures of 0.5 and 1.5 kbar, oxygen fugacity of $\Delta\log f_{O_2}$ (ΔNNO) from −1.6 to +3.6. The melt was derived from low-Fe comendite ND002 from the Olkaria Complex, whose composition is as that of the pre-caldera comendite at Nemrut (Fig. 21, Table 7). According to (Di Carlo et al., 2010), similar mineral phases are formed in pantelleritic melt (NK/A = 1.4) at 1 and 1.5 kbar and $\Delta\log f_{O_2}$ < NNO derived from pantellerite PAN01113 from Pantelleria Island. The compositions of this pantellerite and sample NR-7 are similar. According to QUILF calculations (Table 11), equilibrium crystallization of hedenbergite, ilmenite and fayalite in Nemrut rocks occurred at an oxygen fugacity below the FMQ buffer, $\Delta\log f_{O_2}$ (ΔFMQ) from −1.08 to −1.27 and a pressure higher than 2.3 kbar. These parameters are close to those of experiments under a pressure of 1.5 kbar with comenditic melt at ΔNNO = −1.6 (Scaillet and Macdonald, 2001, 2003) and with pantelleritic melt at $\Delta\log f_{O_2}$ < NNO (Di Carlo et al., 2010). It is interesting to consider more closely the phase diagrams of these melts (Fig. 21).

It follows from data in (Scaillet and Macdonald, 2001) that a pressure increase from 0.5 to 1.5 kbar expands the stability field of anorthoclase, hedenbergite, Fe and Ti oxides into the low-temperature region (to approximately 700°C) at an increase in the water content in the comenditic melt up to its saturation at about 5 wt % water (Fig. 21a). At temperatures above 750–770°C, a decrease in the water content in the melt from 5 to 3 wt % results in a change in the mineral association: the first phases to crystallize are Fe and Ti oxides, and they are followed by hedenbergite, anorthoclase, quartz and fayalite. At an H_2O content of 1–2 wt %, hedenbergite is unstable, and amphibole (ferrorichterite) is formed instead. In pantelleritic melt under a pressure of 1.5 kbar, the first liquidus phase can be either clinopyroxene or titanomagnetite, and a further temperature decrease or a decrease in the water content lead to the crystallization of anorthoclase, aenigmatite, quartz, and amphibole (Fig. 21b). A pressure decrease to 1 kbar results in that the melt nearly saturated with H_2O crystallizes first clinopyroxene (Fig. 21c), and then at 0.5 kbar, this mineral becomes stable with anorthoclase, quartz, amphibole at any temperature (Fig. 21d). A pressure increase enhances water solubility in pantelleritic melt, significantly diminishes the crystallization field of quartz, modifies phase relations between clinopyroxene and anorthoclase (Figs. 21b–21d).

Nemrut comendites and pantellerites contain >90% glass, in which devitrified glass domains are rare. Because of this, the degree of Fe oxidation is thought to reflect the degree of melt oxidation. The

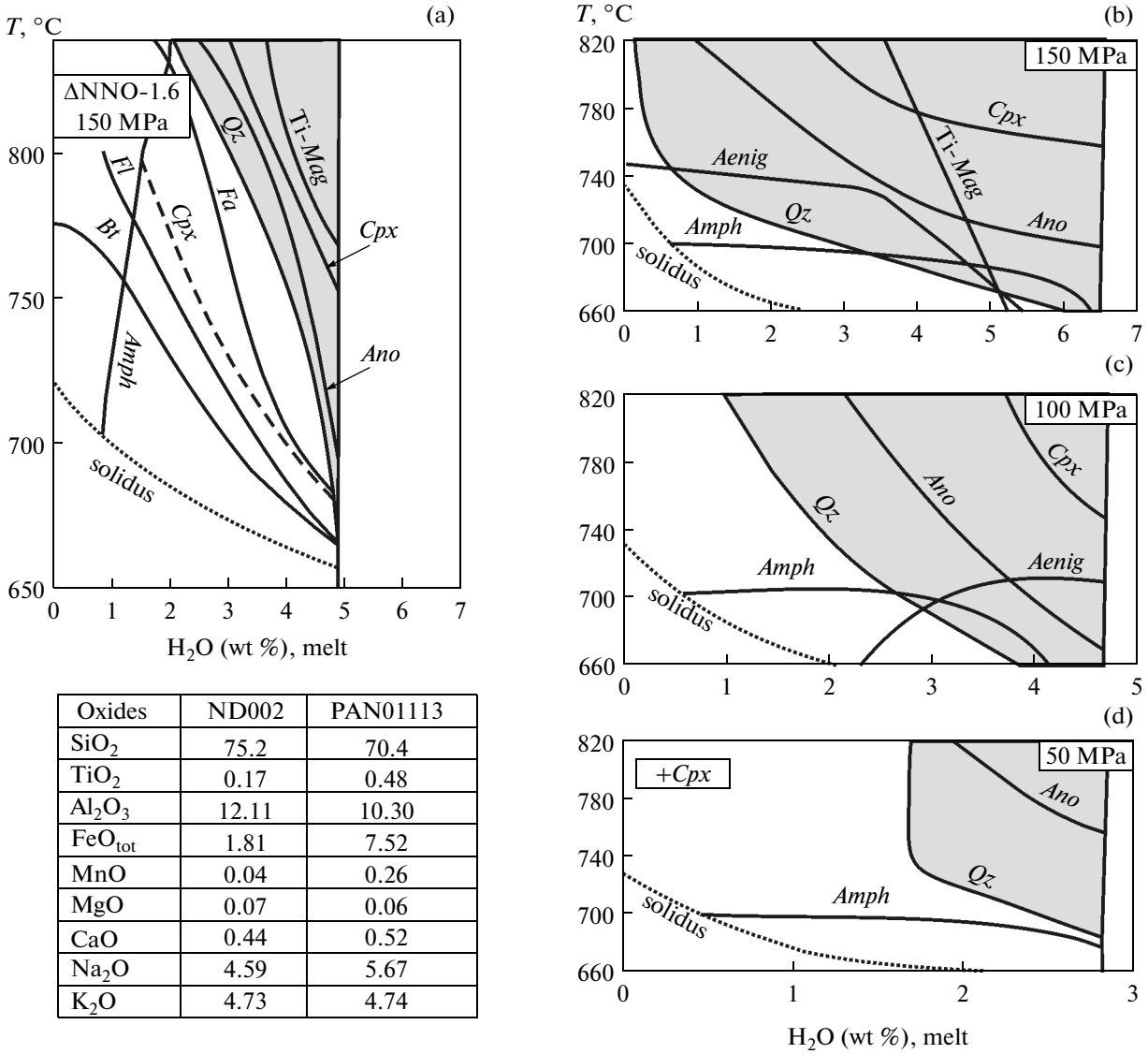

Oxides	ND002	PAN01113
SiO_2	75.2	70.4
TiO_2	0.17	0.48
Al_2O_3	12.11	10.30
FeO_{tot}	1.81	7.52
MnO	0.04	0.26
MgO	0.07	0.06
CaO	0.44	0.52
Na_2O	4.59	5.67
K_2O	4.73	4.74

Fig. 21. Phase diagrams for comenditic and pantelleritic melts. (a) According to Fig. 2 in (Scaillet and Macdonald, 2001); (b–d) according to Fig. 4 in (Di Carlo et al., 2010). The table presents analyses of melts ND002 and PAN01113. The gray field corresponds to the crystallization of quartz-free melts. Phase symbols: Ti-*Mag*—titanomagnetite, *Cpx*—clinopyroxene, *Ano*—feldspar (anorthoclase), *Qz*—quartz, *Amph*—amphibole, *Aenig*—aenigmatite, *Bt*—biotite, *Fa*—fayalite, *Fl*—fluorite.

$Fe_2O_3/(Fe_2O_3 + FeO)$ ratio of the low-Fe comendites, high-Fe comendite NR-23, and pantellerite NR-7 varies insignificantly, from 0.31 to 0.39. The likely reason for this is that the comenditic and pantelleritic magmas occurred under similar redox conditions (Table 11). The arrangement of the crystallization fields of minerals in Fig. 21 suggests that the first minerals to crystallize from the comenditic melt were Fe and Ti oxides and then hedenbergite. For Nemrut volcano, experimental data are consistent with mineral relations in the rocks. In sample NR-23, ilmenite microlites were found as inclusions in hedenbergite (Fig. 2a), while anorthoclase phenocrysts contain hedenbergite inclusions (Fig. 2d), which suggests that the feldspar crystallized later. Fayalite phenocrysts without dissolution traces were found in all samples and suggest their equilibrium with the melt (Figs. 2b, 2c, and 2e). According to experimental data, fayalite can be formed at a pressure of 1.5 kbar ($\Delta NNO = -1.6$) after quartz crystallization in a comenditic melt and is absent from pantelleritic melt. This led us to suggest that the stability field of fayalite expands with increasing pressure if the melt does not contain quartz. This is consistent with experimental data and thermodynamic simulations in the $CaO–FeO–Fe_2O_3–TiO_2–SiO_2$ system (Xirouchakis and Lindsley, 1998), according to which fayalite, hedenbergite and ilmenite (in the absence of quartz) can simultaneously crystallize within a broad pressure range (the calculations were conducted for

pressures up to 3.8 kbar) at temperatures of 650–1000°C and ΔFMQ up to –6.

According to (Scaillet and Macdonald, 2008), the MgO concentration of clinopyroxene decreases from 12–14 to 2.5–3.2 wt % in comenditic melt (experiments with ND002) at an oxygen fugacity of ΔNNO from –1.6 to –2.1, temperature of 788–790°C, and pressure increasing to 1.5 kbar. In pantelleritic melt (experiments with PAN01113), Fe-rich hedenbergite crystallizes that contains 0.4–0.6 wt % MgO regardless of pressure at temperatures of 680–725°C (Di Carlo et al., 2010). These data indicate that a small MgO admixture (0.2–0.6 wt %) in hedenbergite from Nemrut comendites could result from either a low temperature of its crystallization or an elevated pressure (>1.5 kbar).

Nemrut comendites and pantellerites contain no amphibole, likely because the phenocrysts crystallized at temperatures above 700°C from a melt that contained up to 3 wt % water (data on glass in MI, Fig. 12a). No aenigmatite was found in either the comenditic melts with various Fe concentrations (Scaillet and Macdonald, 2001, 2003) or the pantelleritic melts (Scaillet and Macdonald, 2006). In experiments with pantelleritic melt (Di Carlo et al., 2010), the stability field of this mineral expands with increasing pressure at high contents of dissolved water (Figs. 21b–21d). Neither comendite nor pantellerite samples from Nemrut available for us contained aenigmatite. However, this mineral was found (Çubukçu et al., 2012) in the pre-caldera high-Fe comendites and pantellerites. Conceivably, the aenigmatite stability field strongly depends on local temperature, pressure and alkalinity fluctuations and water contents in various portions of the alkaline melts. The occurrence of quartz in the recrystallized enclaves of comenditic trachyte (XE2 in Fig. 3b) in pantellerite NR-7 and in the devitrification products of the matrix glasses of the comendites (Figs. 4h, 4i) and among aggregates of some MI in phenocrysts is explained by low-temperature and low-pressure parameters under which the glass was modified after the melts were quenched. The melts likely lost much of their dissolved water due to degassing during eruptions. Thus, the phase composition of the comendites and pantellerites and the estimated crystallization parameters of their minerals are largely consistent with experimental data.

The rocks produced by the comenditic and pantelleritic magmas significantly differ in alkalinity and concentrations of Fe and trace elements (Table 7, Fig. 10). It follows from our mass balance models and analysis of the geochemistry of the rocks and glasses that the residual melts might likely be formed after 40–70% crystallization of parental trachyte comenditic melts corresponding to comenditic trachyte in composition (Table 15). According to our simulation results, the compositional variations of the comenditic and pantelleritic melts can be explained by variations in the proportions of phases crystallizing from the parental magmas: anorthoclase, hedenbergite, fayalite, Fe and Ti oxides.

The fractional crystallization of trachytic and trachyte comenditic melts during the pre-caldera stage likely produced predominantly Fe-rich comenditic melts. Judging by the proportions of pre-caldera comendite and pantellerite in the volcano (Fig. 1), pantelleritic magmas were also formed, but their amount was subordinate. The variations in the major- and trace-element composition of the post-caldera low-Fe comendites were insignificant (Table 7, Fig. 10). This means that after the origin of the caldera at 30 ± 2 ka (the age of the oldest comendites in the caldera) before the reactivation of Nemrut volcano at historical time at approximately 500 years ago (comendites in the "rift" zone), low-Fe comenditic melt of unvarying composition was erupted. This magma likely came from a single source of little varying composition. This could be the latest portions of the pre-caldera magma (approximately 90 ka, judging from the age of the youngest comenditic trachyte), whose crystallization conditions changed after ignimbrite trachyte eruptions and ensuing collapse of the stratovolcano. Our estimates suggest that mineral phenocrysts of similar composition in the comenditic and pantelleritic melts were formed under similar P–T parameters and an oxygen fugacity below the FMQ buffer (Table 11). The possible reasons for the change in the crystallization regime of the trachyte comenditic melt were variations in the pressure and content of water dissolved in the melt. Pressure can remarkably modify the stability fields of minerals during the crystallization of pantelleritic and comenditic melts, and an increase in the water content of comenditic melt by 3–4 wt % modifies phase proportions and increases the concentrations of hedenbergite, fayalite, Fe and Ti oxides at the sacrifice of anorthoclase (Fig. 21). Variations in pressure and dissolved water content in the parental trachyte comenditic magma could give rise to residual melts of various composition, from pantelleritic to comenditic, with variations in the Fe concentration.

Eruptions of trachybasaltic and low-Fe comenditic magmas occurred approximately 500 years ago in the "rift" zone or at closely spaced eruption centers (Fig. 1). We believe (Peretyazhko et al., 2015) that trachybasaltic magma was injected in the chamber with low-Fe comenditic melt, and this resulted in the hybrid post-caldera benmoreitic magma with anomalously low Ba and Sr concentrations. According to a possible alternative scenario, the low-Fe comenditic melt could be formed by the fractional crystallization of trachybasaltic melt in a local magmatic chamber during the post-caldera stage. The geochemistry of the rocks is generally consistent with this hypothesis, because the configuration of the normalized multielemental patterns and the levels of trace-element con-

centrations of the low-Fe comenditic melt are consistent with the model of the fractional crystallization of the parental trachybasaltic melt (Fig. 10). The time span between the last pre-caldera eruptions of ignimbrite trachyte (100–80 ka) and comenditic magma in the caldera (30 ± 2 ka) is 50–70 ka. Estimates based on U–Th isotopic data suggest that the accumulation rate of comenditic melt in the Olkaria Complex was 2.5×10^{-3} km^3 /year (Heumann and davies, 2002) and that of rhyolite melt of Alid volcano ranged from 2×10^{-4} to 1×10^{-3} km^3 /year (Lowenstern et al., 2006). This accumulation rate was high enough to produce local chambers during the post-caldera evolutionary stage of Nemrut volcano. The chambers were filled with low-Fe comenditic melt generated by the fractional crystallization of trachybasaltic melt, which came from a mantle source. This model is, however, in conflict with the following facts. Trachybasaltic melt is known to fractionate according to the so-called trachytic trend to produce residual melts of trachydacitic and trachytic composition. This conclusion is consistent with both experimental data (Nekvasil et al., 2004) and a common evolutionary compositional trend of rocks of trachybasalt–trachyte–comendite series at both Nemrut itself (Fig. 7) and several other volcanic complexes in various geodynamic environments: oceanic islands, continental rifts, and convergent zones of lithospheric plates (Mungall and Martin, 1995; Bohrson and Reid, 1997; Civetta et al., 1998; Gagnevin et al., 2003; Peccerillo et al., 2003; White et al., 2009; Ronga et al., 2010; LeMasurier et al., 2011; Çubukçu et al., 2012; Field et al., 2013; Andreeva et al., 2014). In Nemrut trachybasalt, the composition of residual glasses in interstices between phenocrysts also corresponds to trachytic melt with 7–8 wt % Na_2O and 1.7–5 wt % K_2O (Peretyazhko et al., 2015). Because of this, fractionation of trachybasaltic melt cannot produce residual comenditic melt without generating intermediate trachytic magmas. No trachytes were formed during the post-caldera stage of Nemrut volcano. The post-caldera low-Fe comendites contain only relics (glass and xenocrysts) of benmoreitic magma and enclaves of post-caldera benmoreites. The presence of benmoreite rocks could have been explained by the fractionation of trachybasaltic melt, but as was demonstrated in (Peretyazhko et al., 2015), these rocks were formed by a hybrid magma of benmoreite composition after the mixing of trachybasaltic and low-Fe comenditic melts.

Magmatic sources are analyzed using paired ratios of incompatible elements, for example, Th/Yb–Ta/Yb, because such ratios cannot be significantly modified by magmatic differentiation. The Th/Yb–Ta/Yb diagram in Fig. 22 shows that all volcanic rocks of Nemrut volcano, such as mugearites, trachytes, trachytic comendites, pantellerites, and comendites, except only its trachybasalts and hybrid rocks (benmoreites), define a compact field above the region of mantle values. The trachybasalts of the "rift" zone possess geochemical characteristics remarkably different from those of this field, and this rock plots between OIB and E-MORB basalts (Figs. 10, 22). This provides grounds to believe that the trachybasaltic magma erupted in the "rift" zone could not be a source of post-caldera low-Fe comenditic melt. The differentiated magma series of Nemrut was likely formed via the fractionation of another parental trachybasaltic melt, which could have had a major-component composition similar to that of basalts in the "rift" zone and which came from a mantle source to the crust more than 1 Ma ago.

Estimated Conditions under Which the Comenditic and Pantelleritic Magmas Were Produced

According to the results of our QUILF calculations, ilmenite, fayalite, and hedenbergite simultaneously crystallized under a pressure of 3 kbar from the pre-caldera high-Fe comenditic and pantelleritic melts and a pressure of >2.3 kbar from the post-caldera high-Fe comenditic melt (Table 11). This conclusion is underlain by the fact that, according to simulations, quartz should crystallize from the melts at pressures lower than these values, and hence, the absence of quartz phenocrysts from the rocks can be interpreted as an indication of elevated pressure in the comenditic and pantelleritic magmas. Seismic data on Nemrut volcano (Çubukçu et al., 2012) indicate that the upper part of the chamber whose low-Fe comenditic melt was erupted in the caldera in the "rift" zone occurs at a depth of 6 km, which corresponds, depending on the assumed density of the continental crust (2600–2800 kg/m^3) to a lithostatic pressure of 2–2.5 kbar. These value are close to the pressure estimates for the post-caldera low-Fe comenditic melt. A lithostatic pressure greater than 3 kbar at the crystallization of the phenocrysts in the pre-caldera comenditic and pantelleritic melts may suggest that the magmatic chamber occurred at depth greater than 10 km. This conclusion is hard to test for the pre-caldera episode of Nemrut volcano, but the estimates themselves are consistent with estimates of the lithostatic pressure at other volcanic centers containing similar rocks. For example, Andreeva et al. (2014) arrived at the conclusion (with reference to seismic profiling data) that the magmatic evolution of Pektusan volcano, which resulted in high-Fe comenditic and pantelleritic residual magmas, could proceed in chambers at depths of 10–12 km. According to (Field et al., 2013), comenditic and pantelleritic magmas could be generated at the fractionation of trachybasaltic melt of Dabbahu volcano under a pressure close to 4.3 kbar at a depth of 10–15 km. Lower pressure estimates of 1–1.5 kbar were obtained by QUILF calculations for the crystallization of comenditic and pantelleritic melts in the Kenya Rift (Ren et al., 2006) and Pantelleria Island (White et al., 2005, 2009). According to experimental data (Di Carlo et al., 2010), the reservoir of pantelleritic

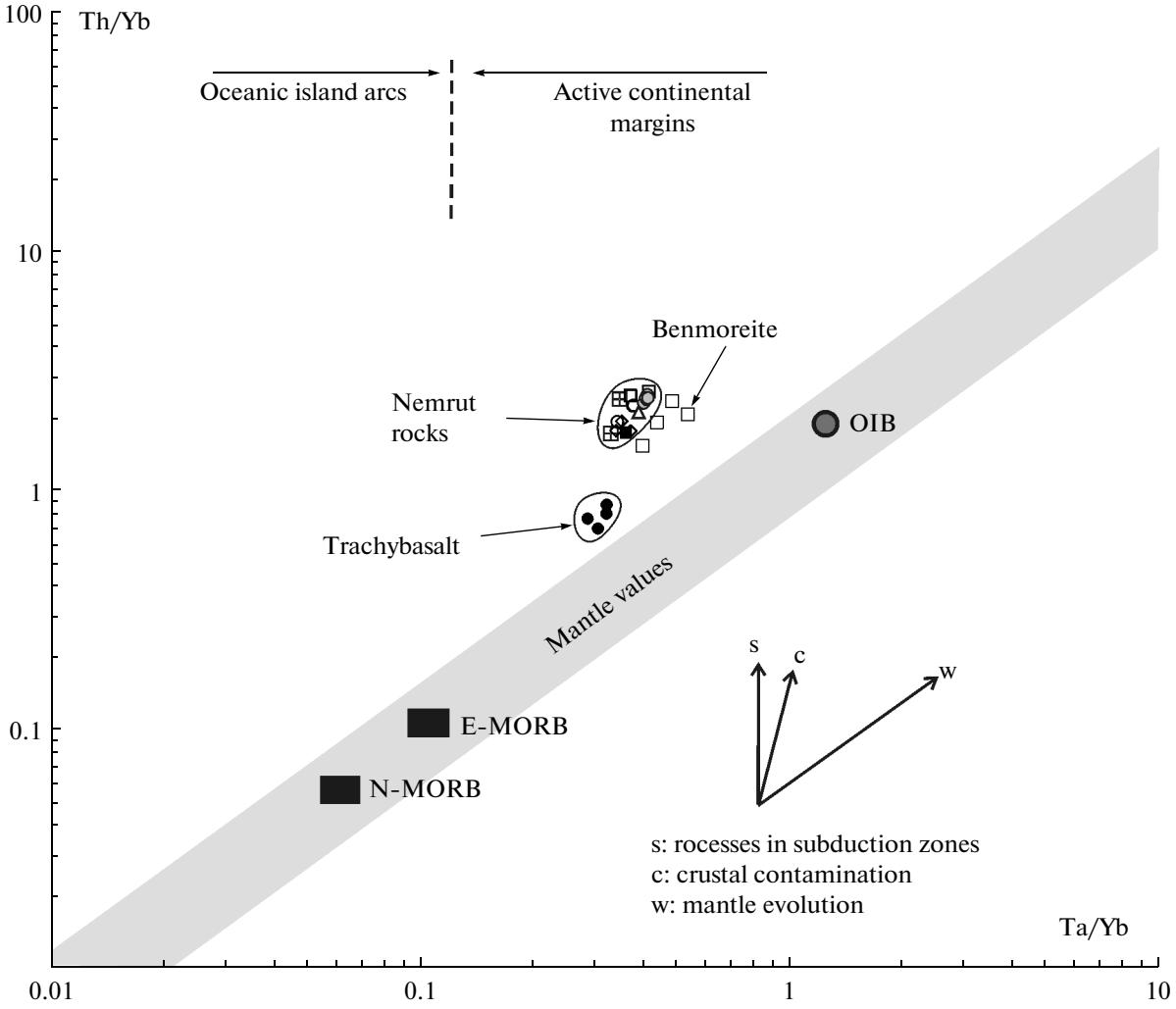

Fig. 22. Th/Yb vs. Ta/Yb diagram for rocks from Nemrut volcano. See Fig. 7 for symbol explanations.

magma beneath Pantelleria Island occurred at a depth of 5 ± 1 km at a pressure of 1.2 ± 0.2 kbar and a temperature of 730 ± 10°C, and the magma contained approximately 4 wt % H_2O at an oxygen fugacity of ΔNNO −1.5. It should also be mentioned that the occurrence of aenigmatite in the rocks cannot be regarded as evidence of low-pressure crystallization of the comenditic and pantelleritic magmas because experimental data in (Di Carlo et al., 2010) indicate that this mineral crystallizes in a water-rich pantelleritic melt (NK/A > 1.2, H_2O > 2.8 wt %) under pressures higher than 1 kbar (Fig. 21).

The model of the evolution of comenditic and pantelleritic melts from low-Fe and minimally alkaline ones to high-Fe comenditic and maximally alkaline pantelleritic melts, which was suggested to explain the origin of the rocks in the Renya Rift (Macdonal et al., 1987; Marshall et al., 2009; Scaillet and Macdonald, 2001, 2003, 2006), is inapplicable to Nemrut volcano. According to mass balance calculations, this evolution can be possible at >75 wt % crystallization of a mixture of quartz and anorthoclase. The segregation of low-temperature (<750°C) residual melt from the magmatic mush at such a high degree of its crystallinity is highly problematic. To be concentrated, such melt should have got an anomalously low viscosity and be highly fluidal. Our calculations (Table 15) indicate that residual comenditic and pantelleritic melts can be generated by trachyte comenditic magma at its no more than 40–50% crystallization. The separation of residual melts from magmatic mush (as in enclave XE3, Figs. 3d, 3e) can be facilitated by fluid bubbles formed at the degassing of the trachyte comenditic melt.

Finds of quartz-free comendite and pantellerite of composition similar to that of rocks in the Olkaria Complex at Nemrut and Dabbahu volcanoes (Field et al., 2013) and the results of mass balance simulations (Table 14) demonstrate that the model suggested for melt evolution in (Macdonald et al., 1987; Marshall et al., 2009; Scaillet and Macdonald, 2001, 2003,

2006) is inapplicable to natural magmatic processes. Researchers who studied comendites and pantellerites of the volcanoes of Gedemsa (Peccerillo et al., 2003), Boseti (Ronga et al., 2010), Dabbahu (Field et al., 2013), Pektusan (Andreeva et al., 2014), volcanoes at the Azores (Mungall and Martin, 1995), Socorro Island (Bohrson and Reid, 1997), Pantelleria Island (Civetta et al., 1998; White et al., 2009), pantelleritic trachyte and pantellerite at the Kerguelen Islands (Gavnevin et al., 2003) and Antarctica (LeMasurier et al., 2011) arrive at the conclusion that comenditic and pantelleritic magmas are generated via successive fractionation of alkali basaltic and trachybasaltic melts with the origin of intermediate trachytic and trachyte comenditic magmas. An analogous conclusion can also be derived for Nemrut volcano. Along with data on the volcanostratigraphy of Nemrut and results of mass balance simulations, this conclusion also follows from the compositional specifics of enclaves in the rocks. As follows from the model of magmatic evolution of rocks in the Kenya Rift (Macdonald et al., 1987; Marshall et al., 2009; Scaillet and Macdonald, 2001, 2003, 2006), quartz- and feldspar-rich residual rocks, which were produced by the massive crystallization of a mixture of quartz and anorthoclase, should have occurred among the enclaves or erupted volcanic rocks. No rocks or magmatic enclaves of such mineralogical composition are typically contained in volcanics of the trachybasalt–trachyte–comendite series. Quartz-feldspathic rocks were found only at Alid volcano in Eritrea (Lowenstern et al., 2006). However, the magmatic evolution of this volcano has not generated any alkaline magmas but ended with the origin of residual rhyolitic melt whose agpaitic index is lower than one. Conversely, the dominant crystallization of anorthoclase together with Fe-rich and accessory minerals during the evolution of trachytic, trachyte comenditic to comenditic, and pantelleritic melts (as follows from our simulations, Table 15) is validated by finds of enclaves of residual rocks (lavas, tuff, ignimbrite) with anomalously high concentrations of Ba (an element enriched in anorthoclase) and sometimes also Ba, Sr, REE, Nb, U, Th (which are accumulated in feldspars, clinopyroxene, Fe and Ti oxides, and accessory minerals) at several volcanic centers, including the Olkaria Complex (Macdonald et al., 2008).

CONCLUSIONS

Data on the eruption succession of Nemrut volcano and results of mass balance simulations of the composition of quartz-devoid volcanic rocks invalidate the model according to which high-Fe comenditic and pantelleritic magmas can be formed via the fractionation of low-Fe comenditic melt. The compositions of the rocks, matrix glasses, melt inclusions and mineral phenocrysts are consistent with the mass balance models for the magmatic evolution of parental trachyte comenditic magma to comenditic and pantelleritic melts. The origin of residual comenditic and pantelleritic melts with broadly varying Fe concentrations and alkalinity during various evolutionary stages of the volcano can be explained by variations in the crystallization conditions of anorthoclase (dominant phase), hedenbergite, fayalite, Fe and Ti oxides in the parental trachyte comenditic magmas depending on pressure and content of water dissolved in the melts.

The trachybasaltic magma erupted in the "rift" zone at approximately 500 years ago could not be a source of the post-caldera comenditic melt. Such a residual melt with narrow variations in the concentrations of major and trace elements was likely generated by the fractional crystallization of trachyte comenditic magma in the latest pre-caldera chamber, which was preserved after the collapse of the stratovolcano edifice and the origin of the caldera. Accessory minerals (REE- and Sr-bearing fluorapatite, zircon) were likely also involved in the fractional crystallization of the melts.

According to our QUILF calculations, the hedenbergite, fayalite and ilmenite phenocrysts crystallized under the following conditions (minimum parameters in the absence of quartz in the melts): 3 kbar, 763°C, $\Delta FMQ = -1.27$ for the low-Fe comendite NR-23; 3.3–3.8 kbar, 715°C, $\Delta FMQ = -1.08$ for the pantellerite NR-7; 2.3 kbar, 748°C, $\Delta FMQ = -1.16$ for the low-Fe comendites. The equilibrium crystallization of anorthoclase phenocrysts proceeded in the comenditic melts at a temperature of approximately 750°C. Data on glasses in MI in anorthoclase, hedenbergite, and fayalite phenocrysts indicate that the comenditic and pantelleritic melts contained 1–3 wt % H_2O.

Analysis of literature data and estimates of conditions under which the Nemrut magmas were formed shows that the local chambers with water undersaturated comenditic and pantelleritic melts can occur at depths of 5 to 10–15 km (lithostatic pressure of 1–4 kbar) at temperatures less than 750°C and oxygen fugacity below the FMQ buffer.

ACKNOWLEDGMENTS

The authors thank Yu.D. Shcherbakov and N.S. Bryanskii (Vinogradov Institute of Geochemistry, Siberian Branch, Russian Academy of Sciences, Irkutsk) for help with LA-ICP-MS analyses.

REFERENCES

Andersen, D.J., Lindsley, D.H., and Davidson, P.M., QUILF: a Pascal program to assess equilibria among Fe–Mg–Mn–Ti oxides, pyroxenes, olivine, and quartz, *Comput. Geosci.*, 1993, vol. 19, pp. 1333–1350.

Andreeva, O.A., Yarmolyuk, V.V., Andreeva, I.A., Li, J.Q., and Li, W.R., The composition and sources of magmas of Changbaishan Tianchi Volcano (China–North Korea), *Dokl. Earth Sci.*, 2014, vol. 456, no. 2, pp. 572–578.

Aydar, E., Gourgaud, A., Ulusoy, I., Digonnet, F., Labazuy, P., Sen, E., Bayhan, H., Kurttas, T., and Tolluoğlu, A.U., Morphological analysis of active Mount Nemrut stratovolcano, eastern Turkey: evidences and possible impact areas of future eruption, *J. Volcanol. Geotherm. Res*, 2003, vol. 123, pp. 301–312.

Bohrson, W.A. and Reid, M.R., Genesis of silicic peralkaline volcanic rocks in an ocean island setting by crustal melting and open system processes, *J. Petrol.*, 1997, vol. 38, pp. 1137–1166.

Civetta, L., D'Antonio, M., Orsi, G., and Tilton, G.R., The geochemistry of volcanic rocks from Pantelleria Island, Sicily channel: petrogenesis and characteristics of the mantle source region, *J. Petrol.*, 1998, vol. 39, pp. 1453–1491.

Çubukçu, H.E., Aydar, E., and Gourgaud, A., Comment on "Volcanostratigraphy" and petrogenesis of the Nemrut stratovolcano (East Anatolian High Plateau): the most recent post-collisional volcanism in "Turkey" by Özdemir et al. [Chemical Geololgy, 226 (2006) 189–211], *Chem. Geol.*, 2007, vol. 245, pp. 120–129.

Çubukçu, H.E., Ulusoy, İ., Aydar, E., Ersoy, O., Şen, E., Gourgaud, A., and Guillou, H., Mt. Nemrut volcano (eastern Turkey): temporal petrological evolution, *J. Volcanol. Geotherm. Res.*, 2012, vol. 209–210, pp. 33–60.

Di Carlo, I., Rotolo, S.G., Scaillet, B., Buccheri, V., and Pichavant, M., Phase equilibrium constraints on pre-eruptive conditions of recent felsic explosive volcanism at Pantelleria Island, Italy. *J. Petrol.*, 2010, vol. 51, pp. 2245–2276.

Ewart, A., Chemical charges accompanying spherulituc crystallization in rhyolitic lavas, Central Volcanic Region, New Zealand, *Mineral. Mag.*, 1971, vol. 38, pp. 424–434.

Fan, Q.C., Sui, J.L., Wang, T.Y., Li, N., and Sun, Q., Eruption history and magma evolution of the trachybasalt in the Tianchi volcano, Changbaishan, *Acta Petrol. Sin.*, 2006, vol. 22, no. 6, pp. 1449–1457.

Field, L., Blundy, J., Brooker, R.A., Wright, T., and Yirgu, G., Magma storage conditions beneath Dabbahu volcano (Ethiopia) constrained by petrology, seismicity and satellite geodesy, *Bull Volcanol.*, 2012, vol. 74, pp. 981–1004.

Field, L., Blundy, J., Calvert, A., and Yirgu, G., Magmatic history of Dabbahu, a composite volcano in the Afar rift, Ethiopia, *Geol. Soc. Am. Bull.*, 2013, vol. 125, pp. 128–147.

Gagnevin, D., Ethien, R., Bonin, B., Moine, B., Fe'raud, G., Gerbe, M.C., Cottin, J.Y., Michon, G., Tourpin, S., Mamias, G., Perrache, C., and Giret, A., Open-system processes in the genesis of silica-oversaturated alkaline rocks of the Rallier-du-Baty Peninsula, Kerguelen Archipelago (Indian Ocean), *J. Volcanol. Geotherm. Res.*, 2003, vol. 123, pp. 267–300.

Ghiorso, M.S. and Evans, B.W., Thermodynamics of rhombohedral oxide solid solutions and a revision of the Fe–Ti two-oxide geothermometer and oxygen-barometer, *Am. J. Sci.*, 2008, vol. 308, pp. 957–1039.

Hanchar, J.M. and Watson, E.B., Zircon saturation thermometry, in *Zircon*, Hanchar. J.M. and Hoskin P.W.O., Eds., *Mineral. Soc. Am., Rev. Mineral.*, 2003, vol. 53, pp. 89–112.

Heumann, A. and Davies, G.R., U–Th disequilibrium and Rb–Sr age constraints on the magmatic evolution of peralkaline rhyolites from Kenya, *J. Petrol.*, 2002, vol. 43, pp. 557–577.

Horn, S. and Schmincke, H.-U., Volatile during the eruption of Baitoushan volcano (China/North Korea) ca. 969 AD, *Bull. Volcanol.*, 2000, vol. 61, pp. 537–555.

Karaoğlu, Ö., Özdemir, Y., Tolluoğlu, A.Ü., Karabıyıkoğlu, M., Köse, O., and Froger, J.-L., Stratigraphy of the volcanic products around Nemrut caldera: implications for reconstruction of the caldera formation, *Turk. J. Earth Sci.*, 2005, vol. 14, pp. 123–143.

Kozlovsky, A.M., Yarmolyuk, V.V., Kovalenko, V.V., Savatenkov, V.M., and Velivetskaya, T.A., Trachytes, comendites, and pantellerites of the late Paleozoic bimodal rift association of the Noen and Tost ranges, southern Mongolia: differentiation and contamination of peralkaline salic melts, *Petrology*, 2007, vol. 15, no. 3, pp. 240–263.

Lavrent'ev, Yu.G., Karmanov, N.S., and Usova, L.V., Electron microprobe determination of mineral composition: microanalyzer or electron microprobe, *Geol. Geofiz.*, 2015, vol. 56, no. 8, pp. 1473–1482.

LeMasurier, W.L., Choi, S.H., Kawachi, Y., Mukasa, S.B., and Rogers, N.W., Evolution of pantellerite–trachyte–phonolite volcanoes by fractional crystallization of basanite magma in a continental rift setting, Marie Byrd Land, Antarctica, *Contrib. Mineral. Petrol.*, 2011, vol. 162, pp. 1175–1199.

Lowenstern, J.B., Charlier, B.L.A., Clynne, M.A., and Wooden, J.L., Extreme U–Th disequilibrium in rift-related basalts, rhyolites and granophyric granite and the time scale of rhyolite generation, intrusion and crystallization at Alid volcanic center, Eritrea, *J. Petrol.*, 2006, vol. 47, pp. 2105–2122.

Macdonald, R., Nomenclature and petrochemistry of the peralkaline oversaturated extrusive rocks, *Bull. Volcanol.*, 1974, vol. 38, pp. 498–516.

Macdonald, R., Baginski, B., Ronga, F., Dzierzanowski, P., Lustrino, M., Marzoli, A., and Melluso, L., Evidence for extreme fractionation of peralkaline silicic magmas, the Boseti volcanic complex, Main Ethiopian Rift, *Mineral. Petrol,* 2012, vol. 104, pp. 163–175.

Macdonald, R. and Belkin, H.E., Compositional variation in minerals of the chevkinite group, *Mineral. Mag.*, 2002, vol. 66, pp. 1075–1098.

Macdonald, R., Belkin, H.E., Fitton, J.G., Rogers, N.W., Nejbert, K., Tindle, A.G., and Marshall, A.S., The roles of fractional crystallization, magma mixing, crystal mush remobilization and volatile–melt interactions in the genesis of a young basalt–peralkaline rhyolite suite, the Greater Olkaria volcanic complex, Kenya rift valley, *J. Petrol.*, 2008, vol. 49, pp. 1515–1547.

Macdonald, R., Belkin, H.E., Wall, F., and Baginski, B., Compositional variation in the chevkinite group: new data from igneous and metamorphic rocks, *Mineral. Mag.,* 2009, vol. 73, pp. 521–540.

Macdonald, R., Davies, G.R., Bliss, C.M., Leat, P.T., Bailey, D.K., and Smith, R.L., Geochemistry of high-silica peralkaline rhyolites, Naivasha, Kenya rift valley, *J. Petrol.*, 1987, vol. 28, pp. 979–1008.

Marshall, A.S., Mcdonald, R., Rogers, N.W., Fitton, J.G., Tindle, A.G., Nejbert, K., and Hinton, R.W., Fractionation of peralkaline silicic magmas: the Greater Olkaria volcanic complex, Kenya Rift Valley, *J. Petrol.*, 2009, vol. 50, pp. 323–359.

McDonough, W.E. and Sun, S., The composition of the Earth, *Chem. Geol.*, 1995, vol. 120, pp. 223–253.

Mungall, J.E. and Martin, R.F., Petrogenesis of basalt–comendite and basalt–pantellerite suites, Terceira, Azores, and some implications for the origin of ocean-island rhyolites, *Contrib. Mineral. Petrol.*, 1995, vol. 119, pp. 43–55.

Nekvasil, H., Dondolini, A., Horn, J., Filiberto, J., Long, H., and Lindsley, D.H., The origin and evolution of silica-saturated alkali suites: an experimental study, *J. Petrol.*, 2004, vol. 45, pp. 693–721.

Özdemir, Y., Karaoglu, Ö., Tolluoglu, A.U., and Gulec, N., Volcanostratigraphy and petrogenesis of the Nemrut stratovolcano, (East Anatolian High Plateau): the most recent post-collisional volcanism in Turkey, *Chem. Geol.*, 2006, vol. 226, pp. 189–211.

Peccerillo, A., Barberio, M.R., Yirgu, G., Ayalew, D., Barbieri, M., and Wu, T.W., Relationships between mafic and peralkaline silicic magmatism in continental rift settings: a petrological, geochemical and isotopic study of the Gedemsa Volcano, Central Ethiopian Rift, *J. Petrol.*, 2003, vol. 44, pp. 2003–2032.

Peretyazhko, I.S., CRYSTAL: a program package for mineralogists, petrologists, and geochemists, *Zap. Vseross. Mineral. O-va*, 1996, no. 3, pp. 141–148.

Peretyazhko, I.S., Genesis of mineralized cavities (miaroles) in granite pegmatites and granites, *Petrology*, 2010, vol. 18, no. 2, pp. 183–208.

Peretyazhko, I.S., Savina, E.A., Karmanov, N.S., and Shcherbakov, Yu.D., Genesis of mugearites and benmoreites of Nemrut Volcano, Eastern Turkey: magma mixing and fractional crystallization of trachybasaltic melt, *Petrology*, 2015, vol. 23, no. 4, pp. 376–403.

Popov, V.K., Sakhno, V.G., Kuzmin, Ya.V., Glascock, M.D., and Choi, B.K., Geochemistry of volcanic glasses from the Pektusan Volcano, *Dokl. Earth Sci.*, 2005, vol. 403, no. 5, pp. 803–807.

Popov, V.K., Sandimirova, G.P., and Velivetskaya, T.A., Strontium, neodymium, and oxygen isotopic variations in the alkali basalt–trachyte–pantellerite–comendite series of Pektusan Volcano, *Dokl. Earth Sci.*, 2008, vol. 419, no. 2, pp. 329–334.

Putirka, K.D., Thermometers and barometers for volcanic systems, *Rev. Mineral. Geochem*, 2008, vol. 69, pp. 61–120.

Ren, M., Omenda, P.A., Anthony, E.Y., White, J.C., Macdonald, R., and Bailey, D.K., Application of the QUILF thermobarometer to the peralkaline trachytes and pantellerites of the Eburru volcanic complex, East African Rift, Kenya, *Lithos*, 2006, vol. 91, pp. 109–124.

Ronga, F., Lustrino, M., Marzoli, A., and Melluso, L., Petrogenesis of basalt-comendite-pantellerite rock suite: the Boseti volcanic complex (Main Ethiopian Rift), *Mineral. Petrol.*, 2010, vol. 98, pp. 227–243.

Sakhno, V.G., Chronology of eruptions, composition, and magmatic evolution of the Pektusan Volcano: evidence from K–Ar, $^{87}Sr/^{86}Sr$, and $\delta^{18}O$ isotope data, *Dokl. Earth Sci.*, 2007a, vol. 412, no. 1, pp. 22–28.

Sakhno, V.G., Isotopic–geochemical characteristics and deep-seated sources of the alkali rocks of the Pektusan Volcano, *Dokl. Earth Sci.*, 2007b, vol. 417A, no. 4, pp. 1386–1392.

Scaillet, B. and Macdonald, R., Phase relations of peralkaline silicic magmas and petrogenetic implications, *J. Petrol.*, 2001, vol. 42, pp. 825–845.

Scaillet, B. and Macdonald, R., Experimental constraints on the relationships between peralkaline rhyolites of the Kenya Rift Valley, *J. Petrol.*, 2003, vol. 44, pp. 1867–1894.

Scaillet, B. and Macdonald, R., Experimental constraints on pre-eruptive conditions of pantelleritic magmas: evidence from the Eburru complex, Kenya Rift, *Lithos*, 2006, vol. 91, pp. 95–108.

Sharpenok, L.N., Kukharenko, E.A., and Kostin, A.E., New provisions for volcanogenic rocks in the petrographic code, *J. Volcano. Seismol.*, 2009, vol. 3, no. 4, pp. 279–294.

Ulusoy, İ., Labazuy, P., Aydar, A., Ersoy, O., and Çubukçu, E., Structure of the Nemrut caldera (Eastern Anatolia, Turkey) and associated hydrothermal fluid circulation, *J. Volcanol. Geotherm. Res.*, 2008, vol. 174, pp. 269–283.

Ulusoy, İ., Çubukçu, E., Aydar, A., Labazuy, P., and Ersoy, O., Volcanological evolution and caldera forming eruptions of Mt. Nemrut (Eastern Turkey), *J. Volcanol. Geotherm. Res.*, 2012, vol. 245–246, pp. 21–39.

White, J.C., Holt, G.S., Parker, D.F., and Ren, M., Trace-element partitioning between alkali feldspar and peralkalic quartz trachyte to rhyolite magma. Part I: systematics of trace-element partitioning, *Am. Mineral.*, 2003, vol. 88, pp. 316–329.

White, J.C., Ren, M., and Parker, D.F., Variation in mineralogy, temperature, and oxygen fugacity in a suite of strongly peralkaline lavas and tuffs, Pantelleria, Italy, *Can. Mineral.*, 2005, vol. 43, pp. 1331–1347.

White, J.C., Parker, D.F., and Ren, M., The origin of trachyte and pantellerite from Pantelleria, Italy: insights from major element, trace element, and thermodynamic modelling, *J. Volcanol. Geotherm. Res.*, 2009, vol. 179, pp. 33–55.

Xirouchakis, D. and Lindsley, D.H., Equilibria among titanite, hedenbergite, fayalite, quartz, ilmenite and magnetite: experiments and internally consistent thermodynamic data for titanite, *Am. Mineral.*, 1998, vol. 83, pp. 712–725.

Yarmolyuk, V.V., *Pozdnepaleozoiskii vulkanizm kontinental'nykh riftogennykh struktur Tsentral'noi Azii* (Late Paleozoic Volcanism of the Continental Structures of Central Asia), Moscow: Nauka, 1983.

Yılmaz, Y., Guner, Y., and Şaroğlu, F., Geology of the Quaternary volcanic centres of the East Anatolia, *J. Volcanol. Geotherm. Res.*, 1998, vol. 85, pp. 173–210.